Supporting Information

Dioxaphosphabicyclooctanes: small caged phosphines from tris(hydroxymethyl)phosphine

James D. Nobbs,* Dillon W. P. Tay, Yoon Hui Yeap, Yong Lun Tiong, Suming Ye, Srinivasulu Aitipamula, Cun Wang, Choon Boon Cheong and Martin van Meurs*

*Institute of Sustainability for Chemicals, Energy and Environment (ISCE²), Agency for Science, Technology and Research (A*STAR), 1 Pesek Road, Jurong Island, Singapore 627833, Republic of Singapore.*

Contents

1. Synthesis of α,β-unsaturated ketones

3-Methyl-1-phenylbut-2-en-1-one

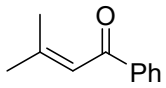

Anhydrous zinc(II) chloride (3.5 g, 25.3 mmol) was suspended in THF (60 mL) and cooled to 0 °C. Phenylmagnesium bromide (0.74M in THF, 32.4 mL, 24.0 mmol) was added dropwise and the mixture allowed to warm to room temperature. After two hours the mixture was again cooled to 0 °C and a mixture of [$Pd(PPh_3)_4$] (1.47 g, 1.27 mmol) and 3,3-dimethylacryloyl chloride (3.0 g, 25.3 mmol) in THF (35 mL) was added dropwise. The mixture was stirred for 40 hours after which time it was quenched with water (0.75 mL). Hexane (200 mL) was then added and the mixture was filtered through celite. The volatiles were removed *in vacuo* and the crude material purified by chromatography (R_f = 0.32) using EtOAc:hexane (1:9) mixture as the eluent. Pale yellow oil. Yield = 3.4 g (88%). ^{1}H NMR (400 MHz, $CDCl_3$): δ 7.95 – 7.90 (2H, m, Ar*H*), 7.55 – 7.49 (1H, m, Ar*H*), 7.48 – 7.41 (2H, m, Ar*H*), 6.75 (1H, sept, $^4J_{HH}$ = 1.3 Hz, C*H*), 2.21 (3H, d, $^4J_{HH}$ = 1.1 Hz, CH_3) and 2.02 ppm (3H, d, $^4J_{HH}$ = 1.1 Hz, CH_3).

4-Methyl-1-phenylpent-3-en-2-one

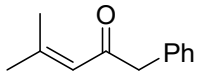

Anhydrous zinc(II) chloride (3.5 g, 25.3 mmol) was suspended in THF (60 mL) and cooled to 0 °C. Benzymagnesium chloride (1.0M in Et_2O, 24.0 mL, 24.0 mmol) was added dropwise and the mixture allowed to warm to room temperature. After two hours the mixture was again cooled to 0°C and a mixture of [$Pd(PPh_3)_4$] (1.47 g, 1.27 mmol) and 3,3-dimethylacryloyl chloride (3.0 g, 25.3 mmol) in THF (35 mL) was added dropwise. The mixture was stirred for 40 hours after which time it was quenched with water (0.75 mL). Hexane (200 mL) was then added and the mixture was filtered through celite. The volatiles were removed *in vacuo* and the crude material purified by chromatography (R_f = 0.34) using EtOAc:hexane (1:9) mixture as the eluent. Pale yellow oil. Yield = 3.7 g (88%). ^{1}H NMR (400 MHz, $CDCl_3$): δ 7.36 – 7.29 9(2H, m, Ar*H*), 7.28 – 7.24 (1H, m, Ar*H*), 7.24 – 7.20 (2H, m, Ar*H*), 6.11 (1H, s, C*H*), 2.15 (3H, s, CH_3) and 1.86 ppm (3H, s, CH_3).

(E)-4-(Pyridin-2-yl)but-3-en-2-one

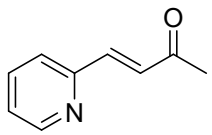

Acetylmethylene-triphenylphosphorane (12.0 g, 37.7 mmol) was stirred in toluene (80 mL). Pyridine-2-carbaldehyde (3.2 g, 2.8 mL, 30.2 mmol) was added and the mixture heated to reflux temperature. After 72 hours the mixture had turned black and the heating was ceased. The volatiles were removed *in vacuo* to give a black solid. Column chromatography was performed using EtOAc:hexanes (1:1) as the eluent. The product eluted first (R_f = 0.73). Yield = 3.0 g (67%). ^{1}H NMR (400 MHz, $CDCl_3$): δ 8.62 (1H, d, $^3J_{HH}$ = 4.7 Hz, Ar*H*), 7.70 (1H, d of t, $^3J_{HH}$ = 7.7 Hz, $^4J_{HH}$ = 1.8 Hz, Ar*H*), 7.49 (1H, d, $^3J_{HH}$ = 16.1 Hz, C*H*), 7.45 (1H, d, $^3J_{HH}$ = 7.8 Hz, Ar*H*), 7.27 – 7.23 (1H, m, Ar*H*), 7.11 (1H, d, $^3J_{HH}$ = 16.1 Hz, C*H*) and 2.37 ppm (3H, s, CH_3). ^{13}C{^{1}H} NMR (101 MHz, $CDCl_3$): δ 198.5 (Ar*C*), 153.2 (Ar*C*), 150.2 (Ar*C*), 142.0 (Ar*C*), 136.9 (*C*H), 130.2 (*C*H), 124.4 (Ar*C*) and 28.1 ppm (*C*H_3).

(3E,7E)-Deca-3,7-diene-2,9-dione

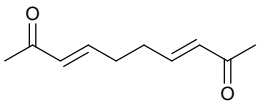

Succinic aldehyde (3.6 g, 41.8 mmol) was dissolved in CH_2Cl_2 (80 mL). Acetylmethylene-triphenylphosphorane (26.6 g , 83.6 mmol) was added giving a pale yellow solution. After 16 hours the solution had turned orange. The volatiles were removed *in vacuo* giving a pale yellow solid. The crude mixture was extracted with Et_2O (200 mL) and the volatiles were removed *in vacuo* to yield an orange oily solid. Column chromatography was performed eluting with EtOAc:hexane (2:3), the product was the third fraction to elute R_f = 0.17. Yellow oil. Yield = 1.2 g (15%). ^{1}H NMR (400 MHz, $CDCl_3$): δ 6.81 – 6.71 (2H, m, C*H*), 6.11 (2H, d, $^3J_{HH}$ = 15.8 Hz, C*H*), 2.44 – 2.40 (4H, m, CH_2) and 2.25 ppm (6H, s, CH_3).

(3E,3'E)-4,4'-(1,2-Phenylene)bis(but-3-en-2-one)

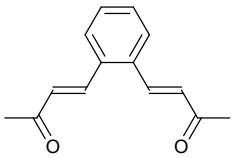

ortho-Phthalilaldehyde (3.2 g, 24.1 mmol) was dissolved in chloroform (200 mL) and then acetylmethylene-triphenylphosphorane (19.2 g, 60.3 mmol) was added. The mixture was heated at reflux temperature for 16 hours. After this time the volatiles were removed *in vacuo* and the crude material was purified by column chromatography eluting with EtOAc:hexanes (3:1). The product eluted in the first fraction (R_f = 0.45). Yield = g (%). ^{1}H NMR (400 MHz, $CDCl_3$): δ 7.85 (2H, d, $^3J_{HH}$ = 16.0 Hz, C*H*), 7.59 -7.55 (2H, m, Ar*H*), 7.42 – 7.38 (2H, m, Ar*H*), 6.61 (2H, d, $^3J_{HH}$ = 16.0 Hz, C*H*) and 2.38 ppm (3H, s, CH_3).

(3E,3'E)-4,4'-(1,3-Phenylene)bis(but-3-en-2-one)

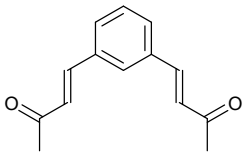

Isophthalaldehyde (3.2 g, 24.0 mmol) was dissolved in $CHCl_3$ (200 mL) and then acetylmethylene-triphenylphosphorane (19.1 g, 60.1 mmol) was added. The mixture was heated at reflux temperature for 72 hours. After this time the volatiles were removed *in vacuo* and the crude material was purified by column chromatography eluting with EtOAc:hexanes (3:1), R_f = 0.62. Yield = 1.6 g (31%). ^{1}H NMR (400 MHz, $CDCl_3$): δ 7.68 (1H, br s, Ar*H*), 7.56 (2H, dd, $^3J_{HH}$ = 7.8 Hz, $^4J_{HH}$ = 1.5 Hz, Ar*H*), 7.50 (2H, d, $^3J_{HH}$ = 16.3 Hz, C*H*), 7.43 (1H, t, $^3J_{HH}$ = 7.5 Hz, Ar*H*), 6.74 (2H, d, $^3J_{HH}$ = 16.3 Hz, C*H*) and 2.38 ppm (6H, s, CH_3).

2. NMR Spectra

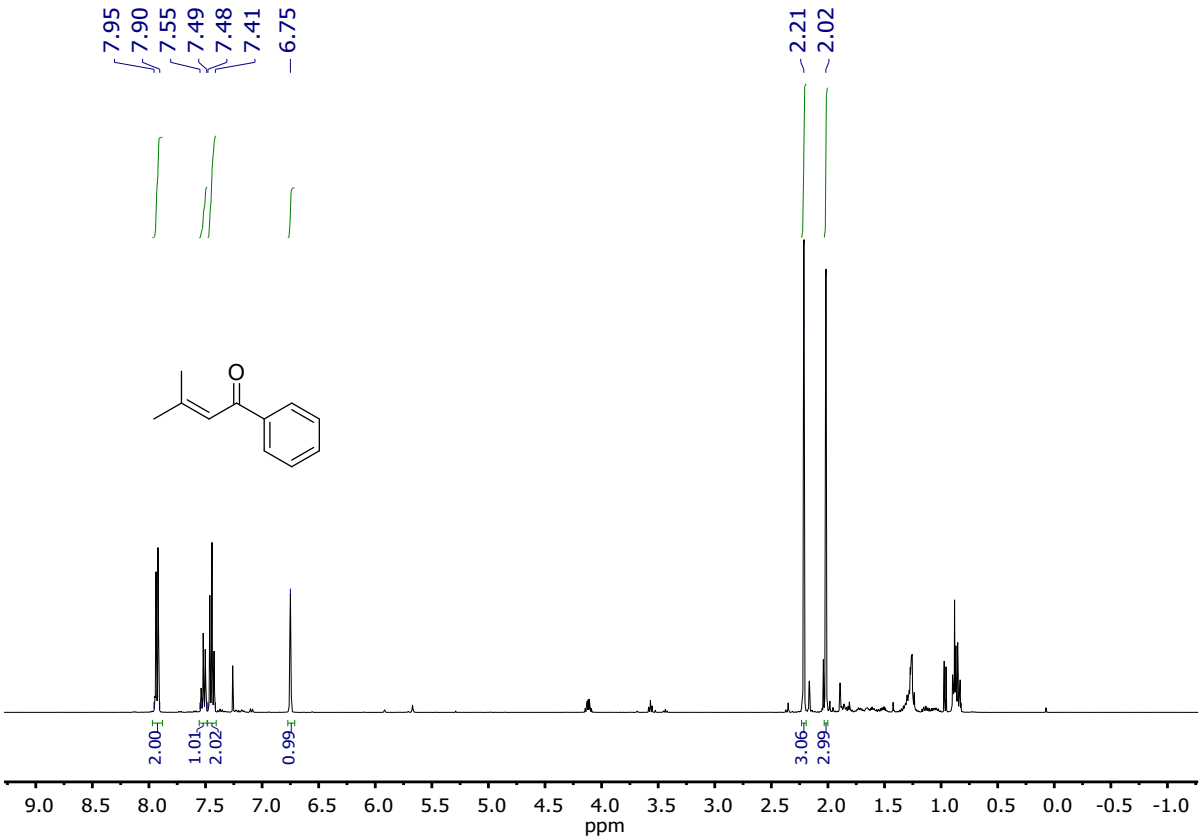

Figure S1. ^{1}H NMR (400 MHz, $CDCl_3$) spectrum of 3-methyl-1-phenylbut-2-en-1-one.

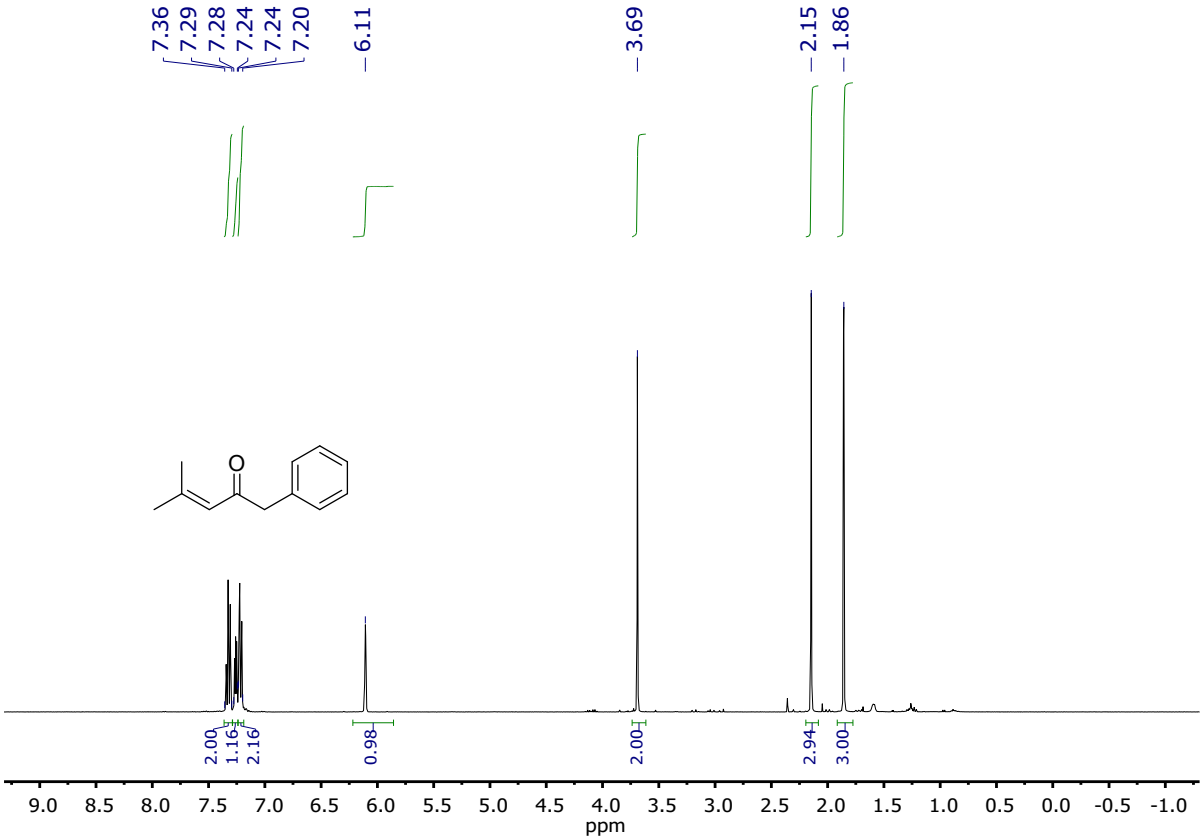

Figure S2. ^{1}H NMR (400 MHz, $CDCl_3$) spectrum of 4-methyl-1-phenylpent-3-en-2-one.

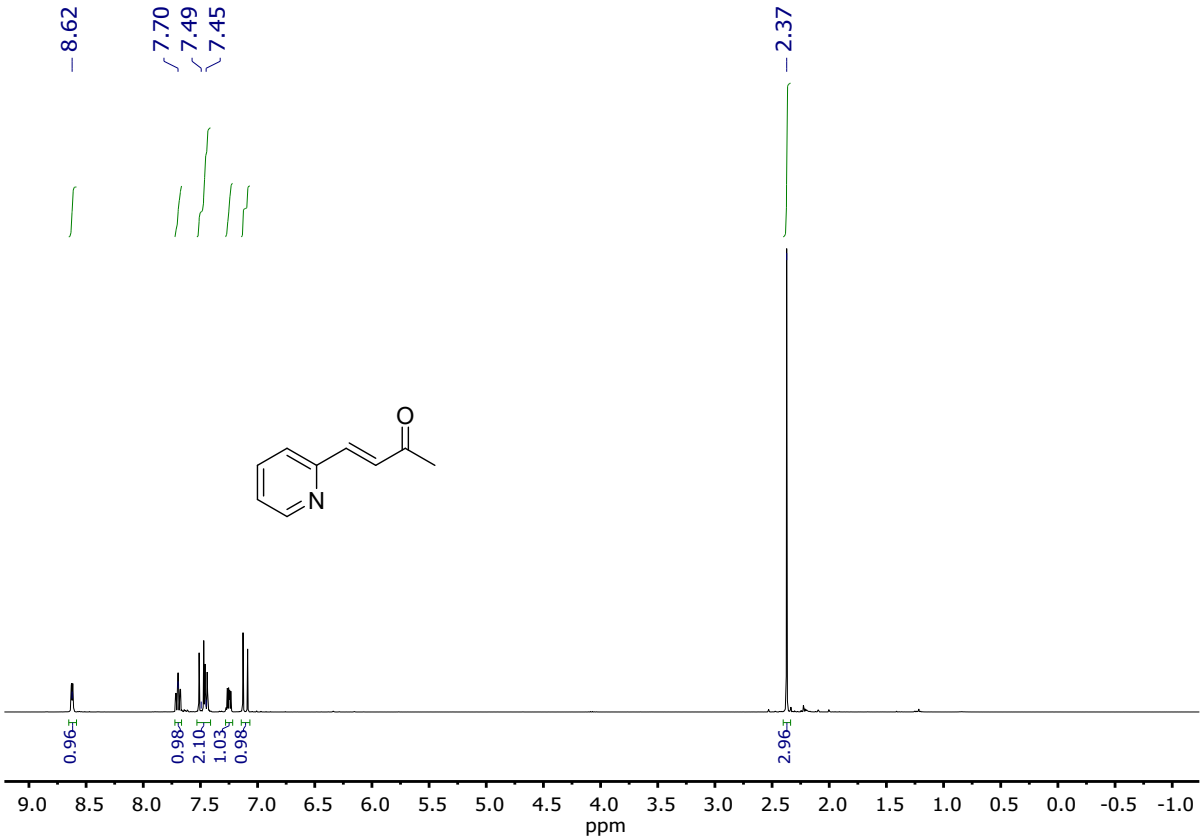

Figure S3. ^{1}H NMR (400 MHz, $CDCl_3$) spectrum of (*E*)-4-(pyridin-2-yl)but-3-en-2-one.

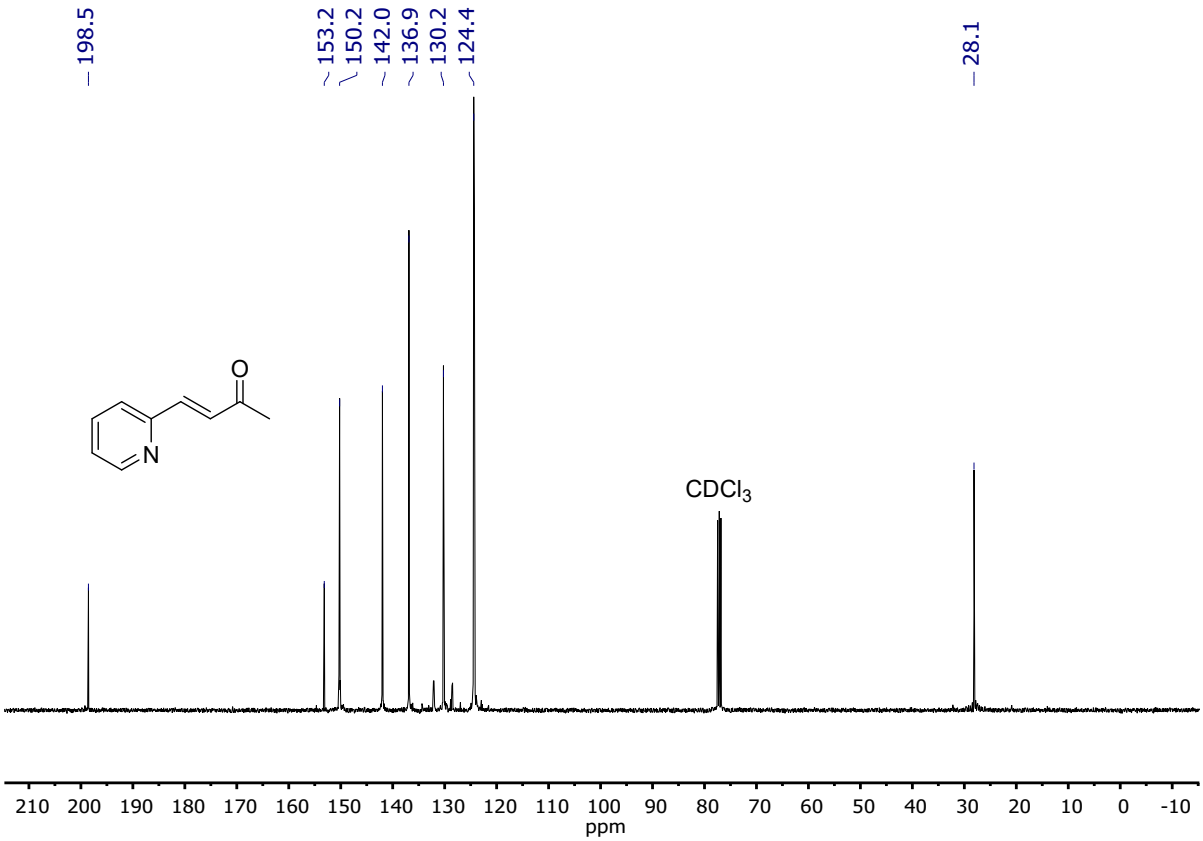

Figure S4. $^{13}C\{^{1}H\}$ NMR (101 MHz, $CDCl_3$) of (*E*)-4-(pyridin-2-yl)but-3-en-2-one.

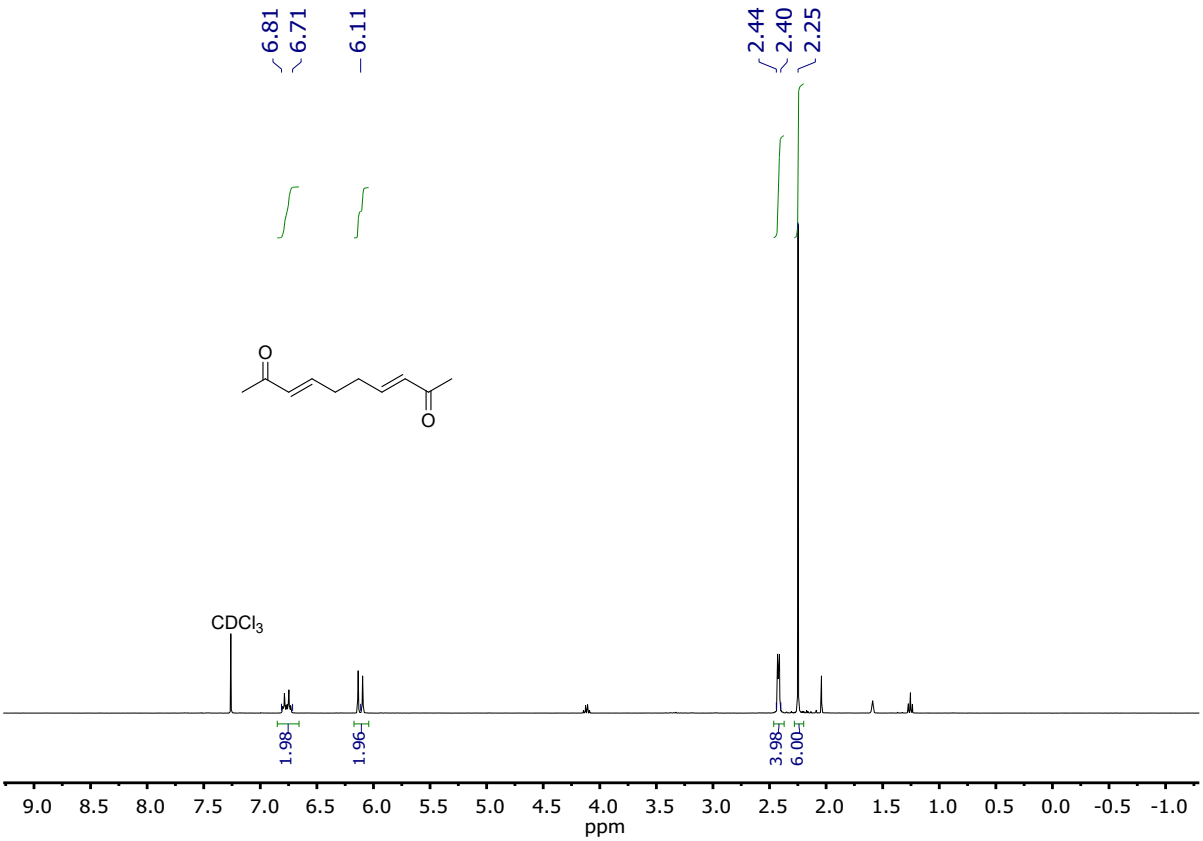

Figure S5. ^{1}H NMR (400 MHz, $CDCl_3$) spectrum of (3*E*,7*E*)-deca-3,7-diene-2,9-dione.

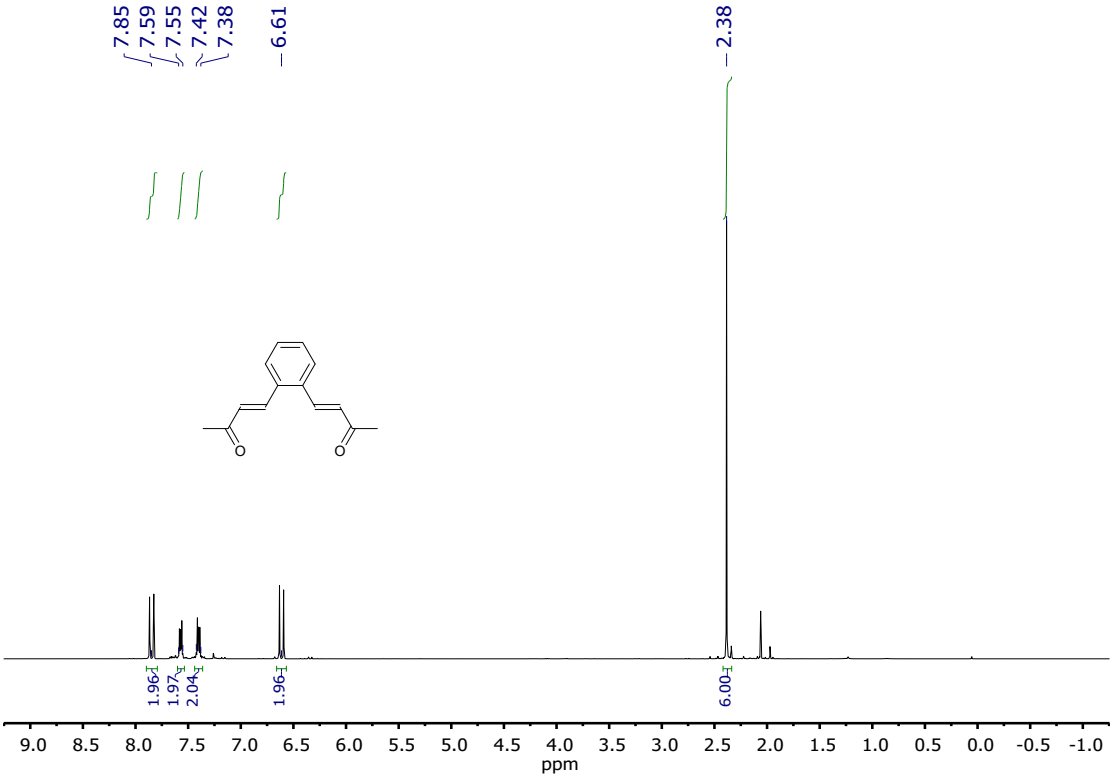

Figure S6. ^{1}H NMR (400 MHz, $CDCl_3$) spectrum of (3*E*,3'*E*)-4,4'-(1,2-phenylene)bis(but-3-en-2-one).

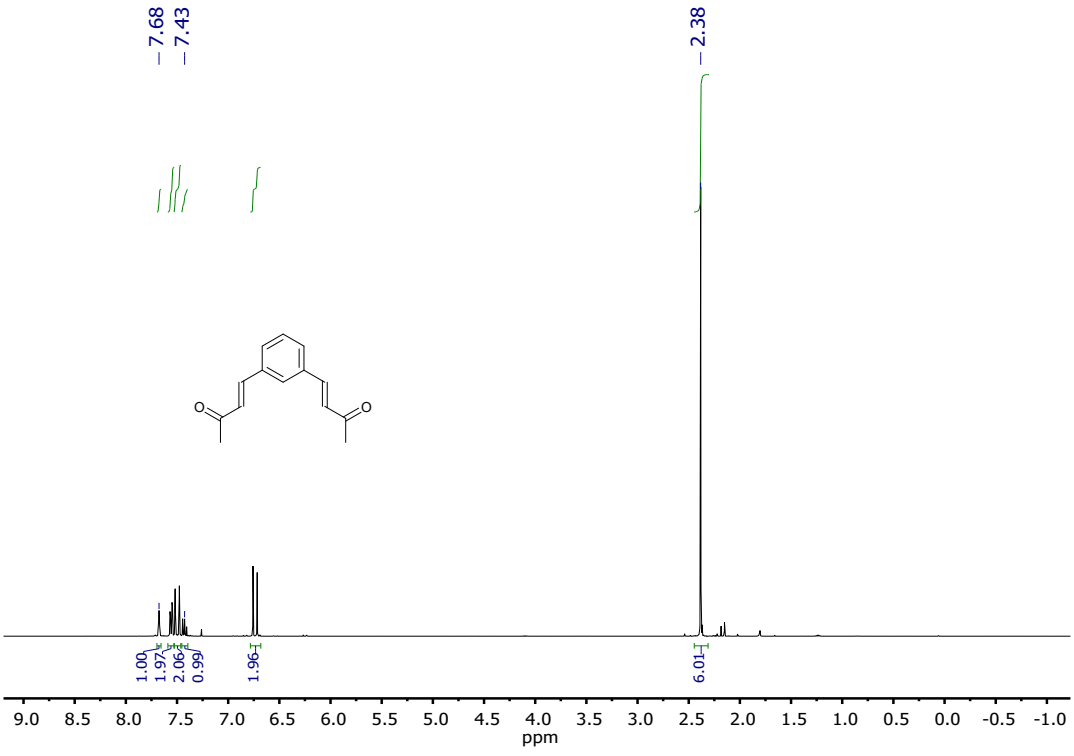

Figure S7. ^{1}H NMR (400 MHz, $CDCl_3$) spectrum of (3*E*,3'*E*)-4,4'-(1,3-phenylene)bis(but-3-en-2-one).

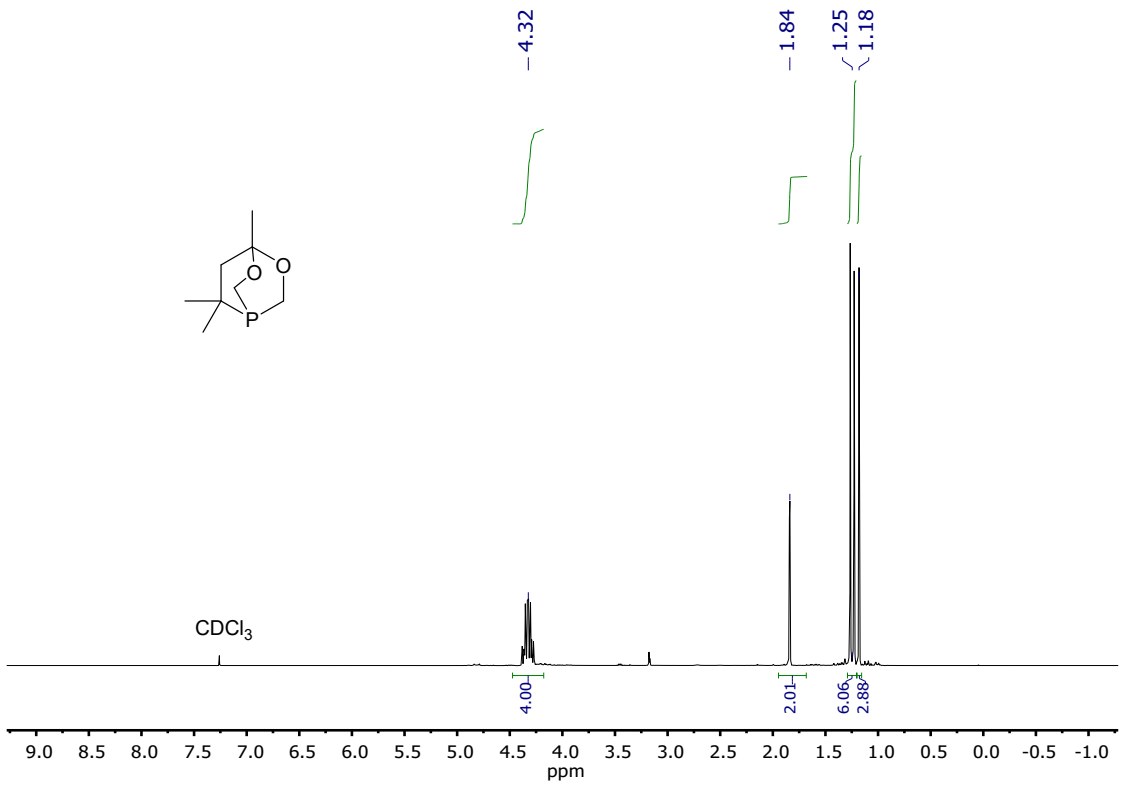

Figure S8. ^{1}H NMR (400 MHz, $CDCl_3$) spectrum of **L1**, 4,7,7-trimethyl-3,5-dioxa-1-phosphabicyclo[2.2.2]octane.

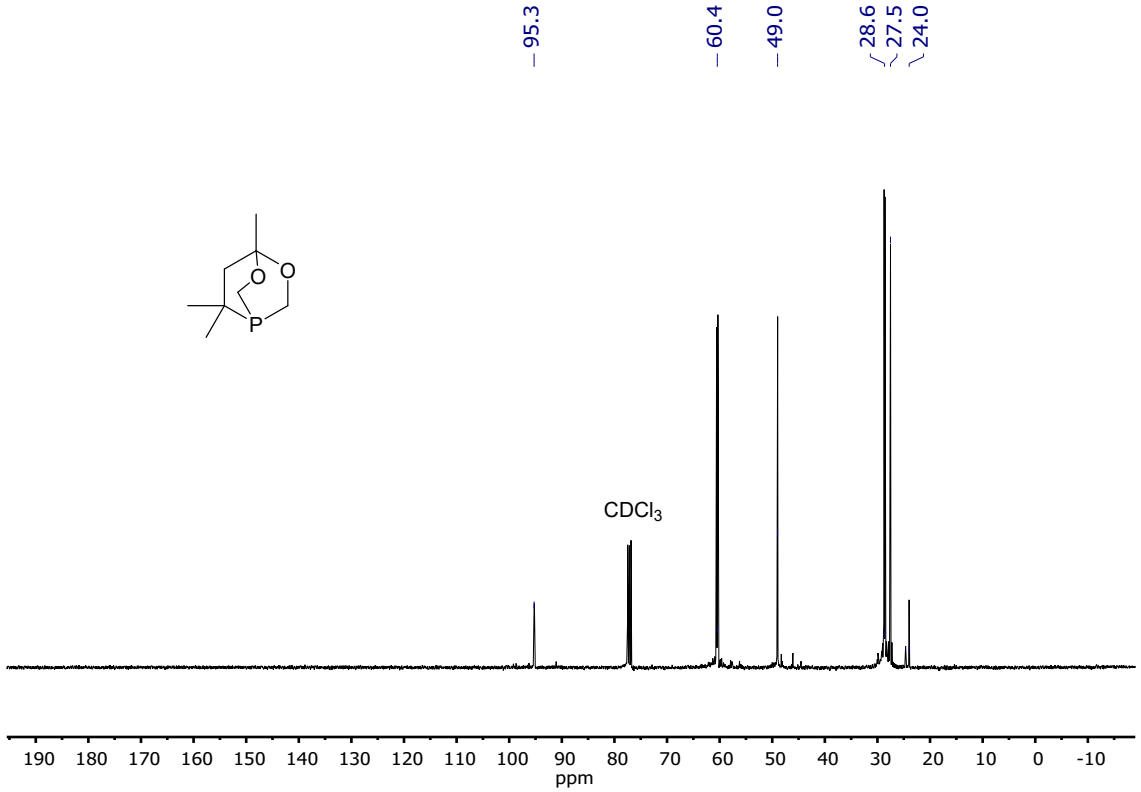

Figure S9. $^{13}C\{^{1}H\}$ NMR (101 MHz, $CDCl_3$) spectrum of **L1**, 4,7,7-trimethyl-3,5-dioxa-1-phosphabicyclo[2.2.2]octane.

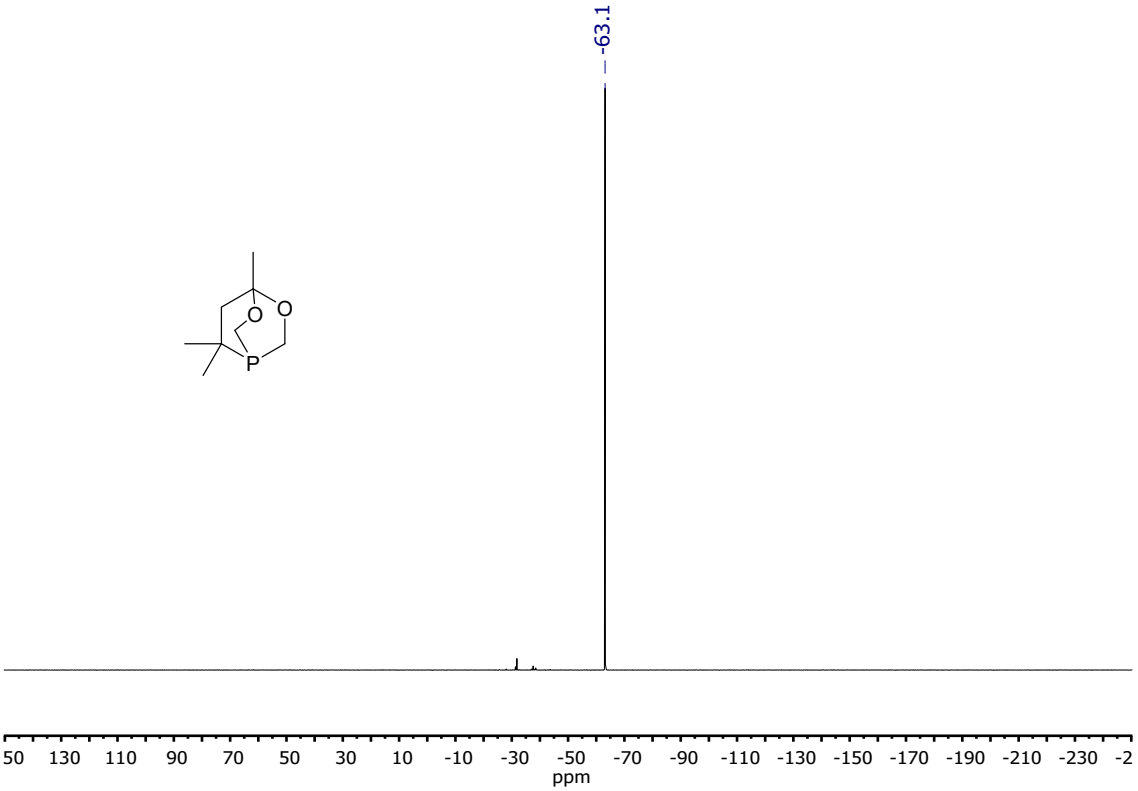

Figure S10. $^{31}P\{^{1}H\}$ NMR (162 MHz, $CDCl_3$) spectrum of **L1**, 4,7,7-trimethyl-3,5-dioxa-1-phosphabicyclo[2.2.2]octane.

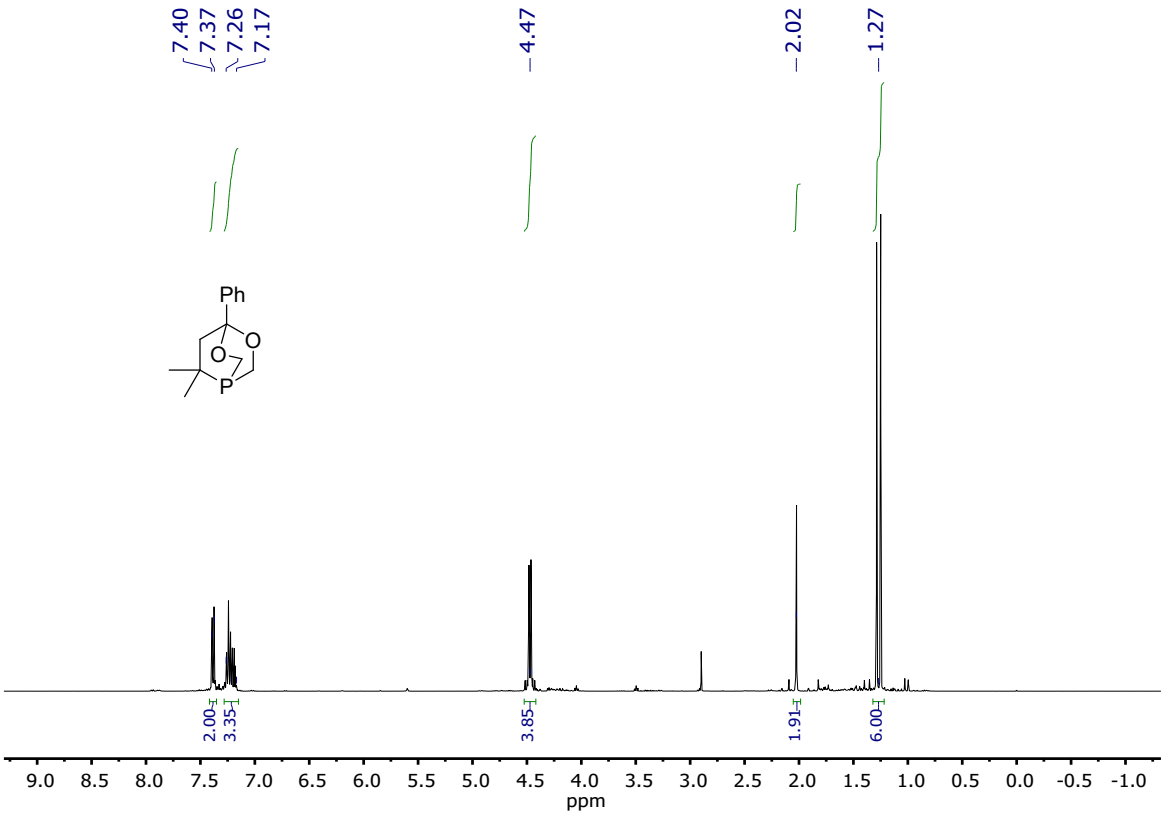

Figure S11. ^{1}H NMR (400 MHz, $CDCl_3$) spectrum of **L2**, 4-phenyl-7,7-dimethyl-3,5-dioxa-1-phosphabicyclo[2.2.2]octane.

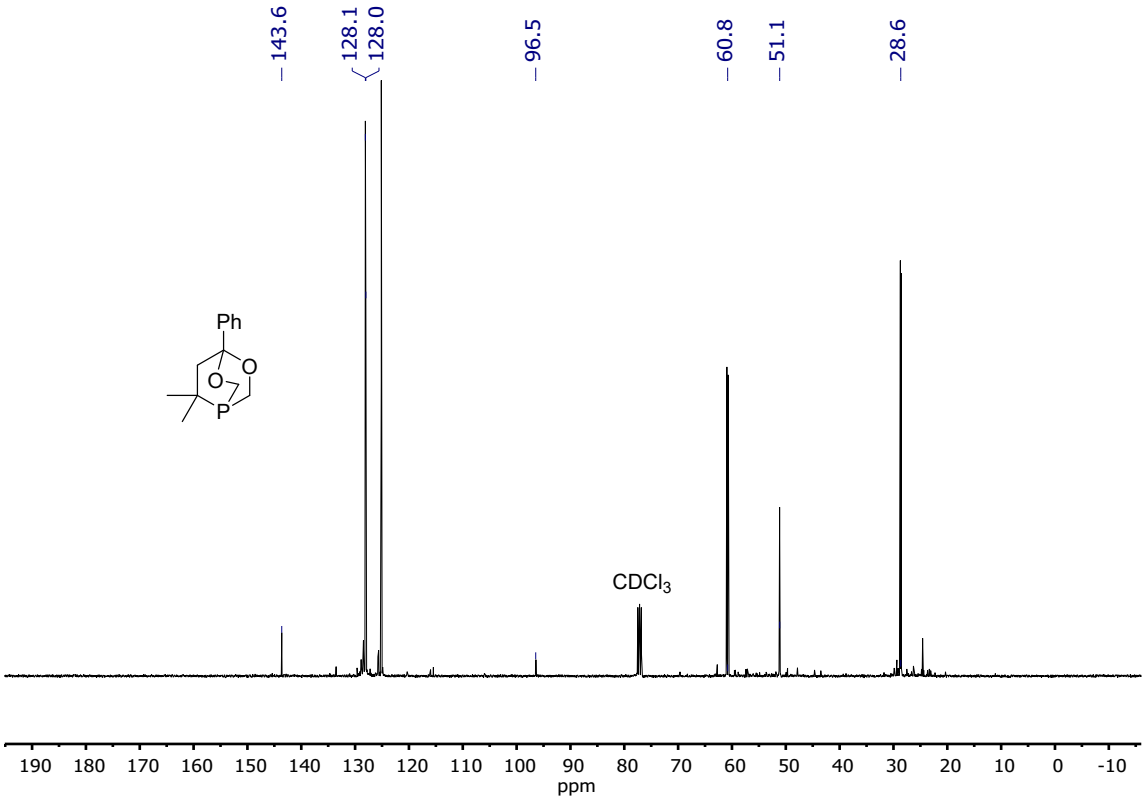

Figure S12. $^{13}C\{^{1}H\}$ NMR (101 MHz, $CDCl_3$) spectrum of **L2**, 4-phenyl-7,7-dimethyl-3,5-dioxa-1-phosphabicyclo[2.2.2]octane.

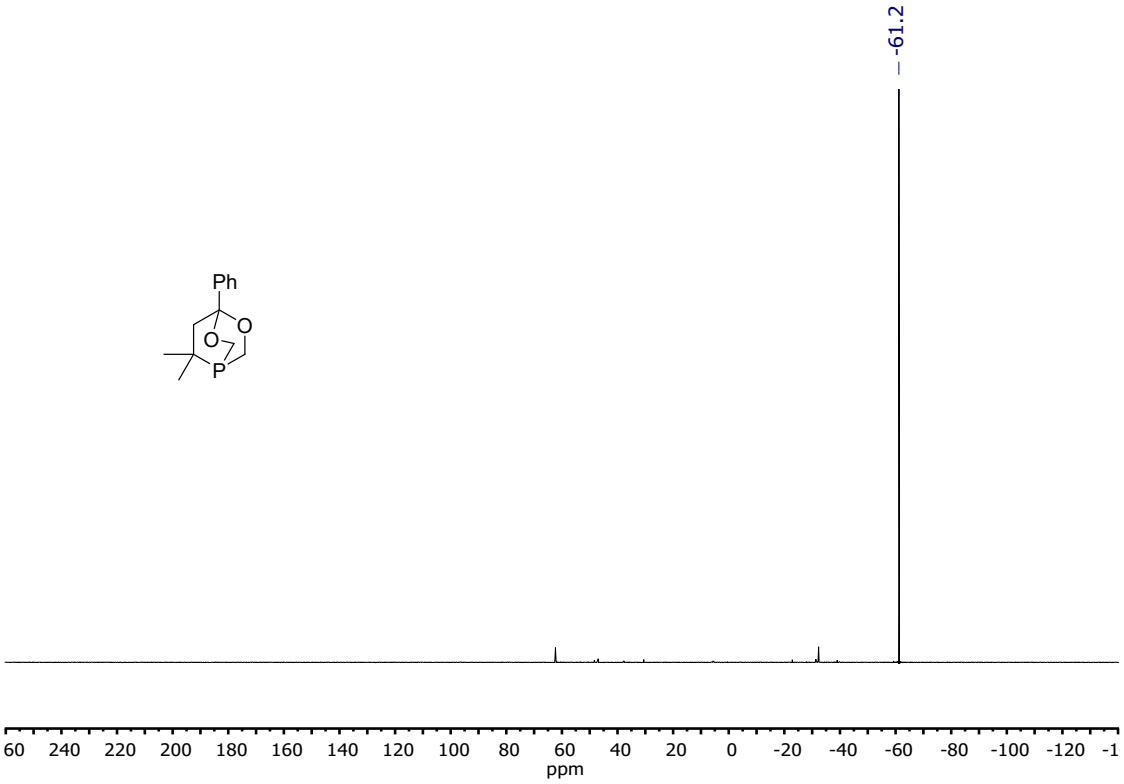

Figure S13. $^{31}P\{^{1}H\}$ NMR (162 MHz, $CDCl_3$) spectrum of **L2**, 4-phenyl-7,7-dimethyl-3,5-dioxa-1-phosphabicyclo[2.2.2]octane.

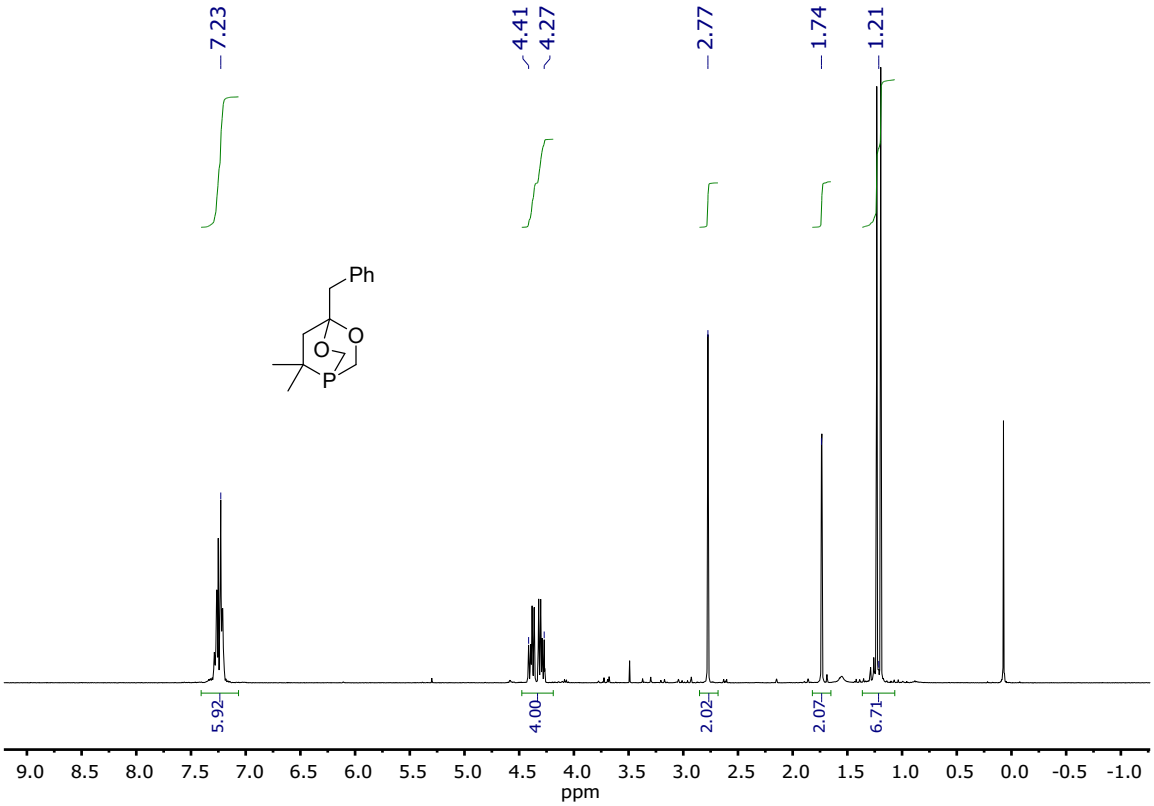

Figure S14. ^{1}H NMR (400 MHz, $CDCl_3$) spectrum of **L3**, 4-benzyl-7,7-dimethyl-3,5-dioxa-1-phosphabicyclo[2.2.2]octane.

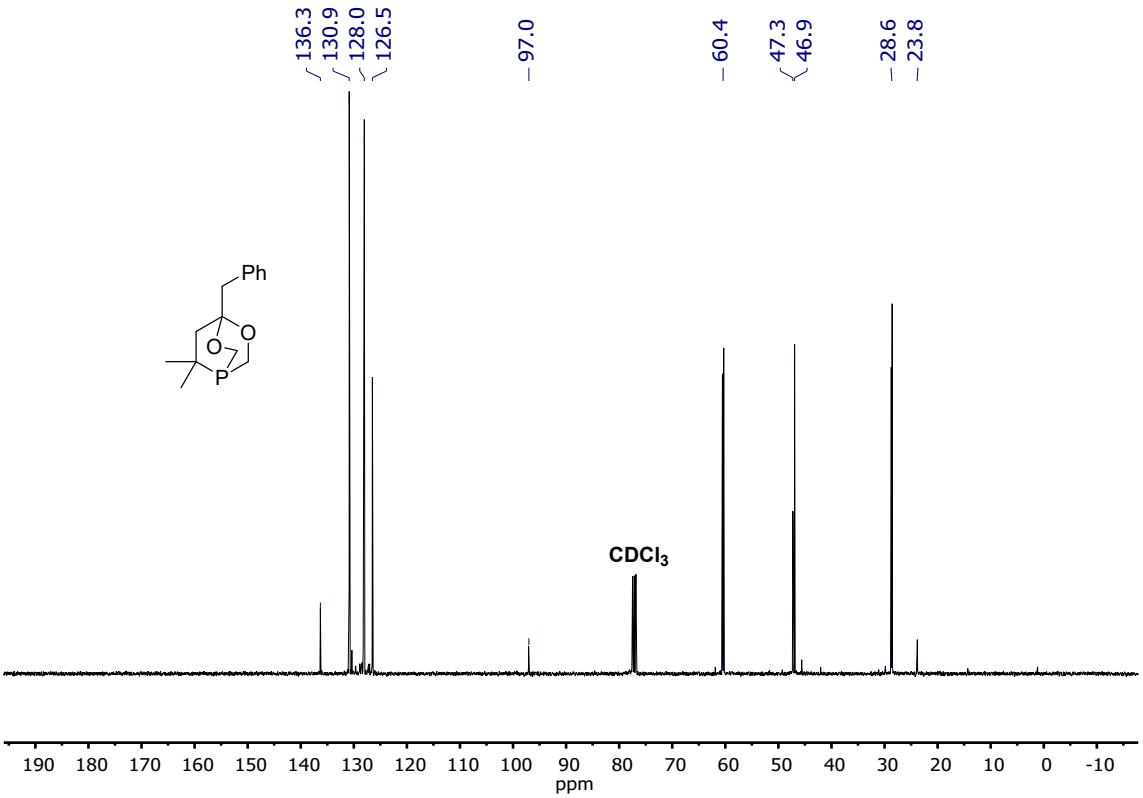

Figure S15. $^{13}C\{^{1}H\}$ NMR (101 MHz, $CDCl_3$) spectrum of **L3**, 4-benzyl-7,7-dimethyl-3,5-dioxa-1-phosphabicyclo[2.2.2]octane.

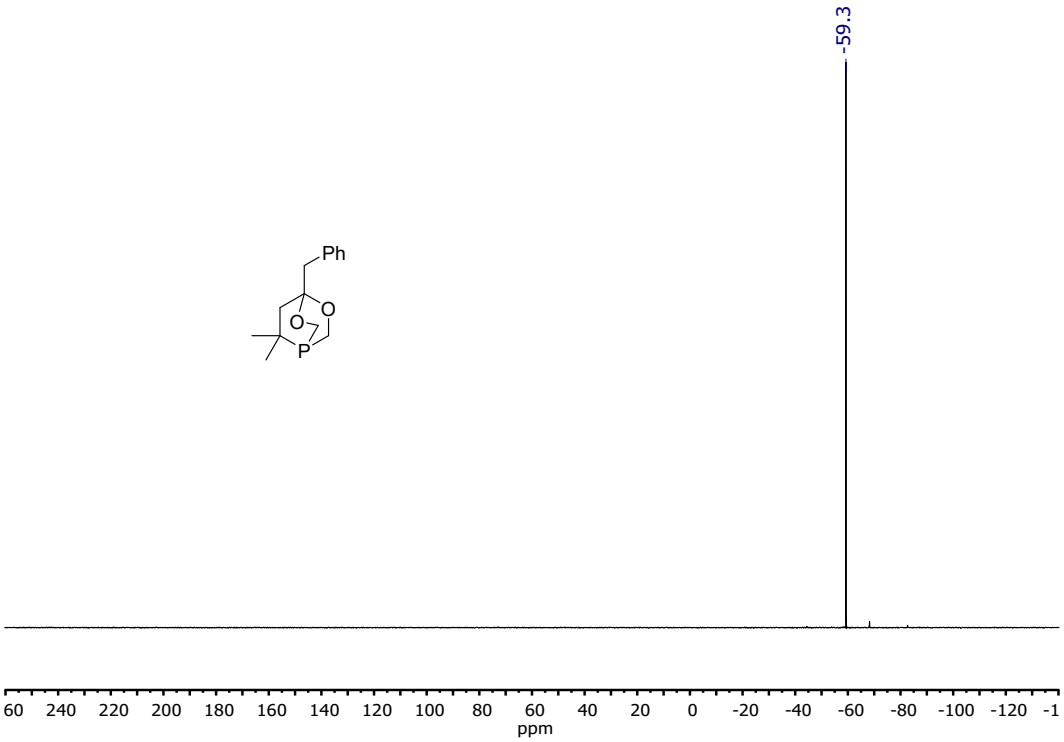

Figure S16. $^{31}P\{^{1}H\}$ NMR (162 MHz, $CDCl_3$) spectrum of **L3**, 4-benzyl-7,7-dimethyl-3,5-dioxa-1-phosphabicyclo[2.2.2]octane.

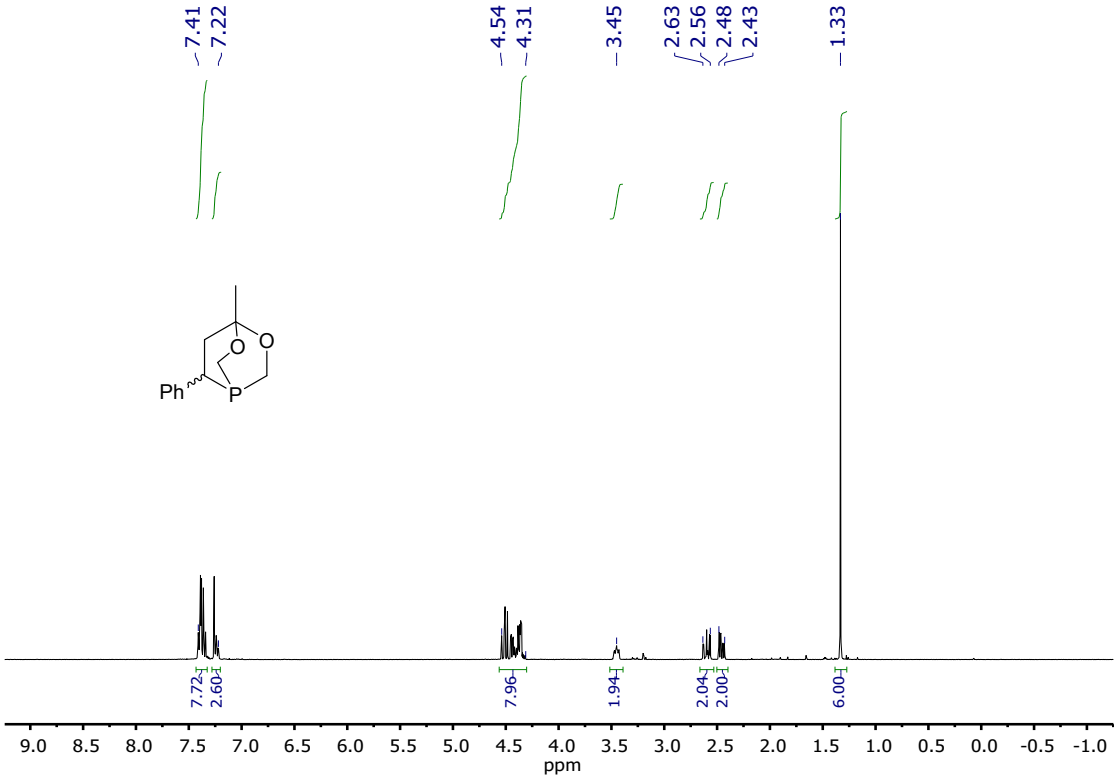

Figure S17. ^{1}H NMR (400 MHz, $CDCl_3$) spectrum of **L4**, 4-methyl-7-phenyl-3,5-dioxa-1-phosphabicyclo[2.2.2]octane.

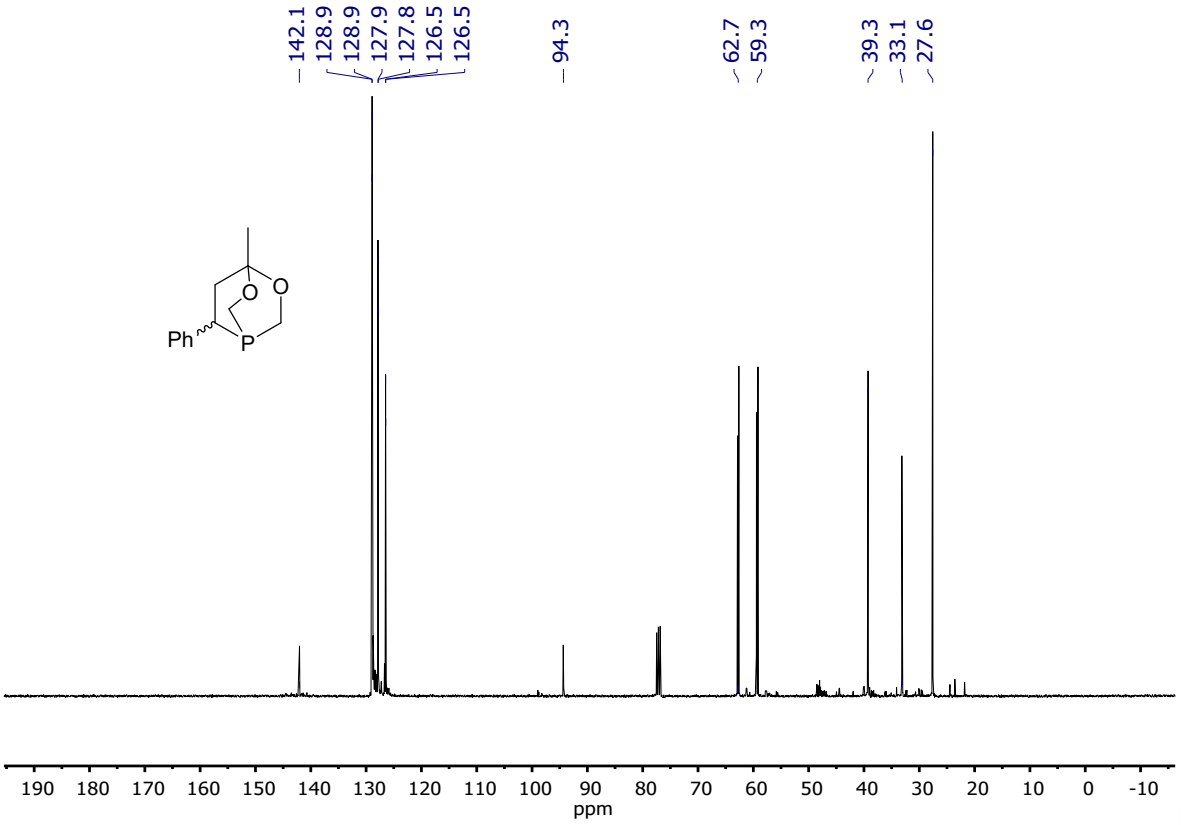

Figure S18. $^{13}C\{^{1}H\}$ NMR (101 MHz, $CDCl_3$) spectrum of **L4**, 4-methyl-7-phenyl-3,5-dioxa-phosphabicyclo[2.2.2]octane.

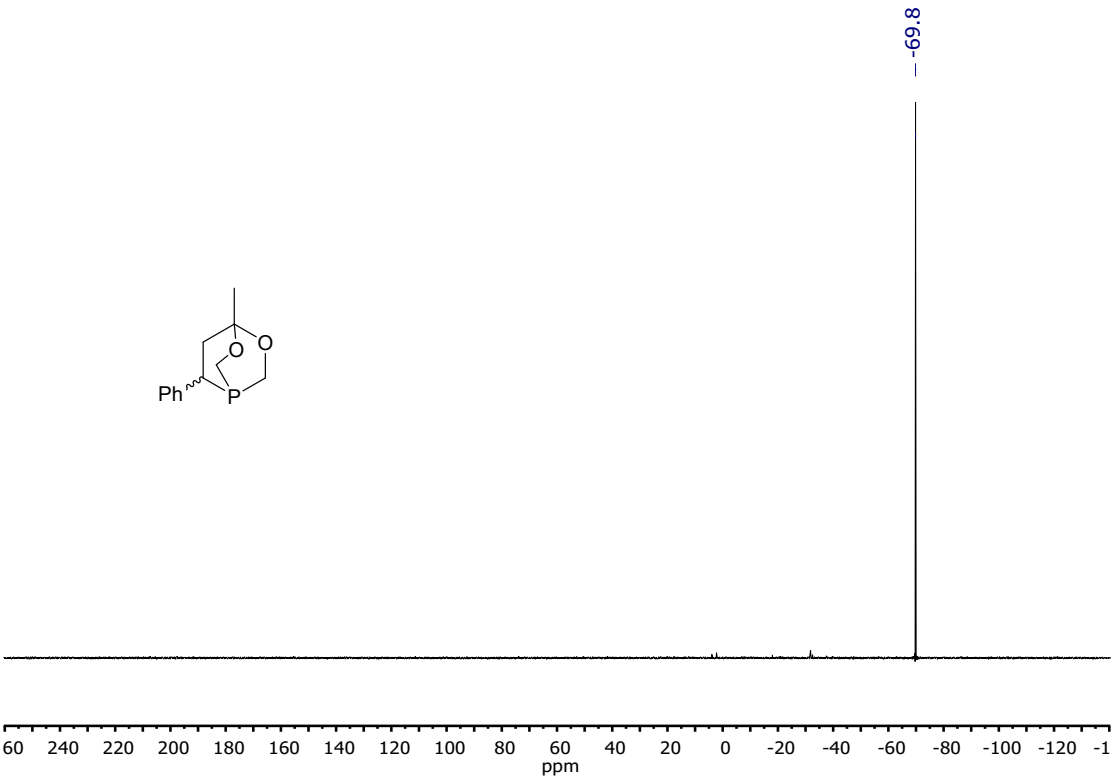

Figure S19. $^{31}P\{^{1}H\}$ NMR (162 MHz, $CDCl_3$) spectrum of **L4**, 4-methyl-7-phenyl-3,5-dioxa-1-phosphabicyclo[2.2.2]octane.

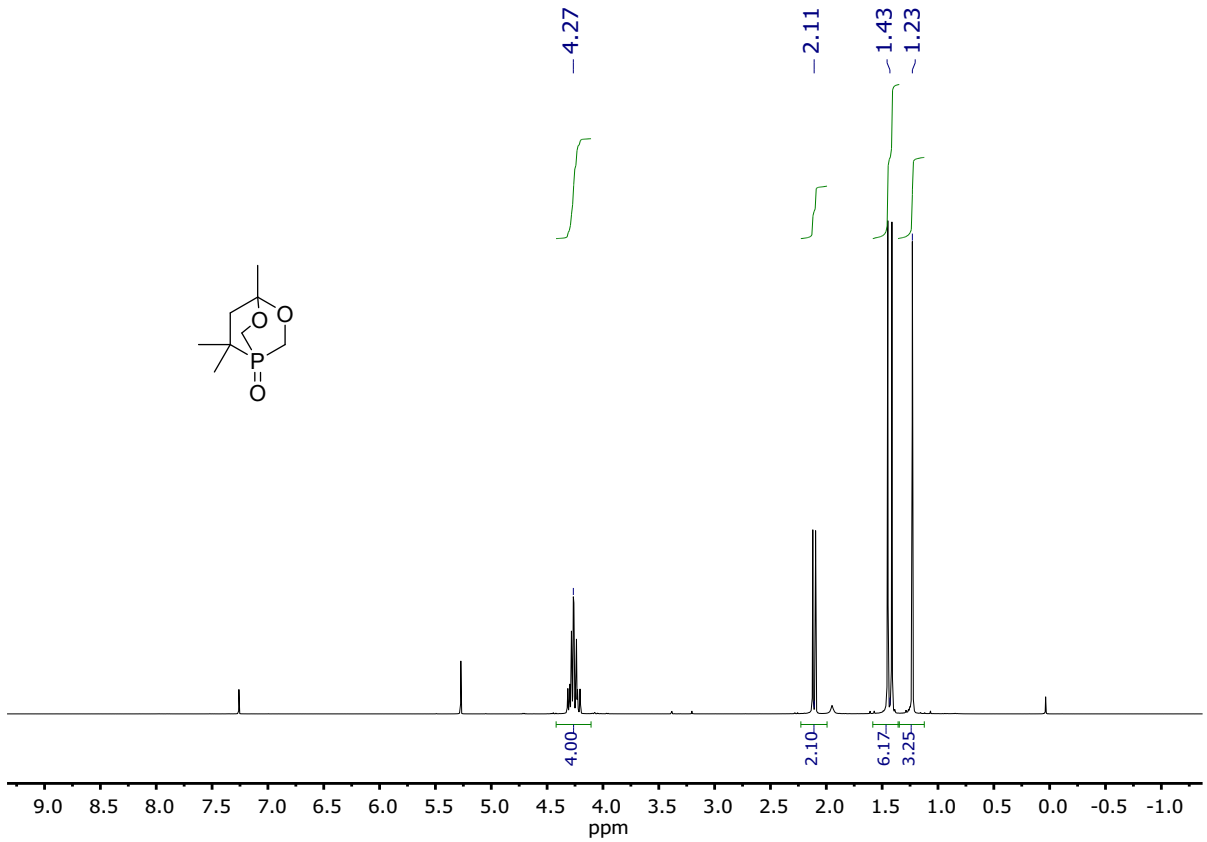

Figure S20. ^{1}H NMR (400 MHz, $CDCl_3$) spectrum of **L1(O)**, 4,7,7-trimethyl-3,5-dioxa-1-phosphabicyclo[2.2.2]octane oxide.

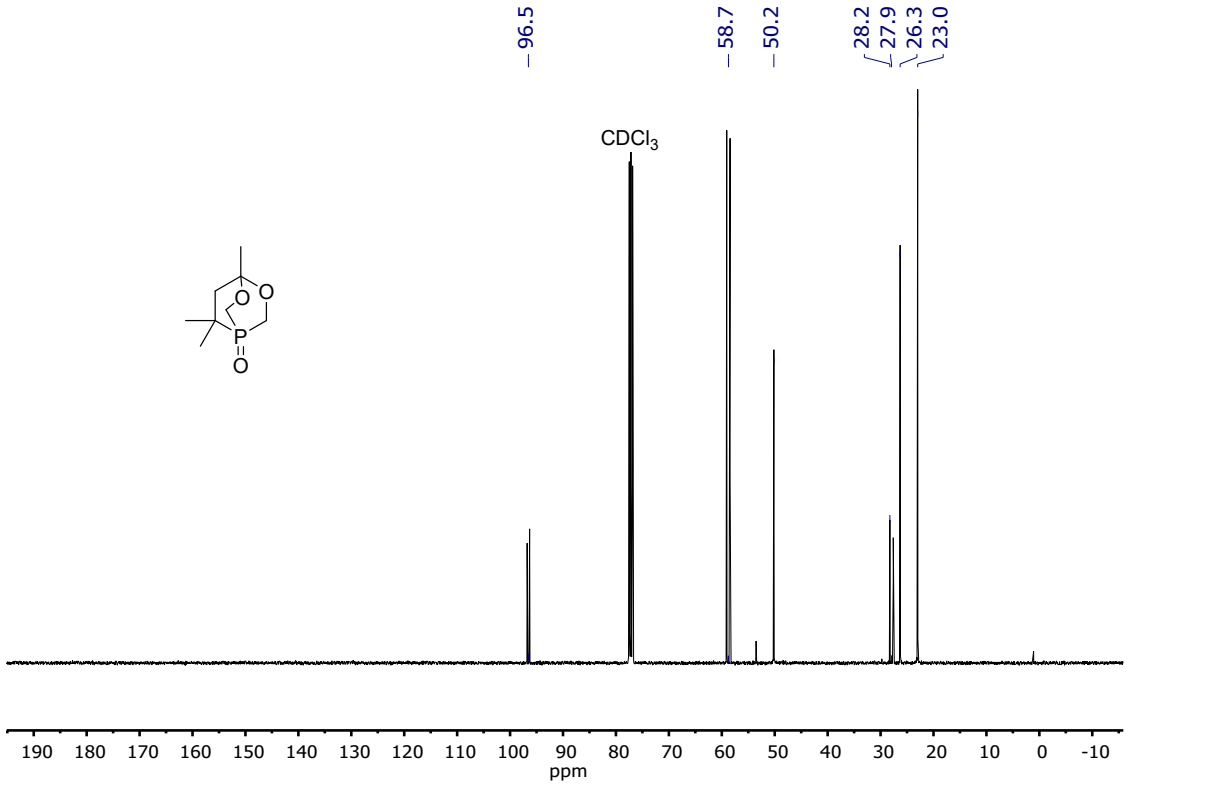

Figure S21. $^{13}C\{^{1}H\}$ NMR (101 MHz, $CDCl_3$) spectrum of **L1(O)**, 4,7,7-trimethyl-3,5-dioxa-1-phosphabicyclo[2.2.2]octane oxide.

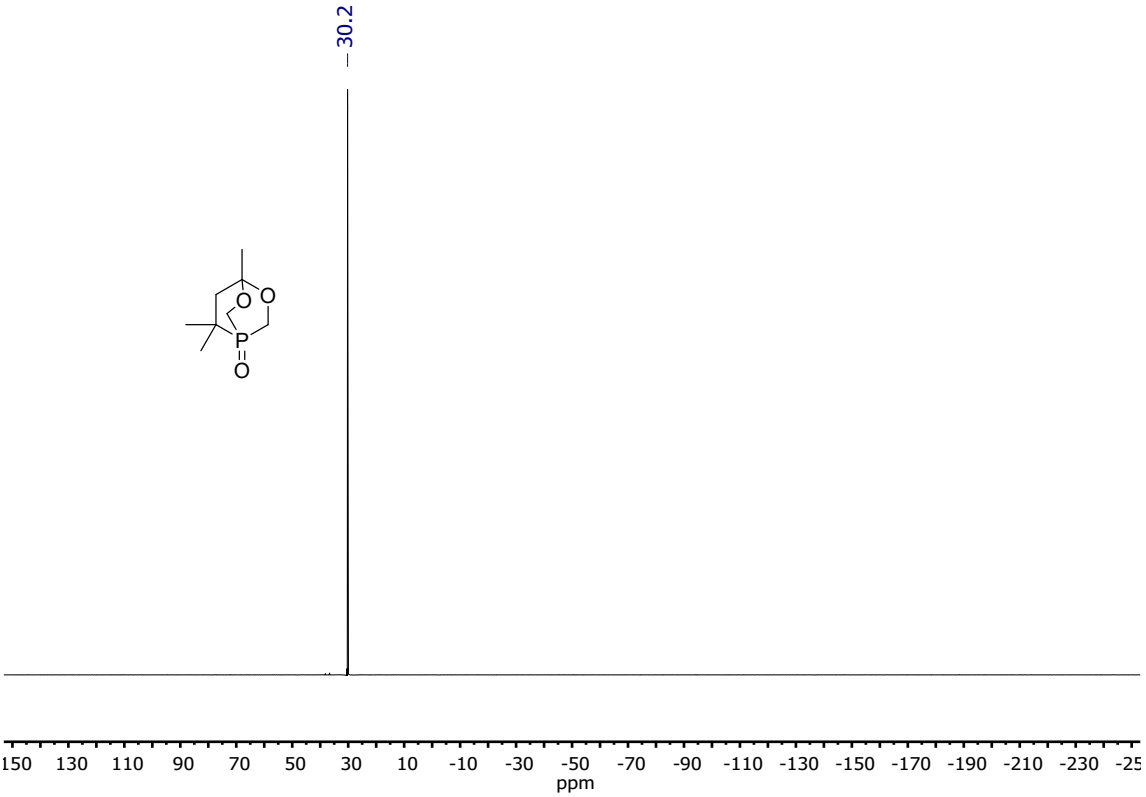

Figure S22. $^{31}P\{^{1}H\}$ NMR (162 MHz, $CDCl_3$) spectrum of **L1(O)**, 4,7,7-trimethyl-3,5-dioxa-1-phosphabicyclo[2.2.2]octane oxide.

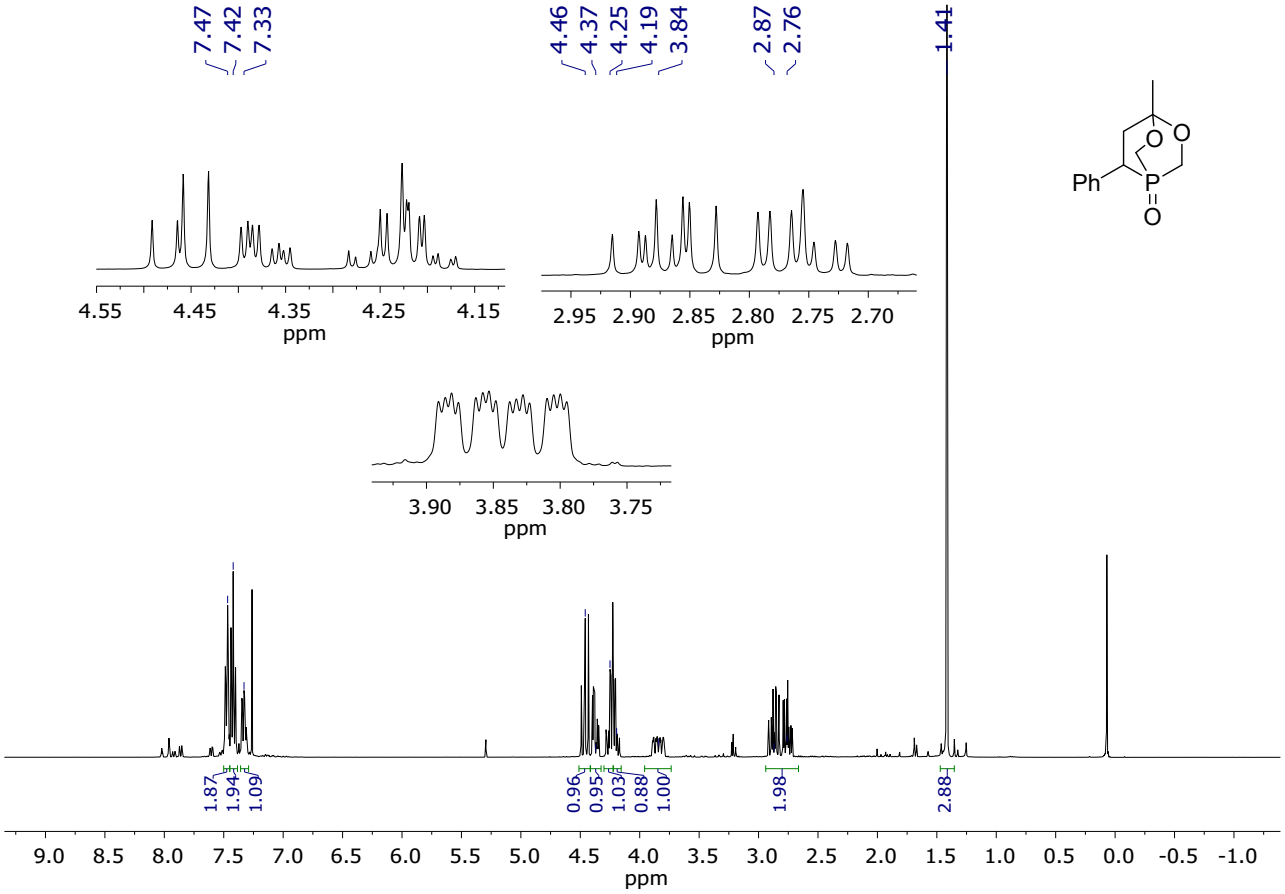

Figure S23. ^{1}H NMR (400 MHz, $CDCl_3$) spectrum of **L4(O)**, 4-methyl-7-phenyl-3,5-dioxa-1-phosphabicyclo[2.2.2]octane oxide.

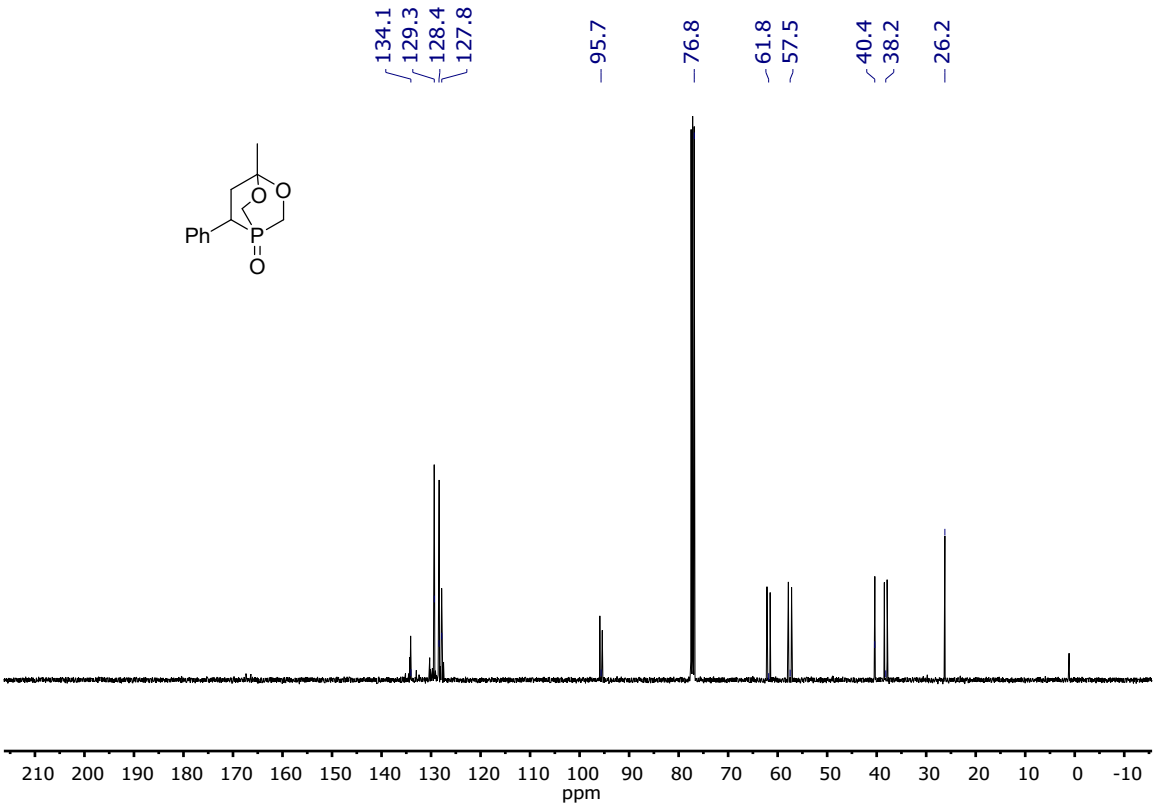

Figure S24. $^{13}C\{^{1}H\}$ NMR (101 MHz, $CDCl_3$) spectrum of **L4(O)**, 4-methyl-7-phenyl-3,5-dioxa-1-phosphabicyclo[2.2.2]octane oxide.

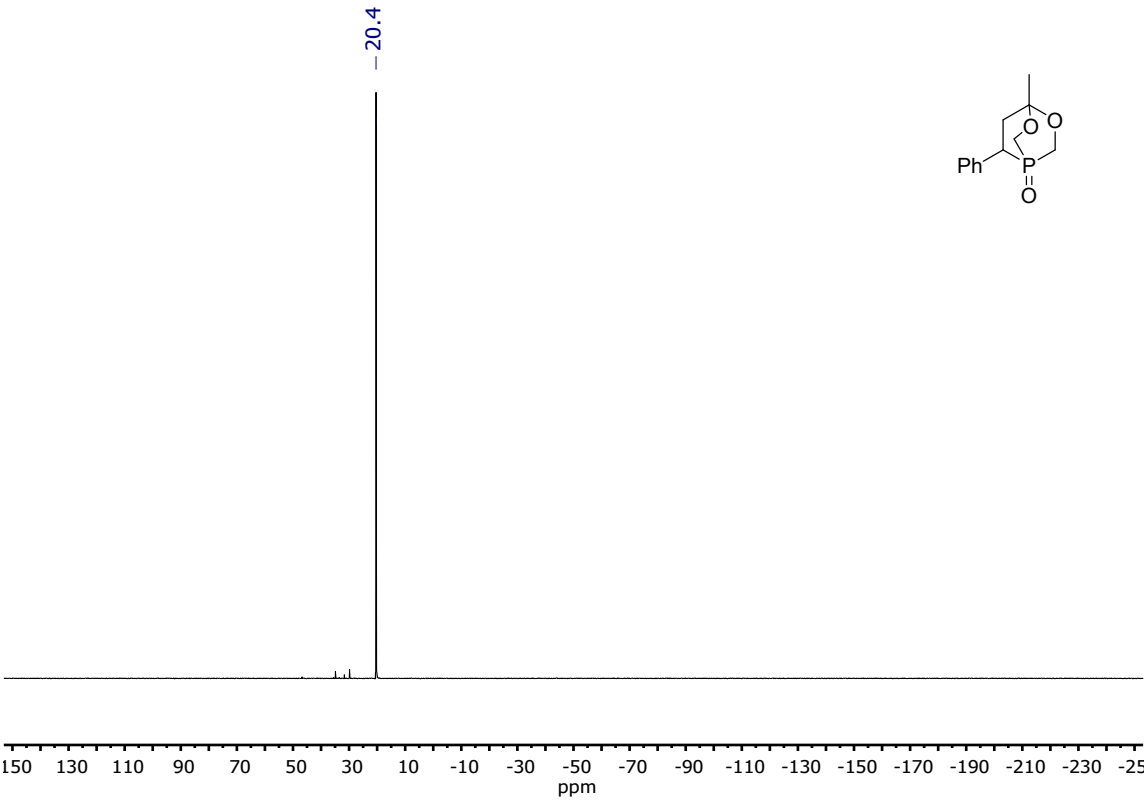

Figure S25. $^{31}P\{^{1}H\}$ NMR (162 MHz, $CDCl_3$) spectrum of **L4(O)**, 4-methyl-7-phenyl-3,5-dioxa-1-phosphabicyclo[2.2.2]octane oxide.

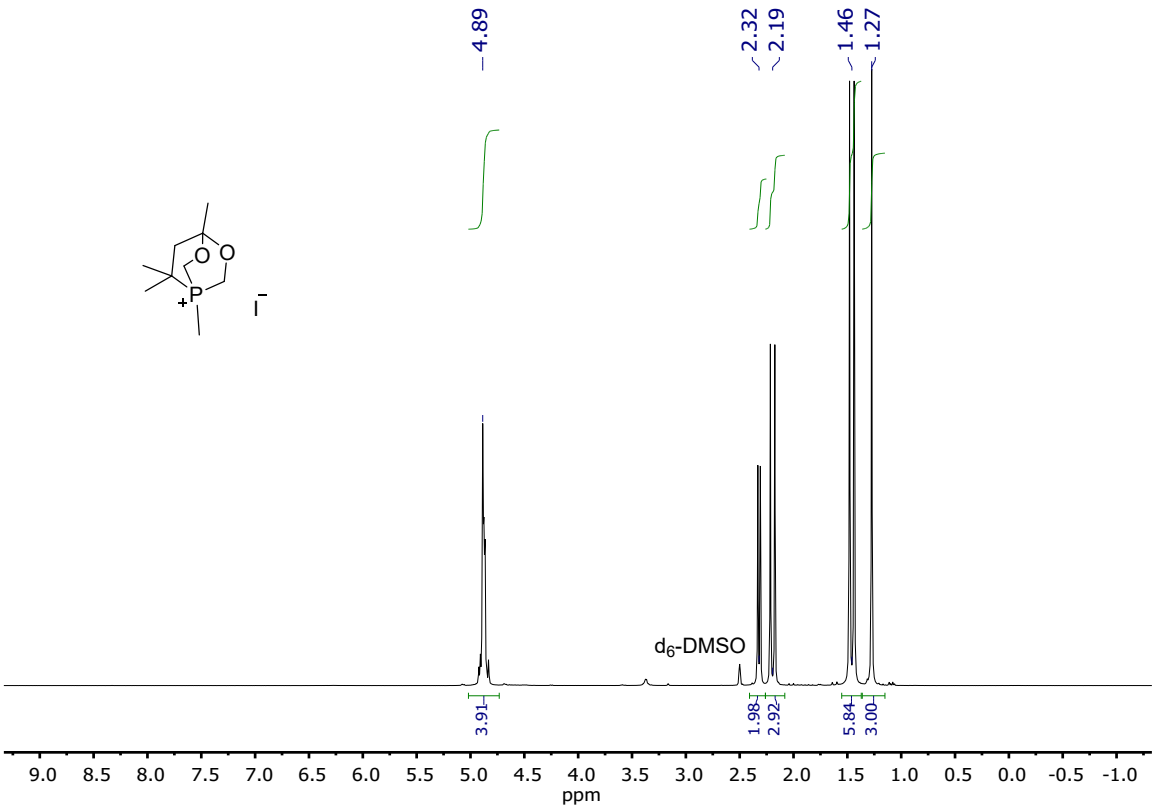

Figure S26. ^{1}H NMR (400 MHz, d_6-DMSO) spectrum of **[MeL1]$^{+}$I^{-}**, 1,4,7,7-tetramethyl-3,5-dioxa-1-phosphabicyclo[2.2.2]octan-1-ium iodide.

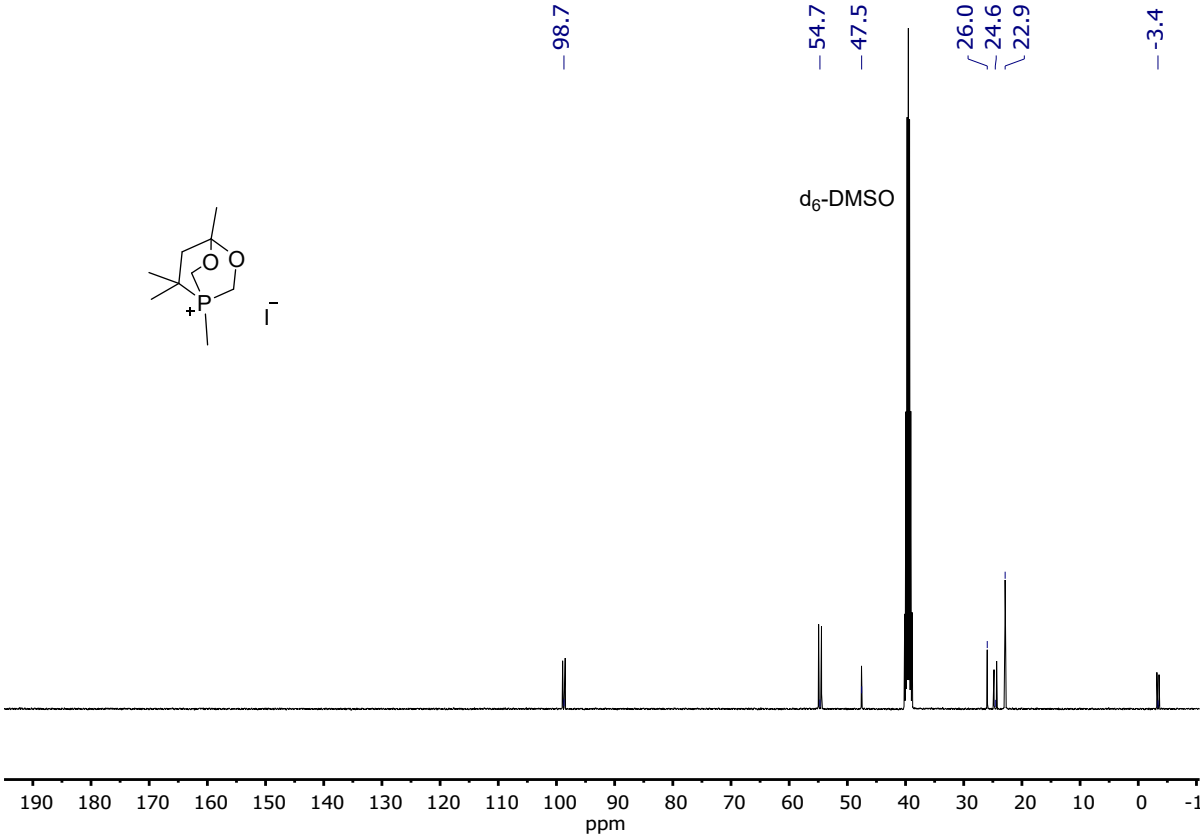

Figure S27. ^{13}C{^{1}H} NMR (101 MHz, d_6-DMSO) spectrum **[MeL1]$^{+}$I^{-}**, 1,4,7,7-tetramethyl-3,5-dioxa-1-phosphabicyclo[2.2.2]octan-1-ium iodide.

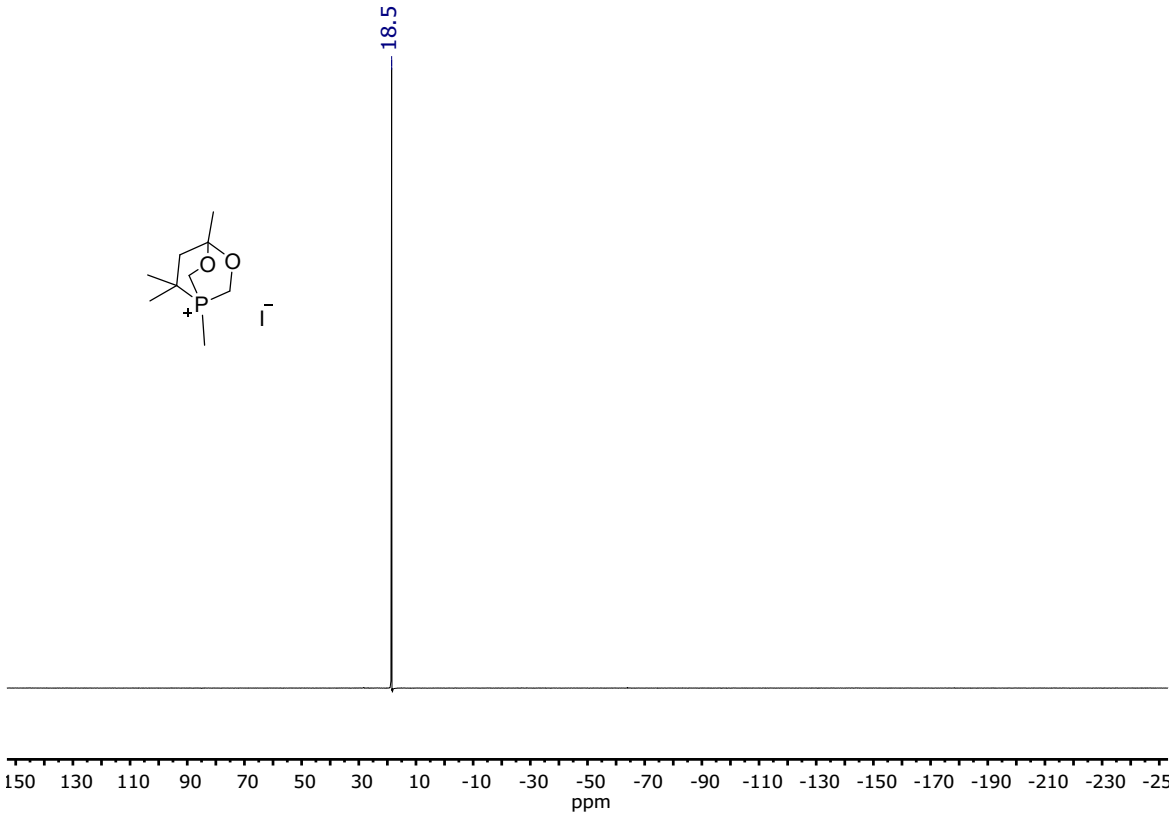

Figure S28. $^{31}P\{^{1}H\}$ NMR (162 MHz, d_6-DMSO) spectrum **[MeL1]$^{+}$I^{-}**, 1,4,7,7-tetramethyl-3,5-dioxa-1-phosphabicyclo[2.2.2]octan-1-ium iodide.

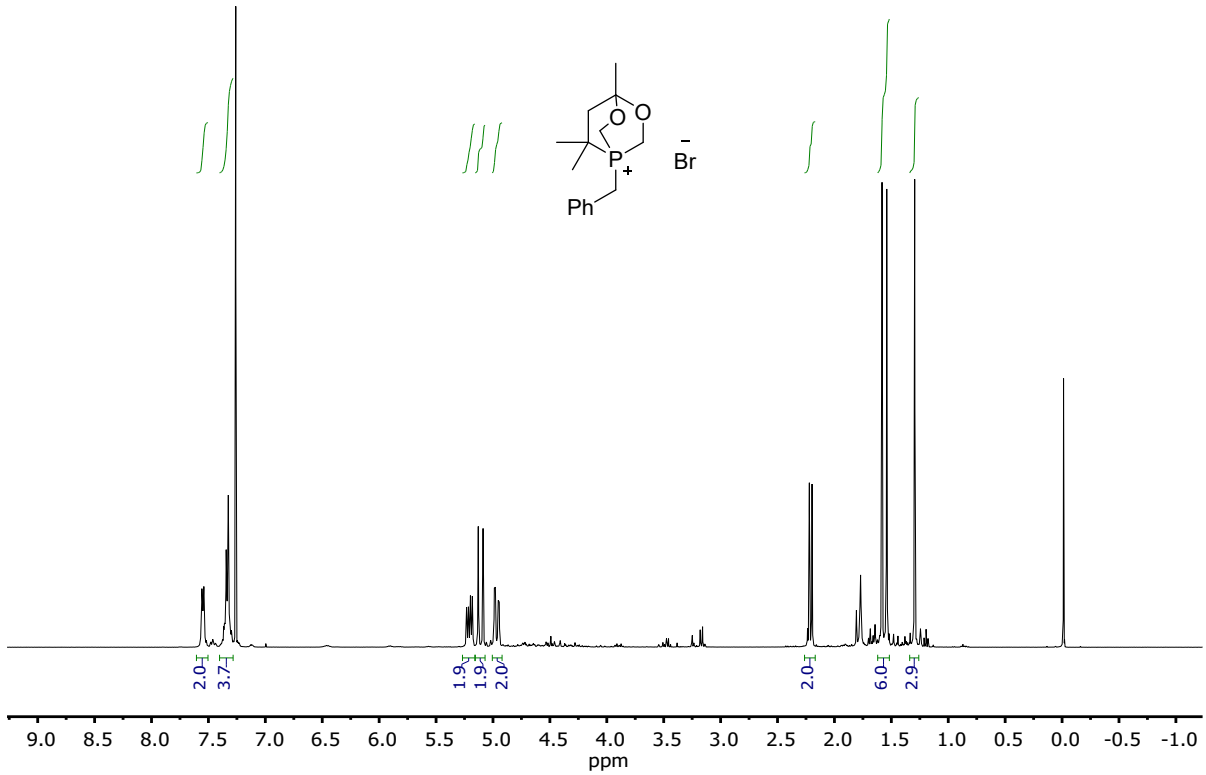

Figure S29. ^{1}H NMR (400 MHz, $CDCl_3$) spectrum of **[BnL1]$^{+}$Br^{-}**.

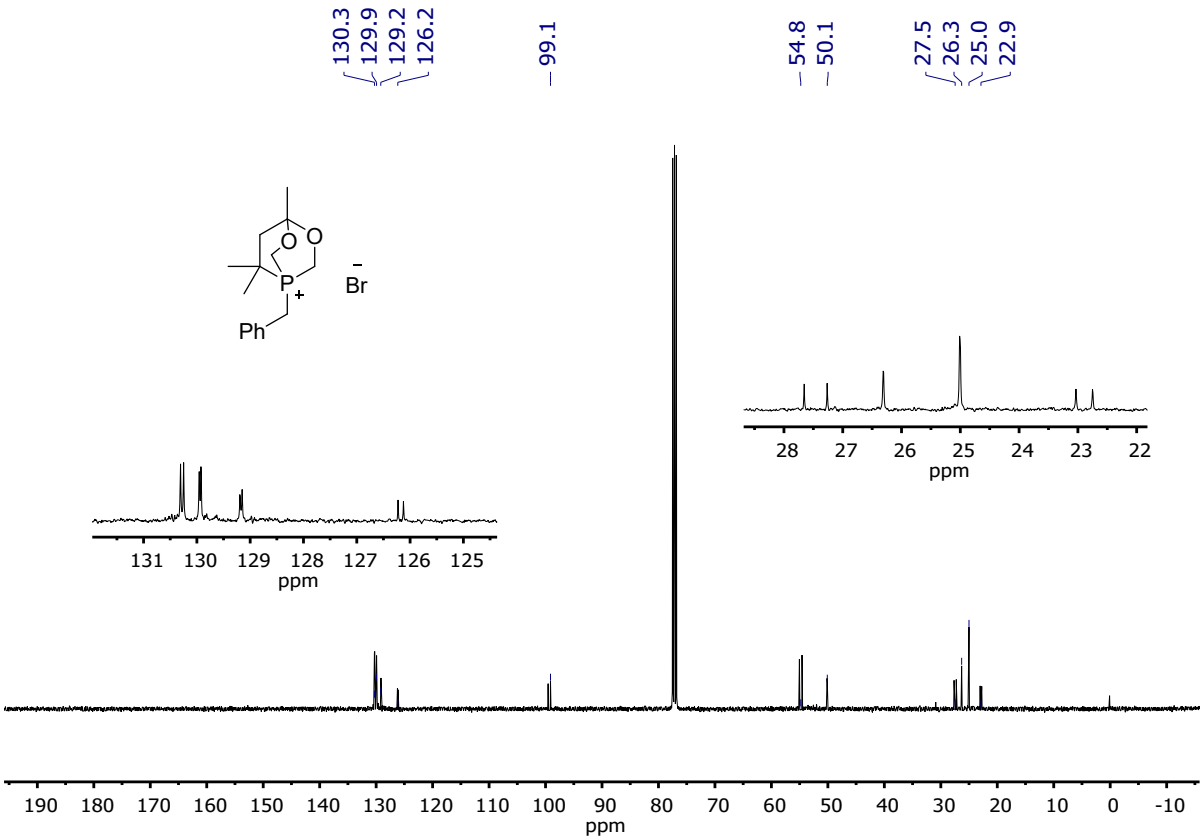

Figure S30. $^{13}C\{^{1}H\}$ NMR (101 MHz, $CDCl_3$) spectrum of **[BnL1]$^{+}$Br^{-}**.

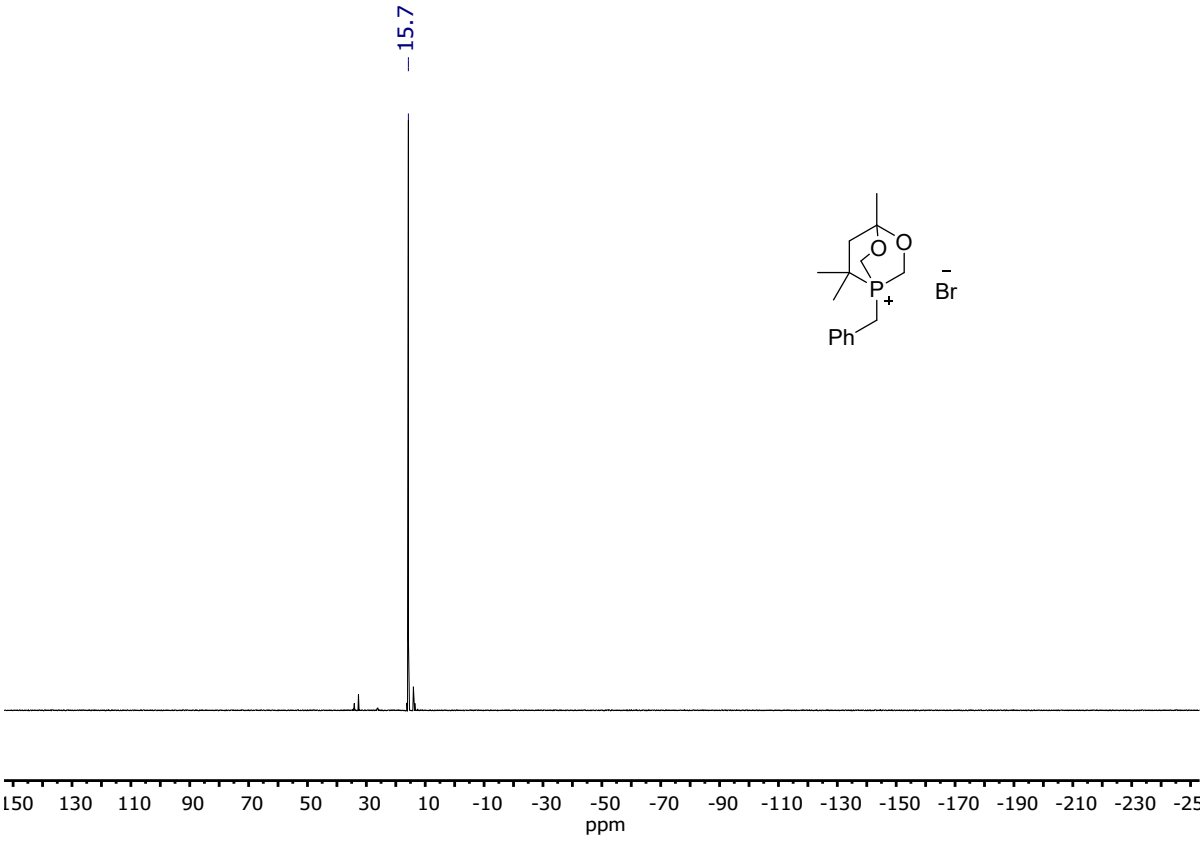

Figure S31. $^{31}P\{^{1}H\}$ NMR (162 MHz, $CDCl_3$) spectrum of **[BnL1]$^{+}$Br^{-}**.

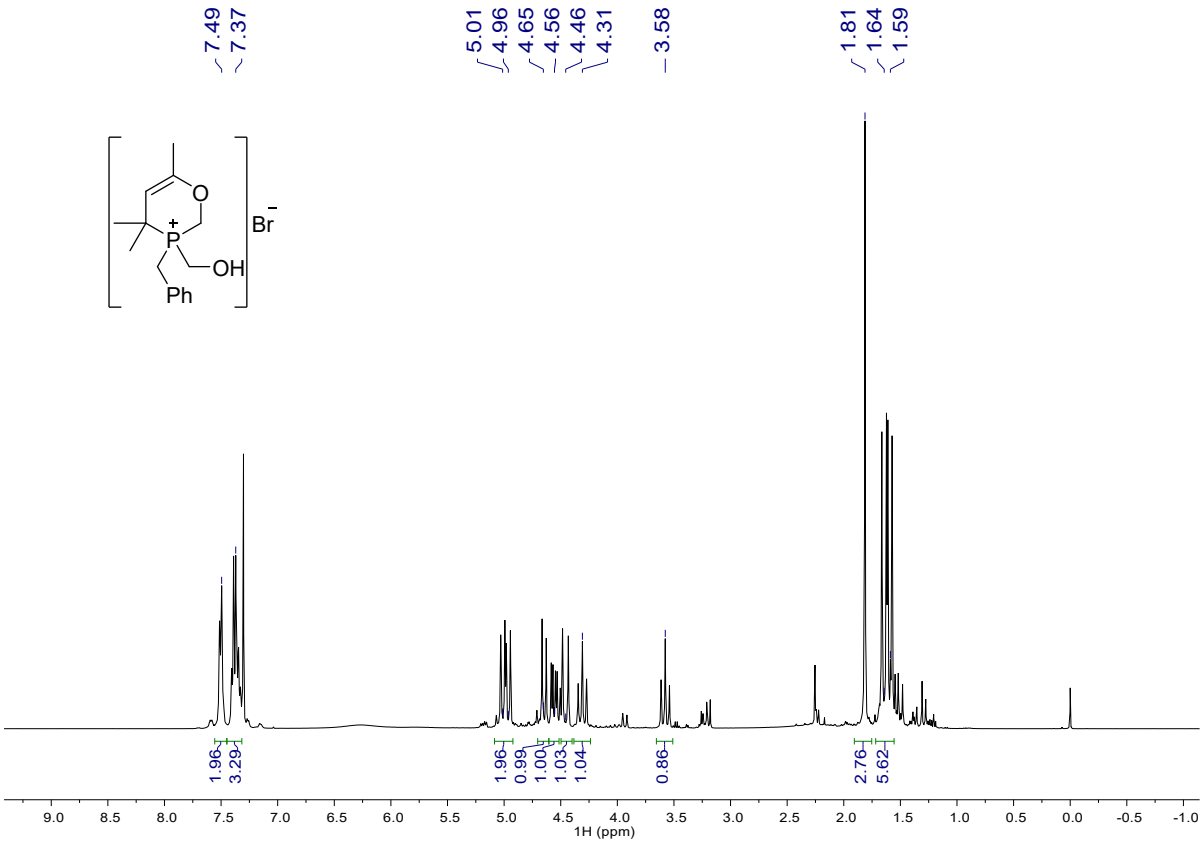

Figure S32. ^{1}H NMR (400 MHz, $CDCl_3$) spectrum of **D1**.

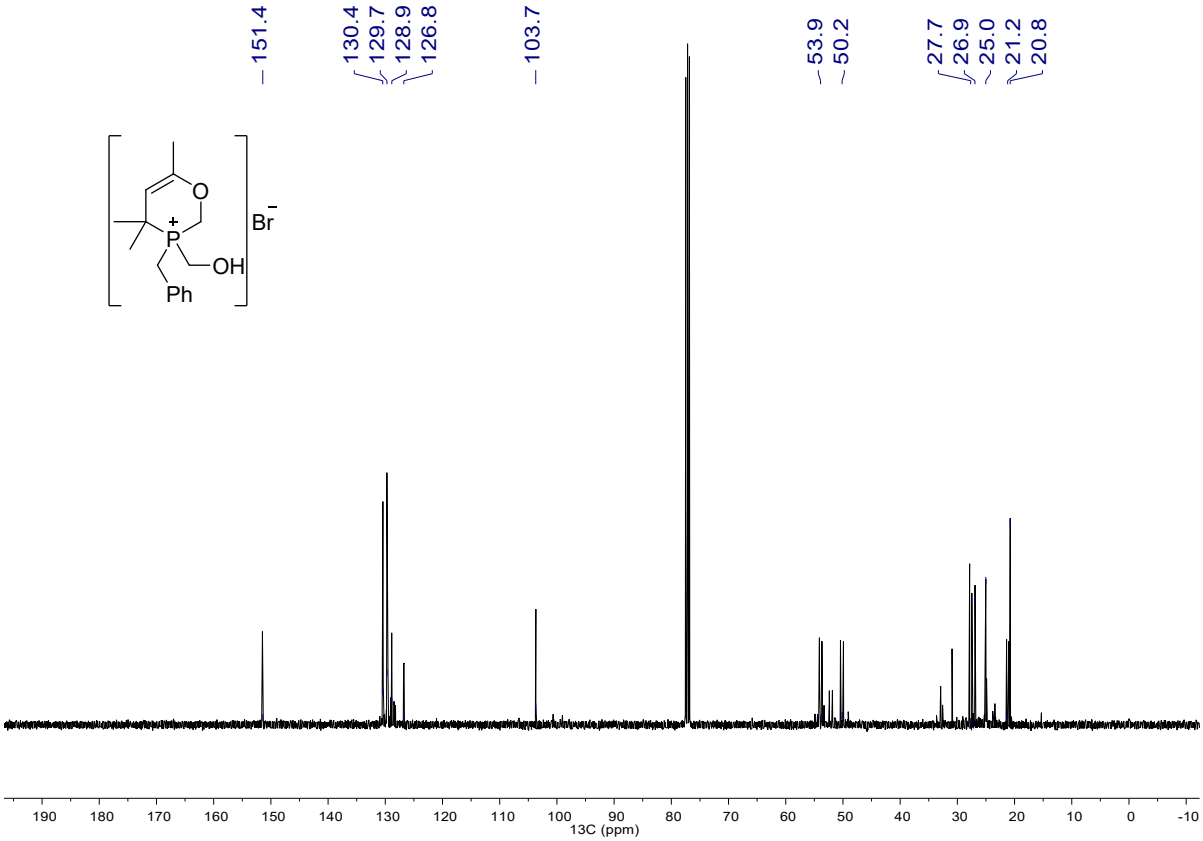

Figure S33. $^{13}C\{^{1}H\}$ NMR (101 MHz, $CDCl_3$) spectrum of **D1**.

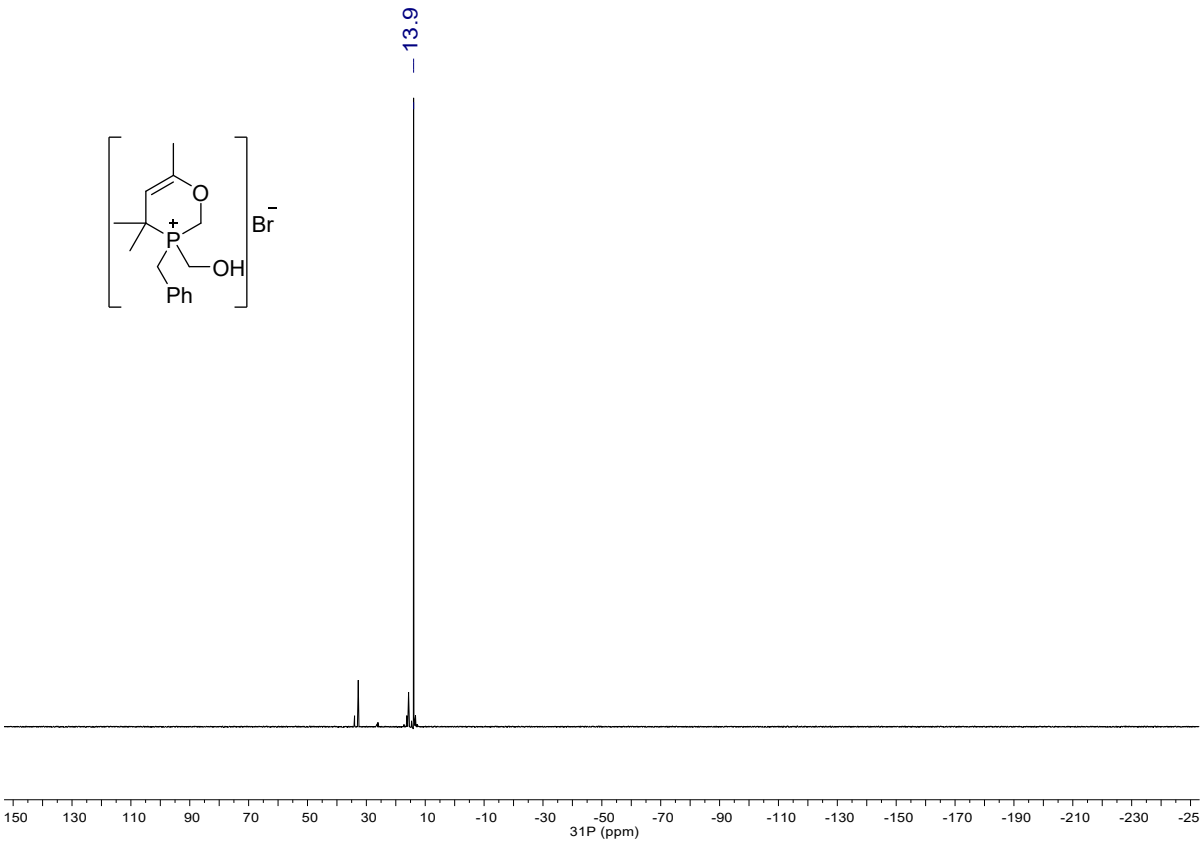

Figure S34. $^{31}P\{^{1}H\}$ NMR (162 MHz, $CDCl_3$) spectrum of **D1**.

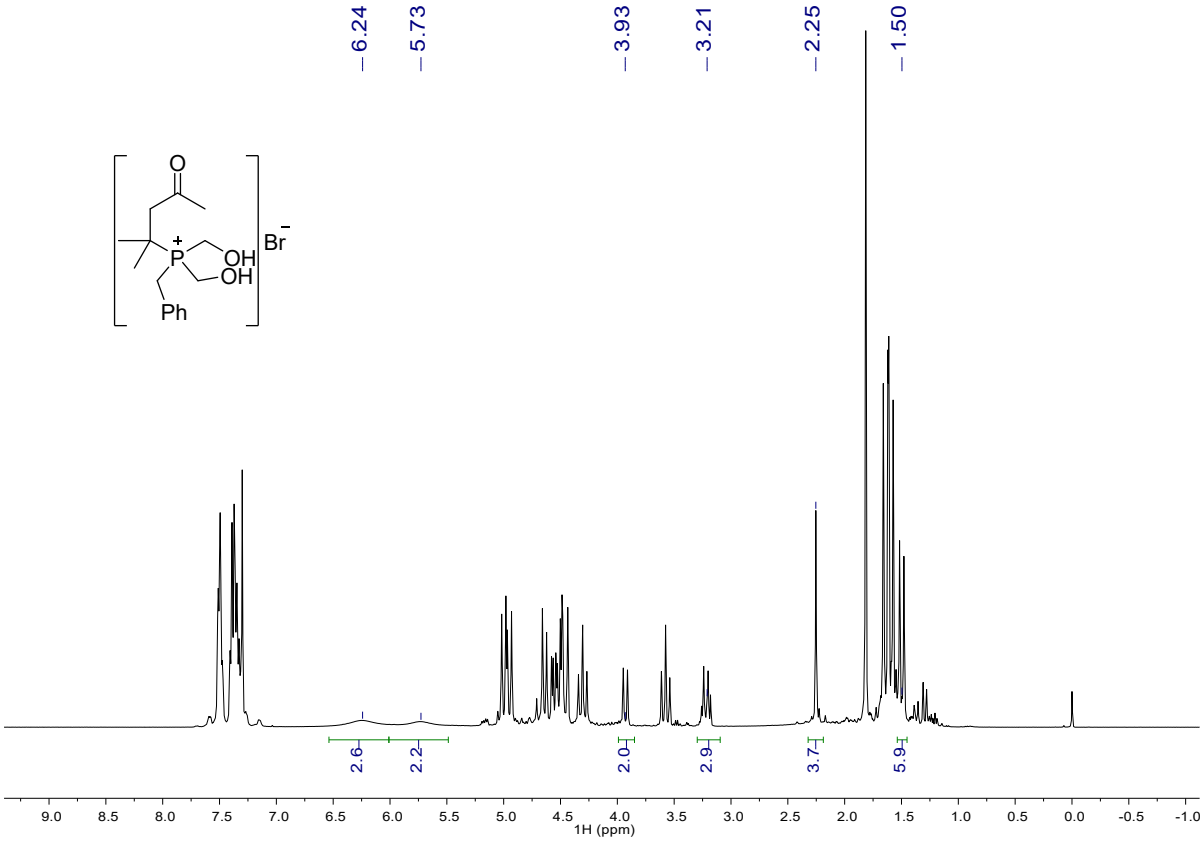

Figure S35. ^{1}H NMR (400 MHz, $CDCl_3$) spectrum of **D2**, (note: **D2** is the minor product).

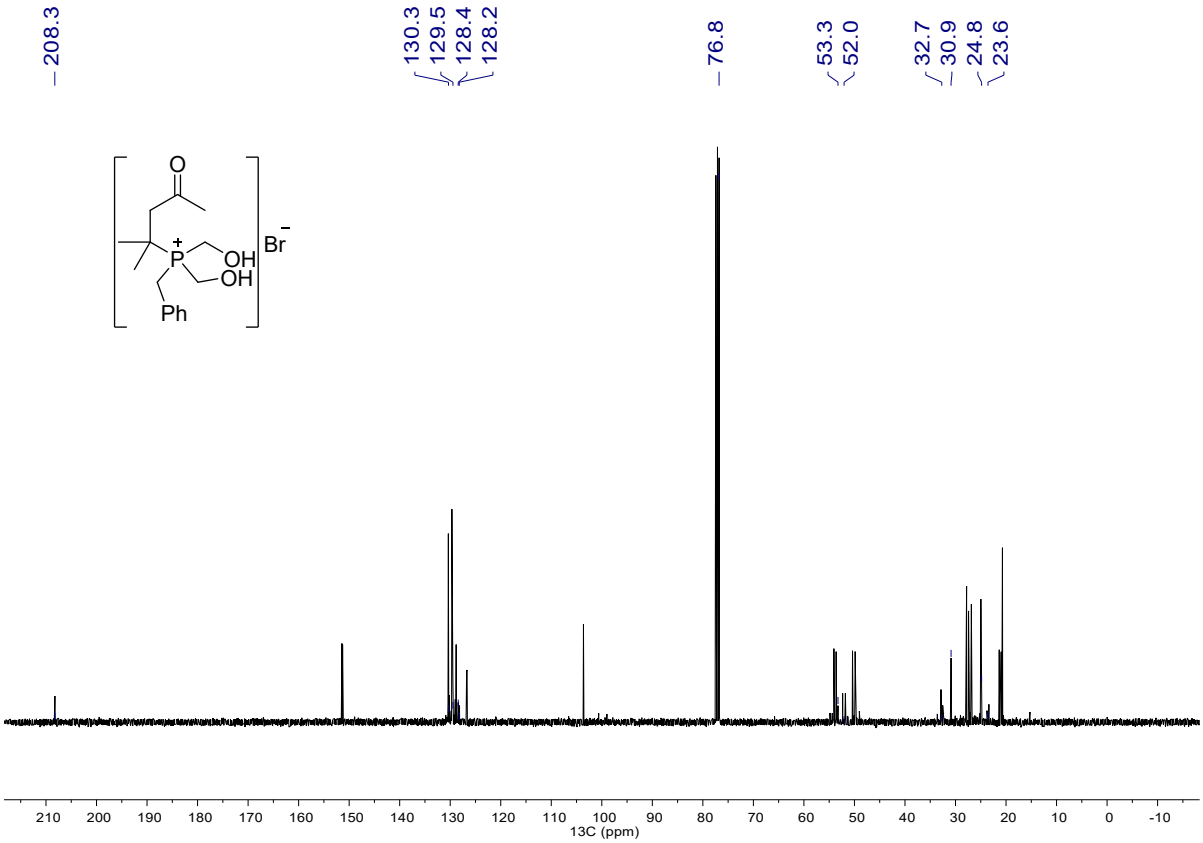

Figure S36. $^{13}C\{^{1}H\}$ NMR (101 MHz, $CDCl_3$) spectrum of **D2**, (note: **D2** is the minor product).

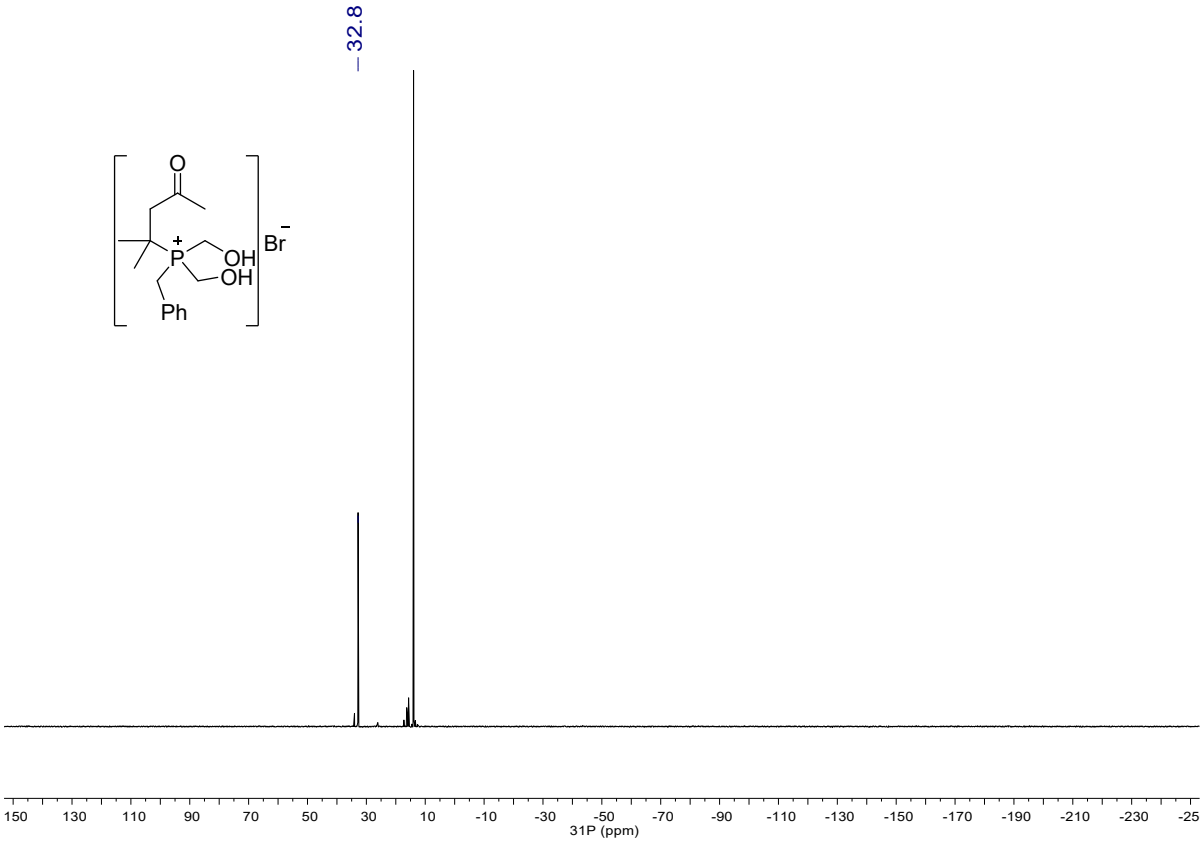

Figure S37. $^{31}P\{^{1}H\}$ NMR (162 MHz, $CDCl_3$) spectrum of **D2**, (note: **D2** is the minor product).

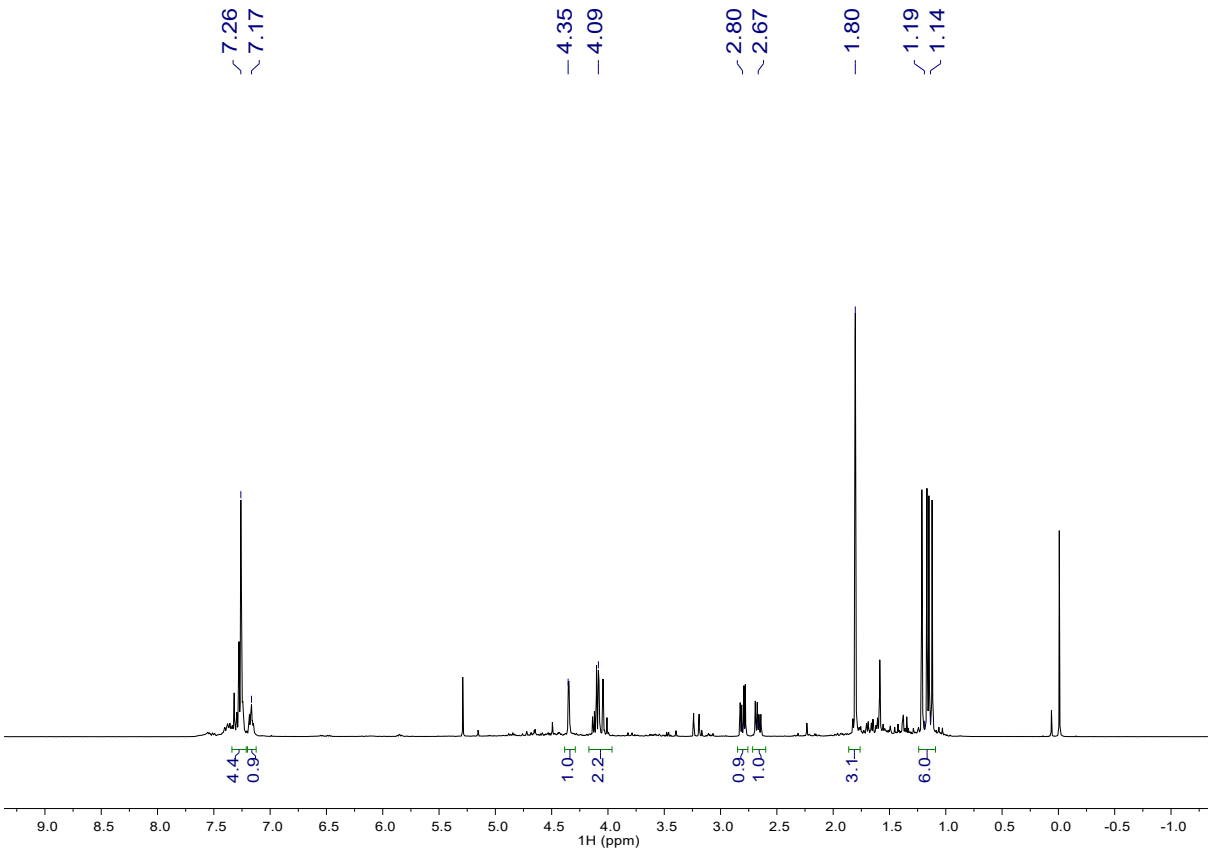

Figure S38. ^{1}H NMR (400 MHz, $CDCl_3$) spectrum of **D3**.

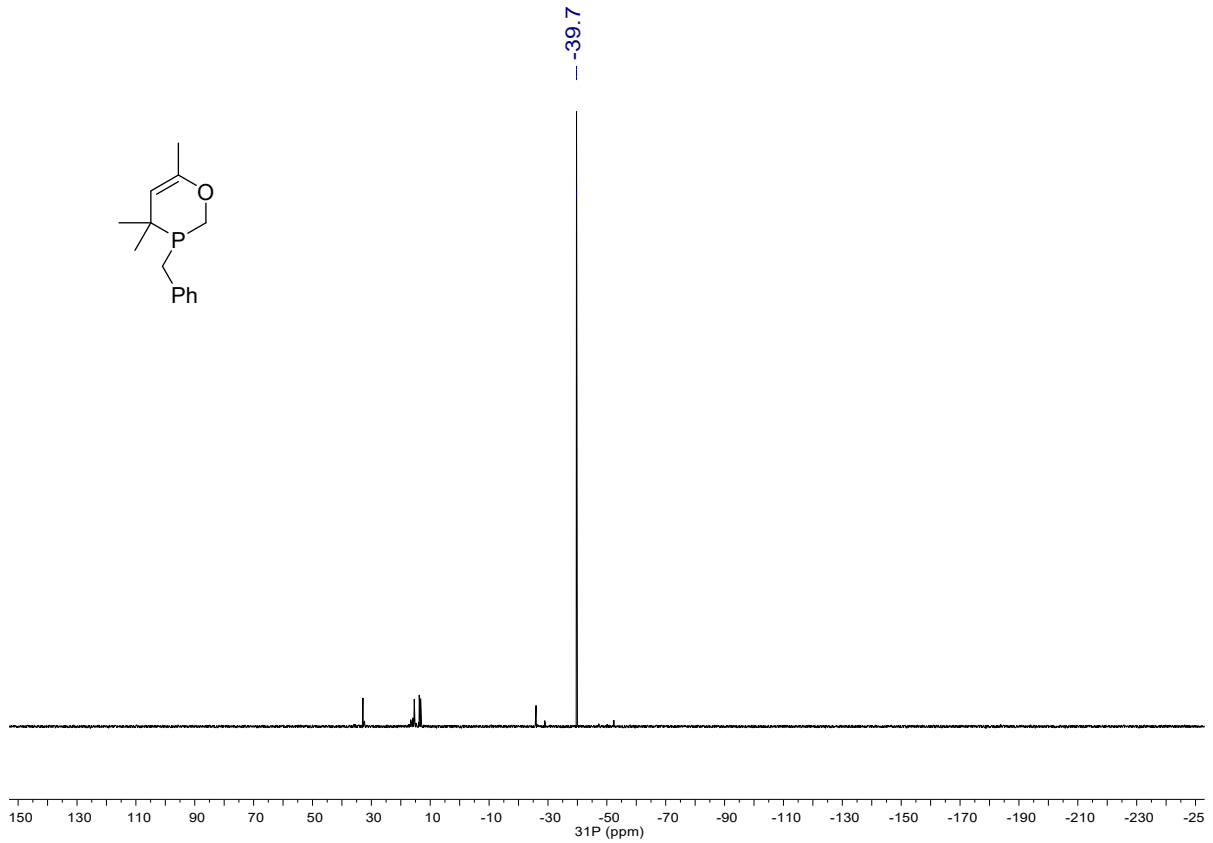

Figure S39. $^{31}P\{^{1}H\}$ NMR (162 MHz, $CDCl_3$) spectrum of **D3**.

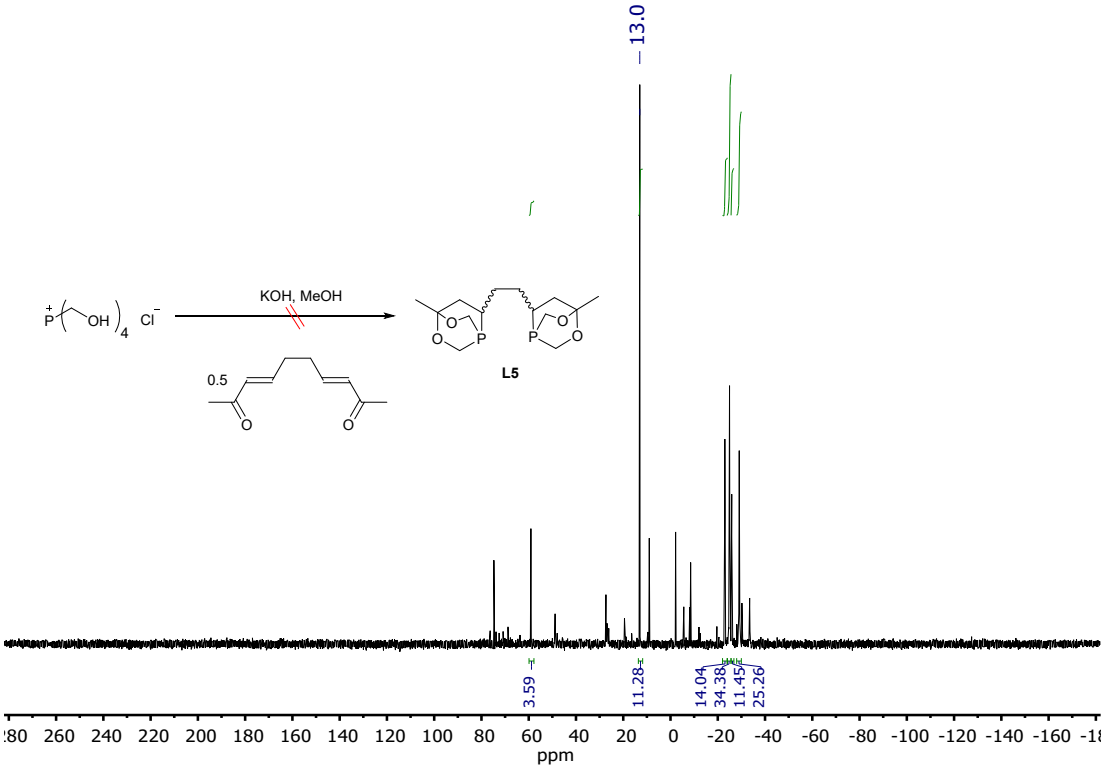

Figure S40. $^{31}P\{^{1}H\}$ NMR (162 MHz, $CDCl_3$) spectrum of the reaction between $[P(CH_2OH)_4]Cl$ and ethylene-*bis*-enone which gave a mixture of products with no signals consistent with **L5**.

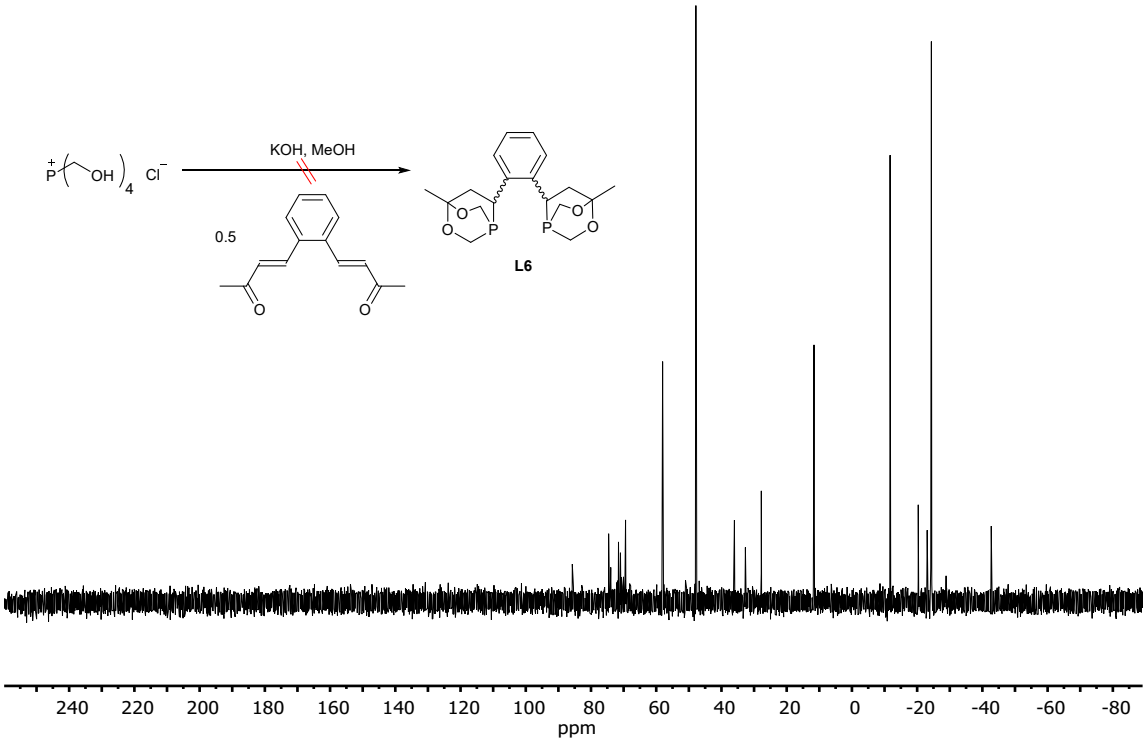

Figure S41. $^{31}P\{^{1}H\}$ NMR (162 MHz, $CDCl_3$) spectrum of the reaction between $[P(CH_2OH)_4]Cl$ and ortho-phenylene-*bis*-enone, gave a mixture of products with no signals consistent with **L6**.

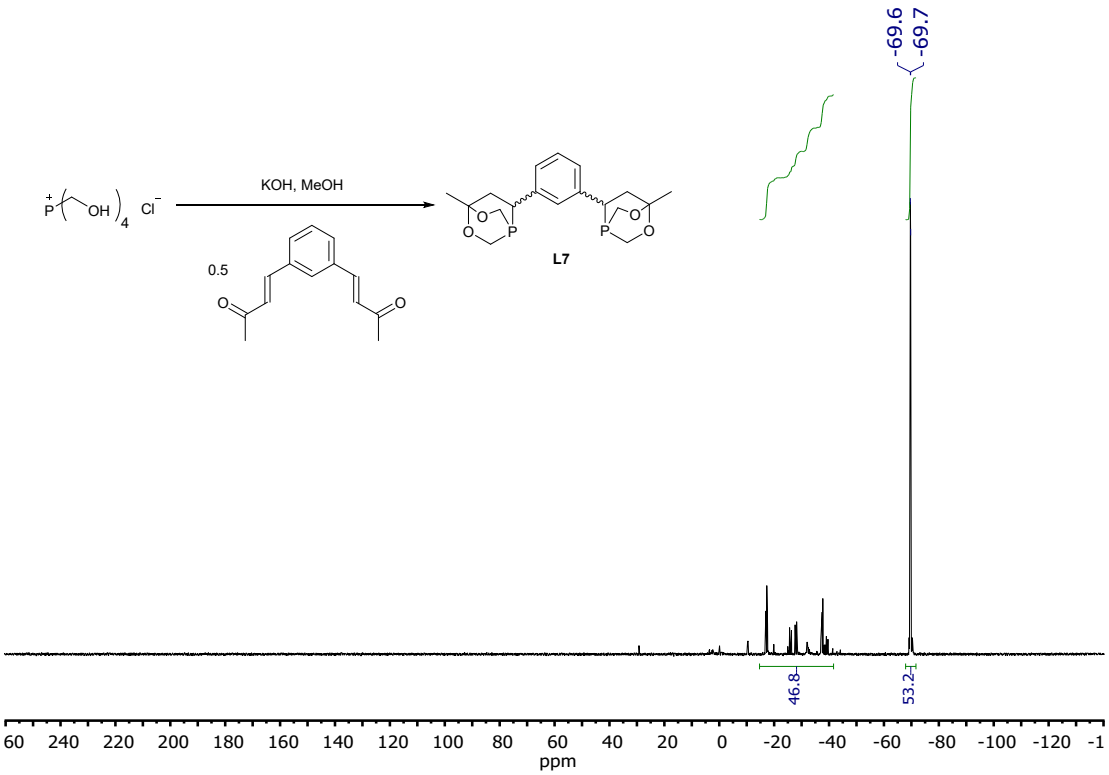

Figure S42. $^{31}P\{^{1}H\}$ NMR (162 MHz, $CDCl_3$) spectrum of the reaction between $[P(CH_2OH)_4]Cl$ and meta-phenylene-*bis*-enone gave a mixture of products with the major product (−69.6 and −69.7 ppm) consistent with **L7**.

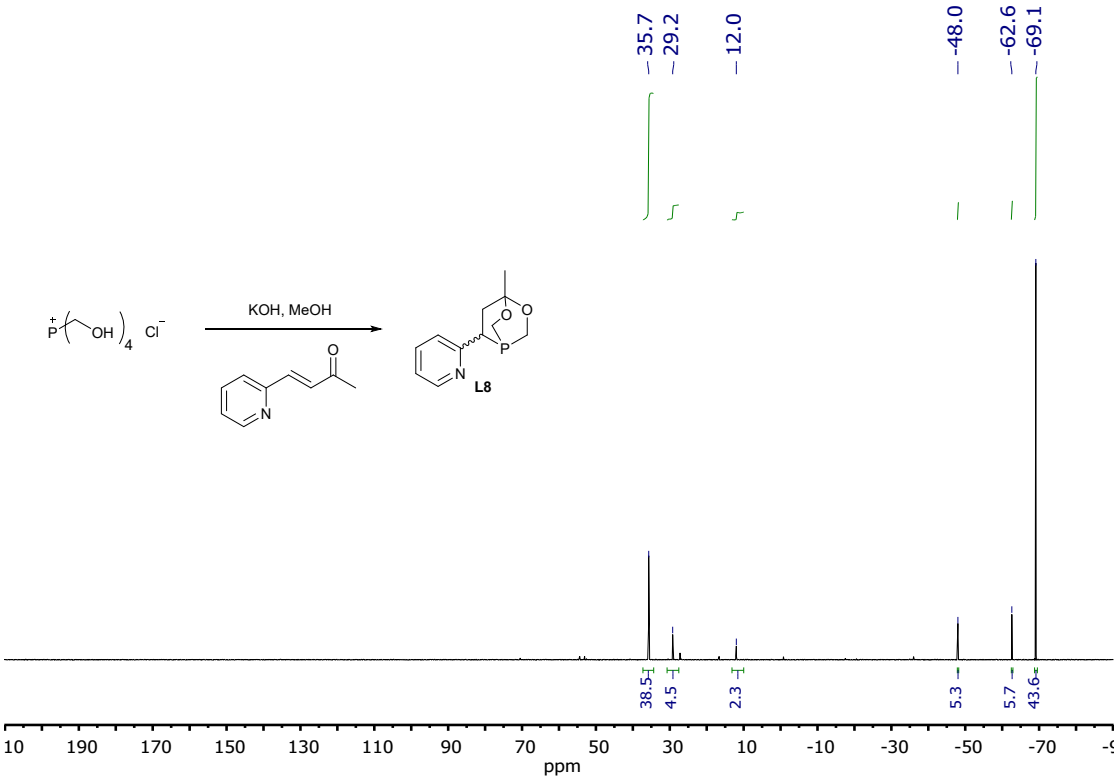

Figure S43. ^{31}P NMR (162 MHz, $CDCl_3$) spectrum of the crude mixture obtained from the reaction between $[P(CH_2OH)_4]Cl$ and pyridine-enone with the major signal (−69.1 ppm) consistent with **L8**.

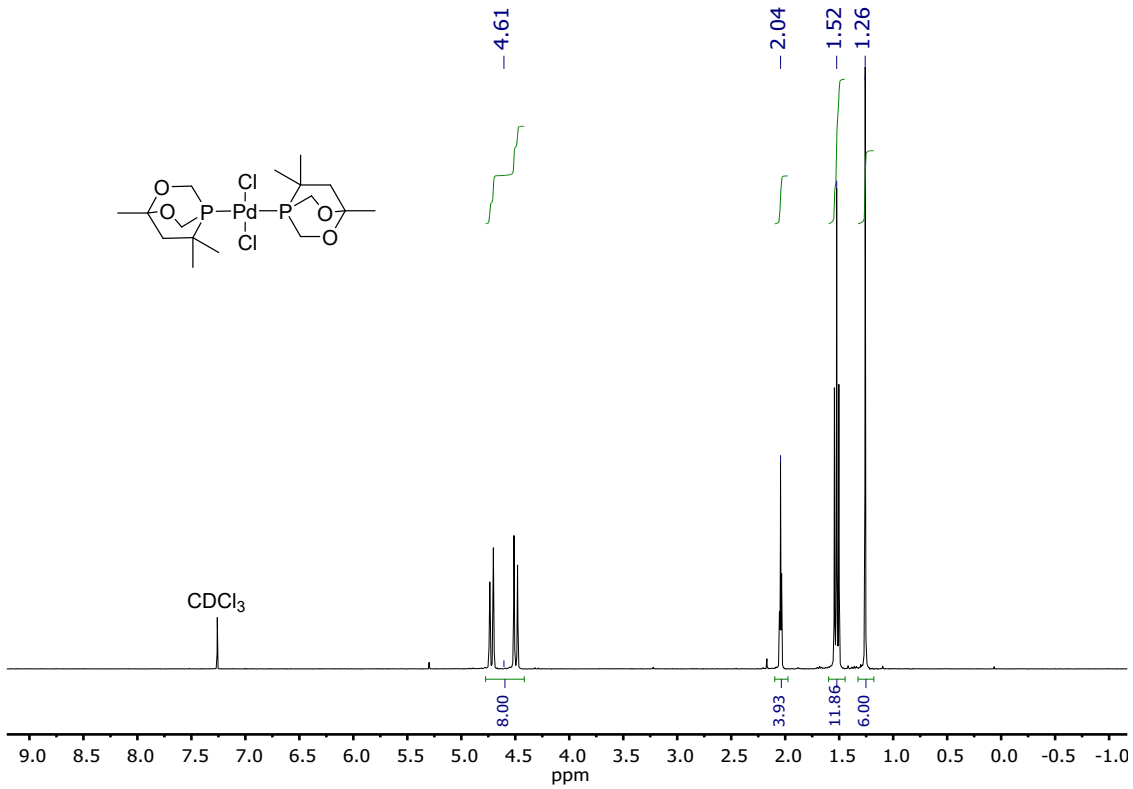

Figure S44. ^{1}H NMR (400 MHz, $CDCl_3$) spectrum of [Pd(**L1**)$_2$Cl$_2$].

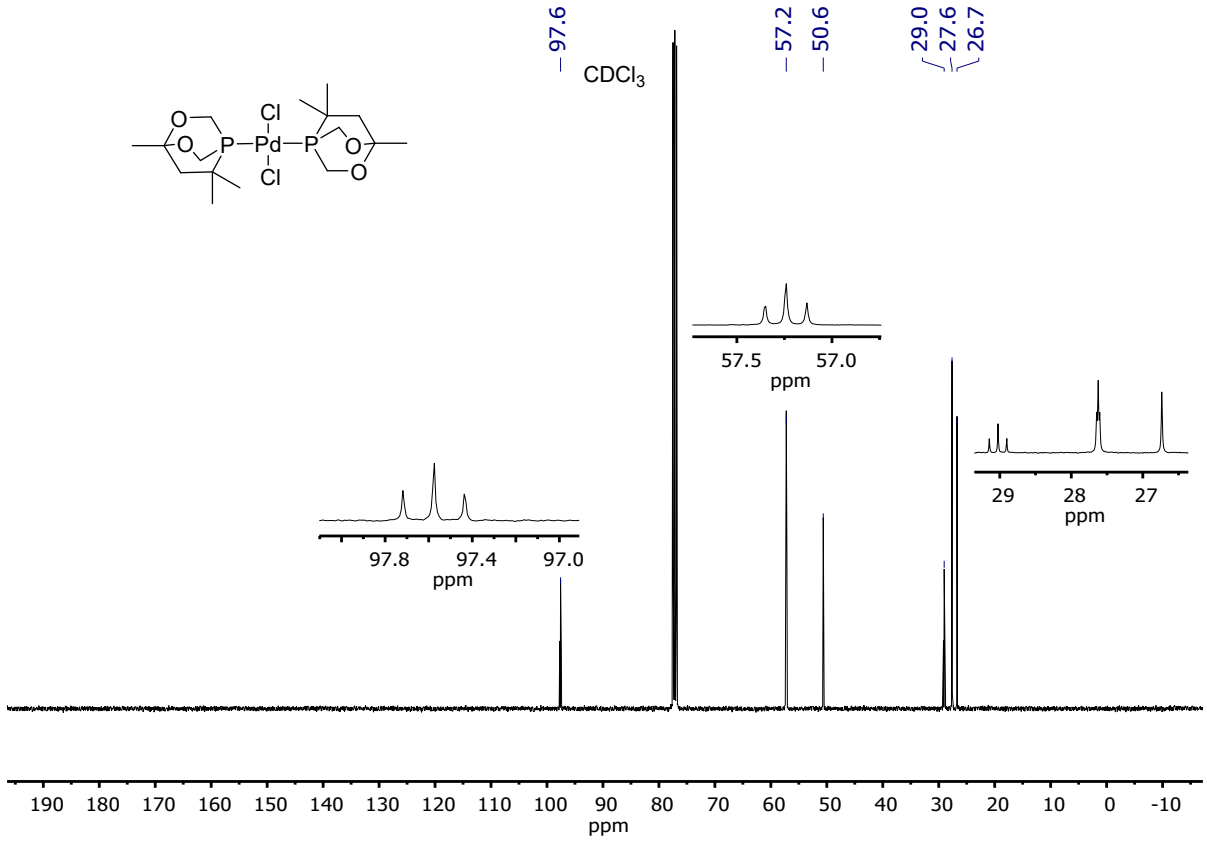

Figure S45. $^{13}C\{^{1}H\}$ NMR (101 MHz, $CDCl_3$) spectrum of [Pd(**L1**)$_2$Cl$_2$].

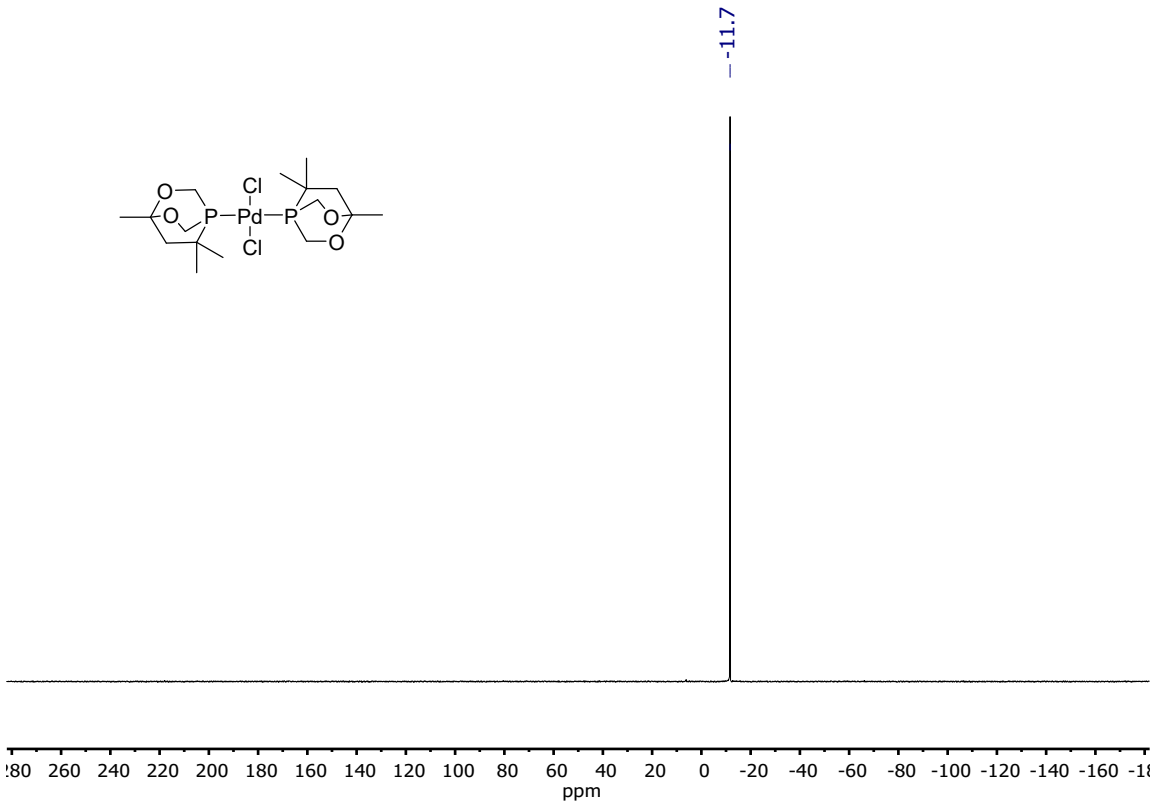

Figure S46. $^{31}P\{^{1}H\}$ NMR (162 MHz, $CDCl_3$) spectrum of $[Pd(\mathbf{L1})_2Cl_2]$.

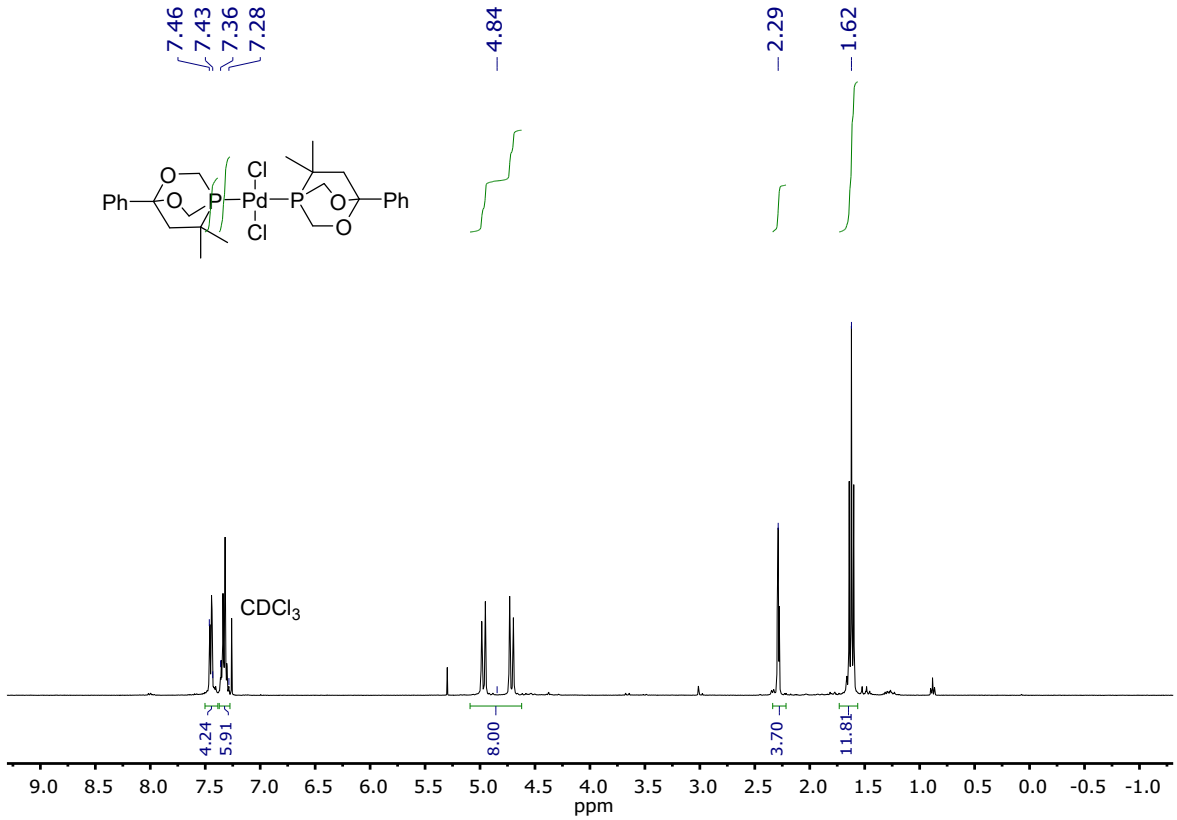

Figure S47. ^{1}H NMR (400 MHz, $CDCl_3$) spectrum of $[Pd(\mathbf{L2})_2Cl_2]$.

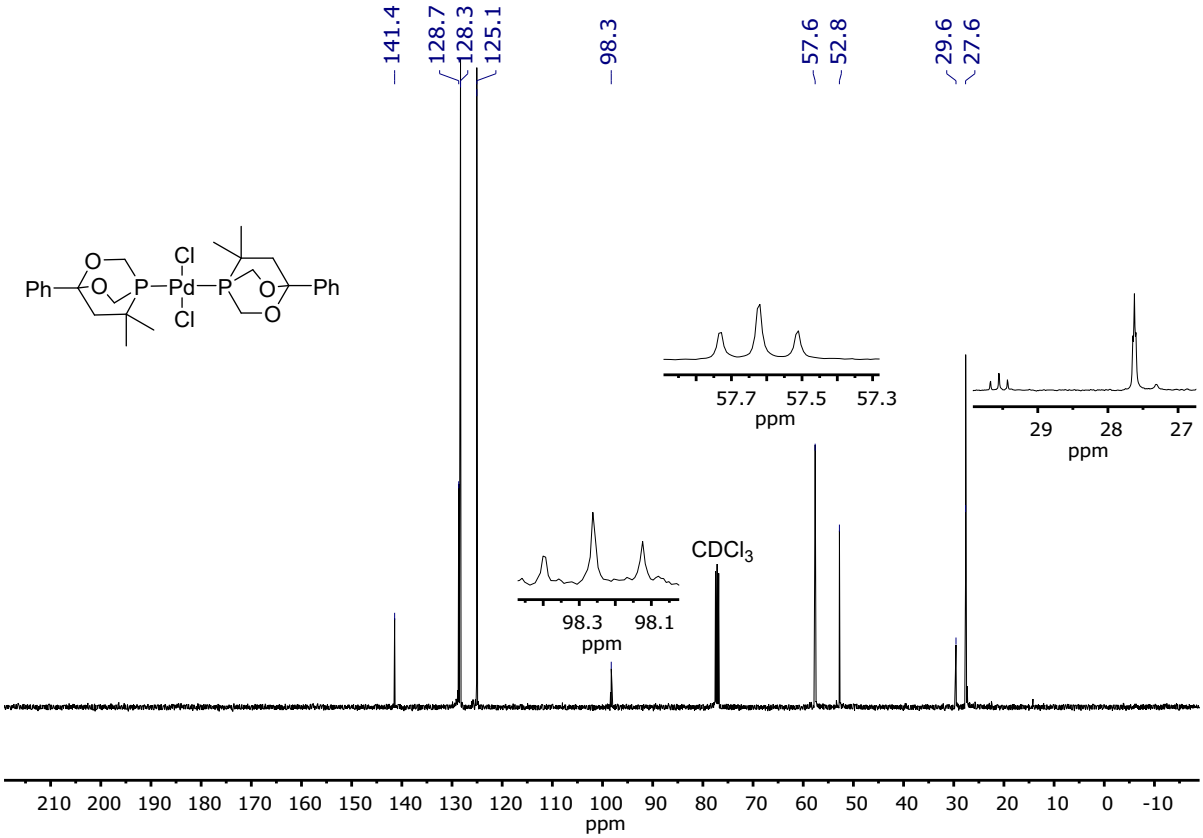

Figure S48. $^{13}C\{^{1}H\}$ NMR (101 MHz, $CDCl_3$) spectrum of [Pd(**L2**)$_2$Cl$_2$].

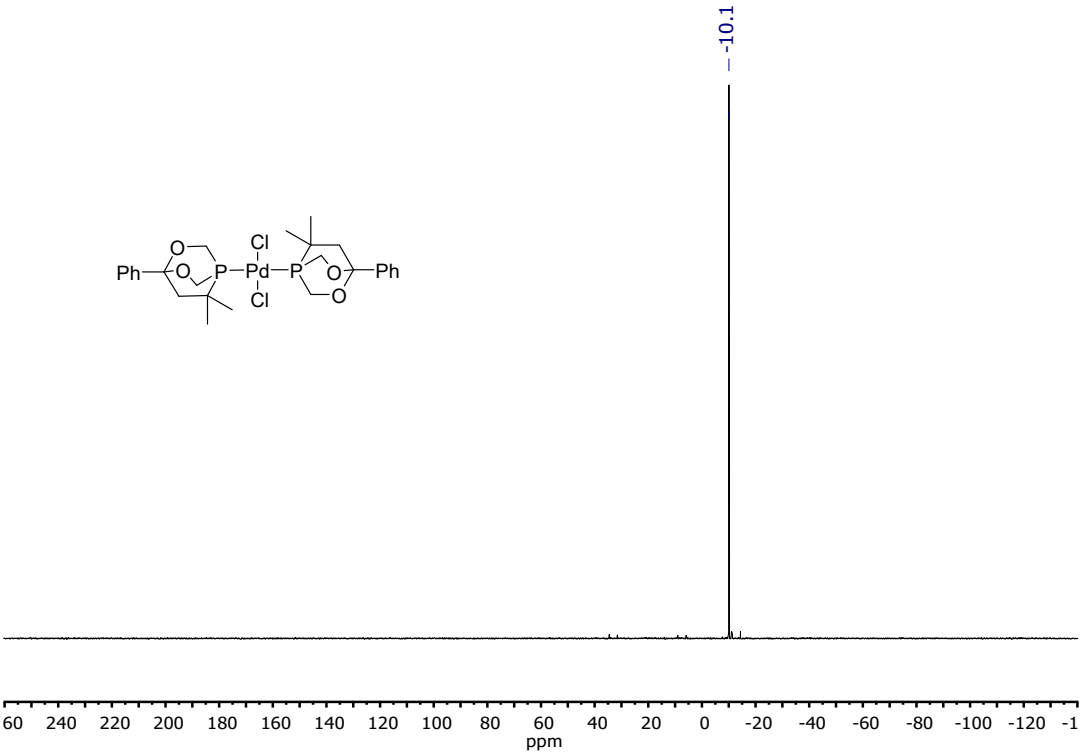

Figure S49. $^{31}P\{^{1}H\}$ NMR (162 MHz, $CDCl_3$) spectrum of [Pd(**L2**)$_2$Cl$_2$].

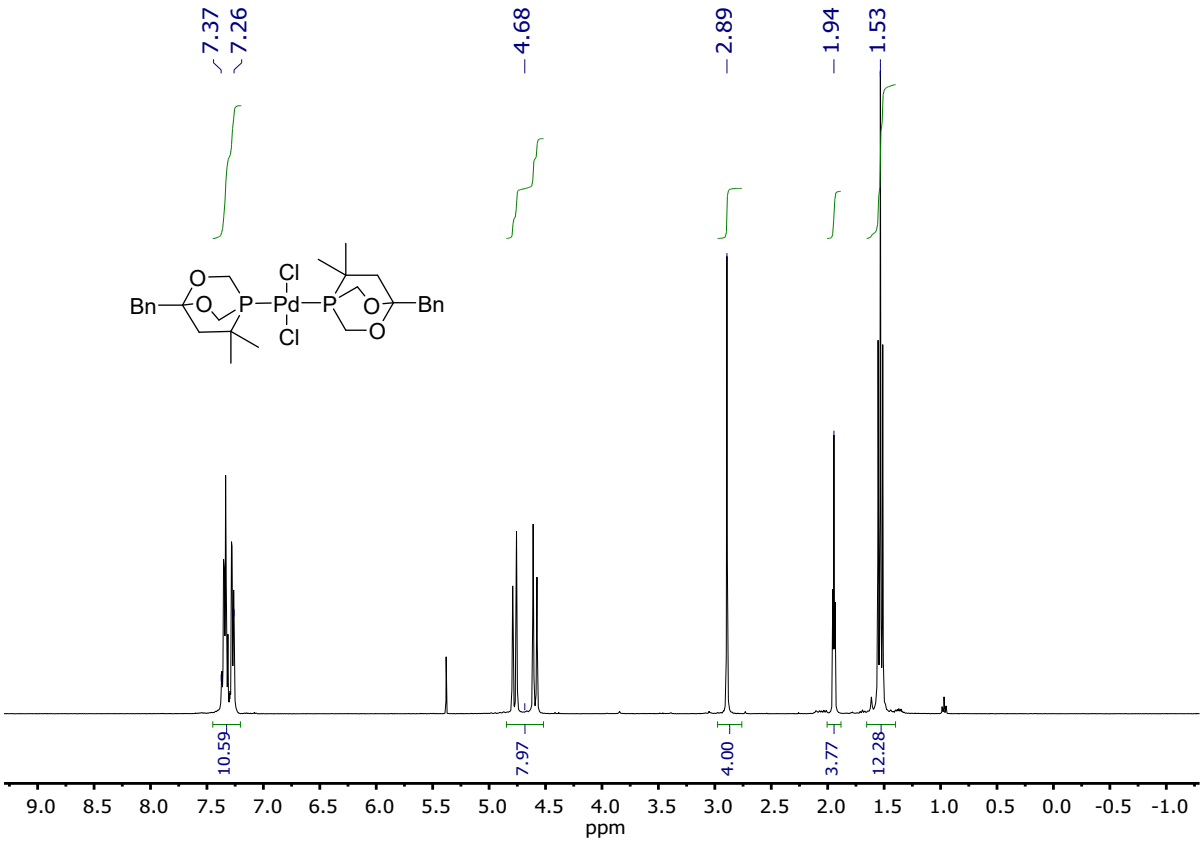

Figure S50. ^{1}H NMR (400 MHz, $CDCl_3$) spectrum of [Pd(**L3**)$_2$Cl$_2$].

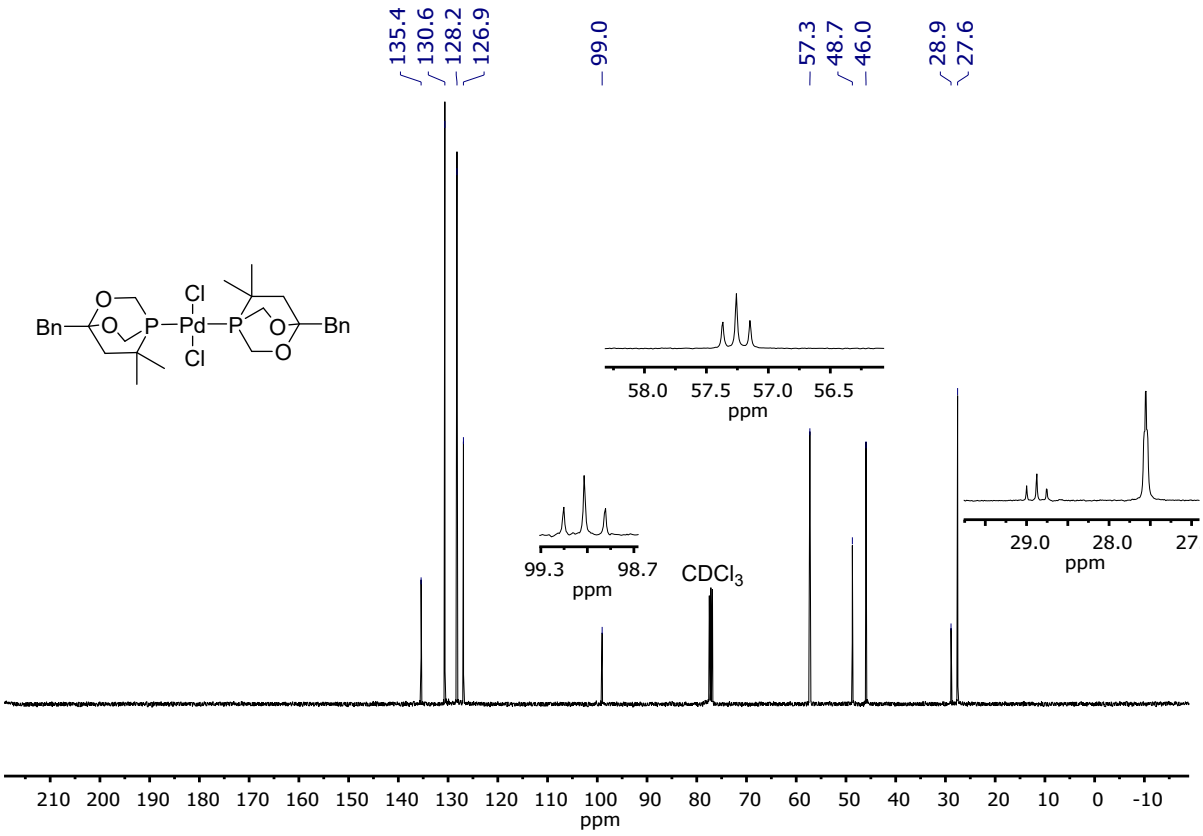

Figure S51. $^{13}C\{^{1}H\}$ NMR (101 MHz, $CDCl_3$) spectrum of [Pd(**L3**)$_2$Cl$_2$].

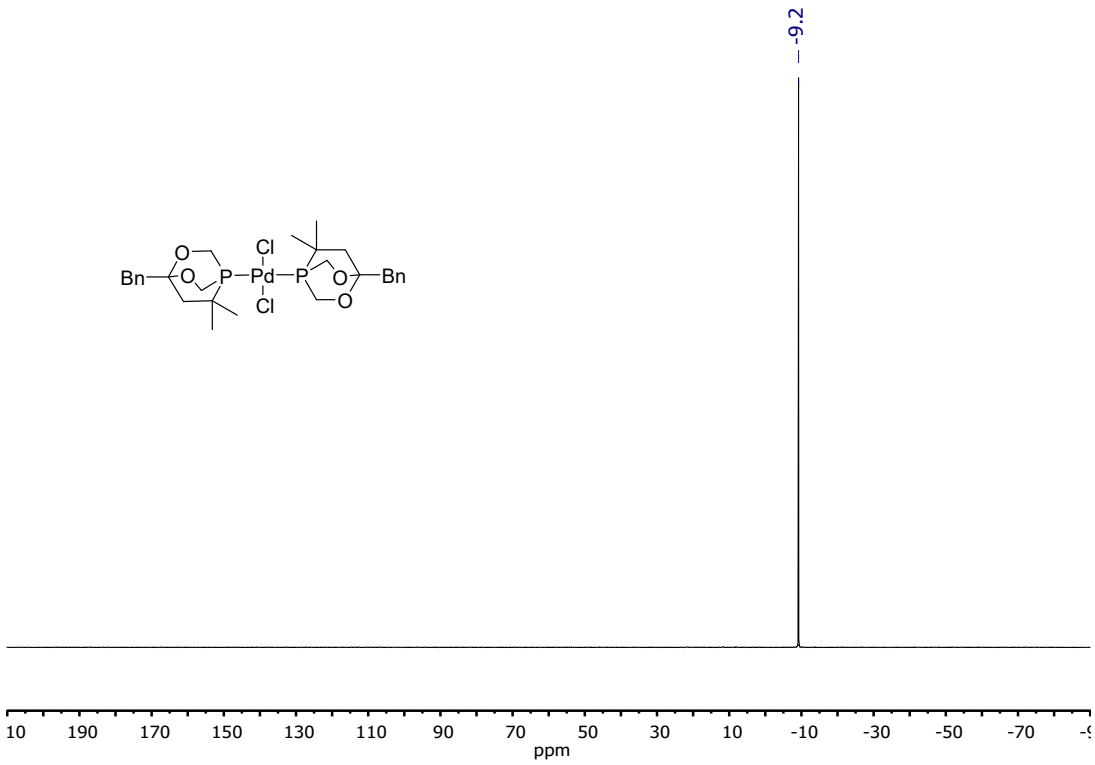

Figure S52. $^{31}P\{^{1}H\}$ NMR (162 MHz, $CDCl_3$) spectrum of [Pd(**L3**)$_2$Cl$_2$].

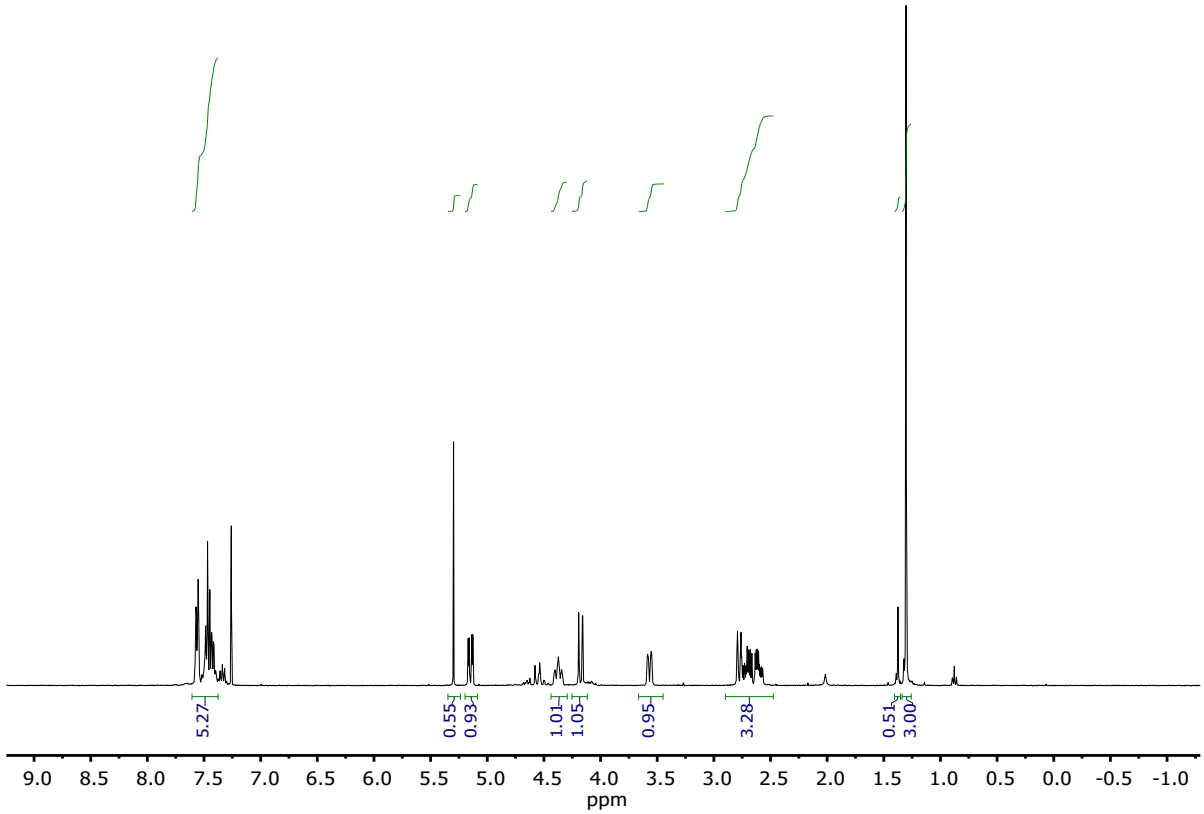

Figure S53. ^{1}H NMR (400 MHz, $CDCl_3$) spectrum of [Pd(**L4**)$_2$Cl$_2$].

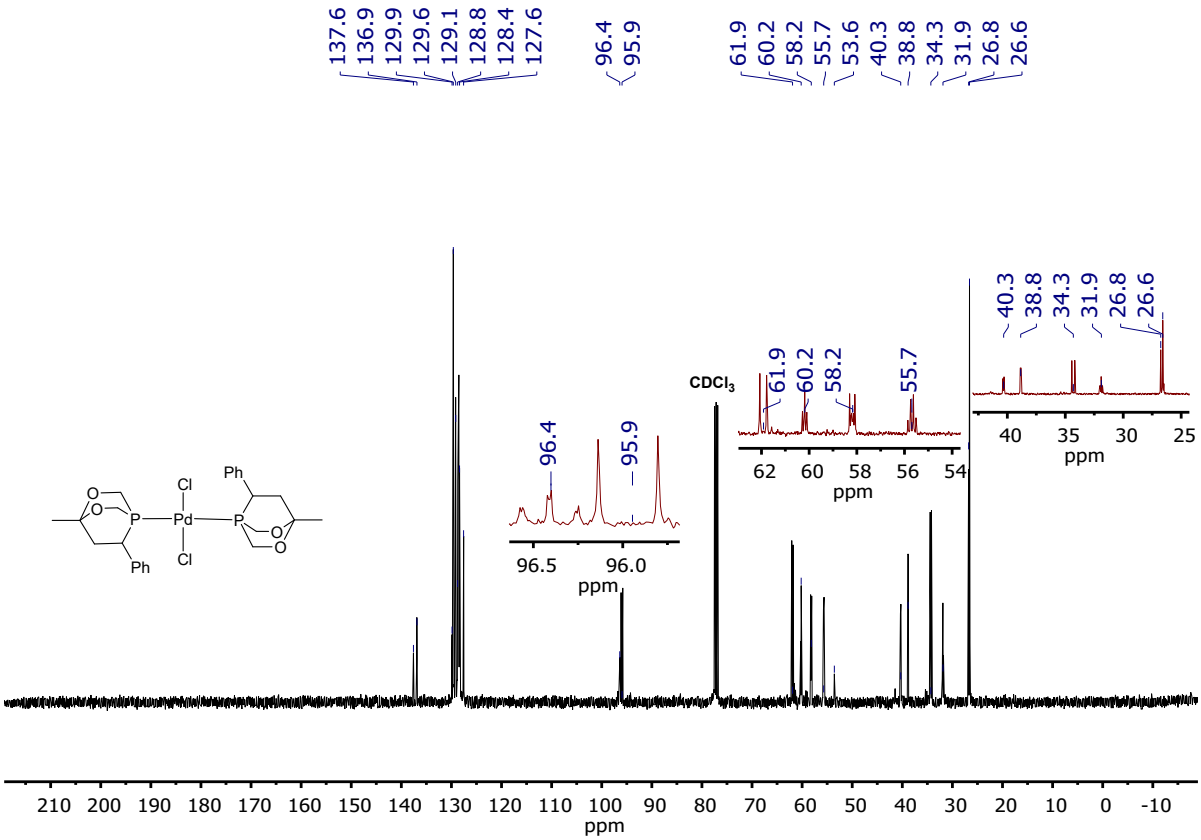

Figure S54. $^{13}C\{^{1}H\}$ NMR (101 MHz, $CDCl_3$) spectrum of [Pd(**L4**)$_2$Cl$_2$].

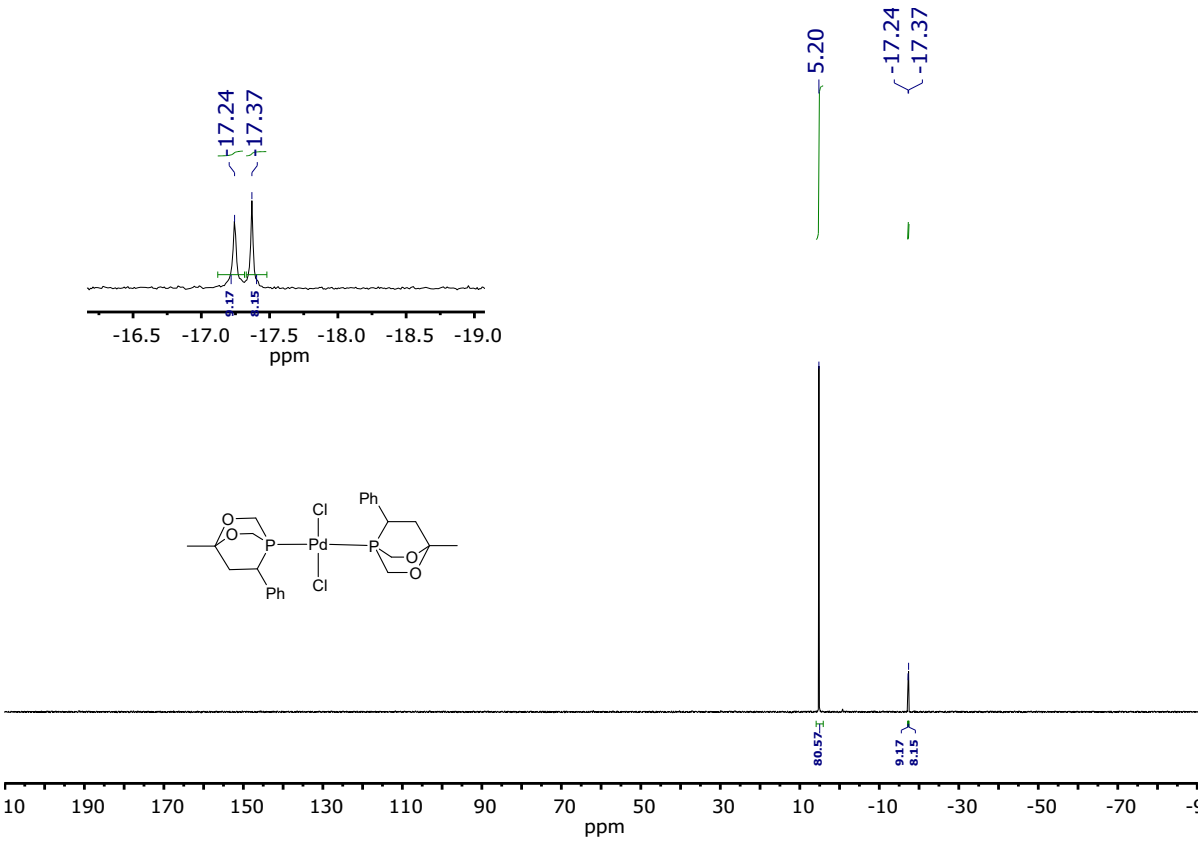

Figure S55. $^{31}P\{^{1}H\}$ NMR (162 MHz, $CDCl_3$) spectrum of [Pd(**L4**)$_2$Cl$_2$].

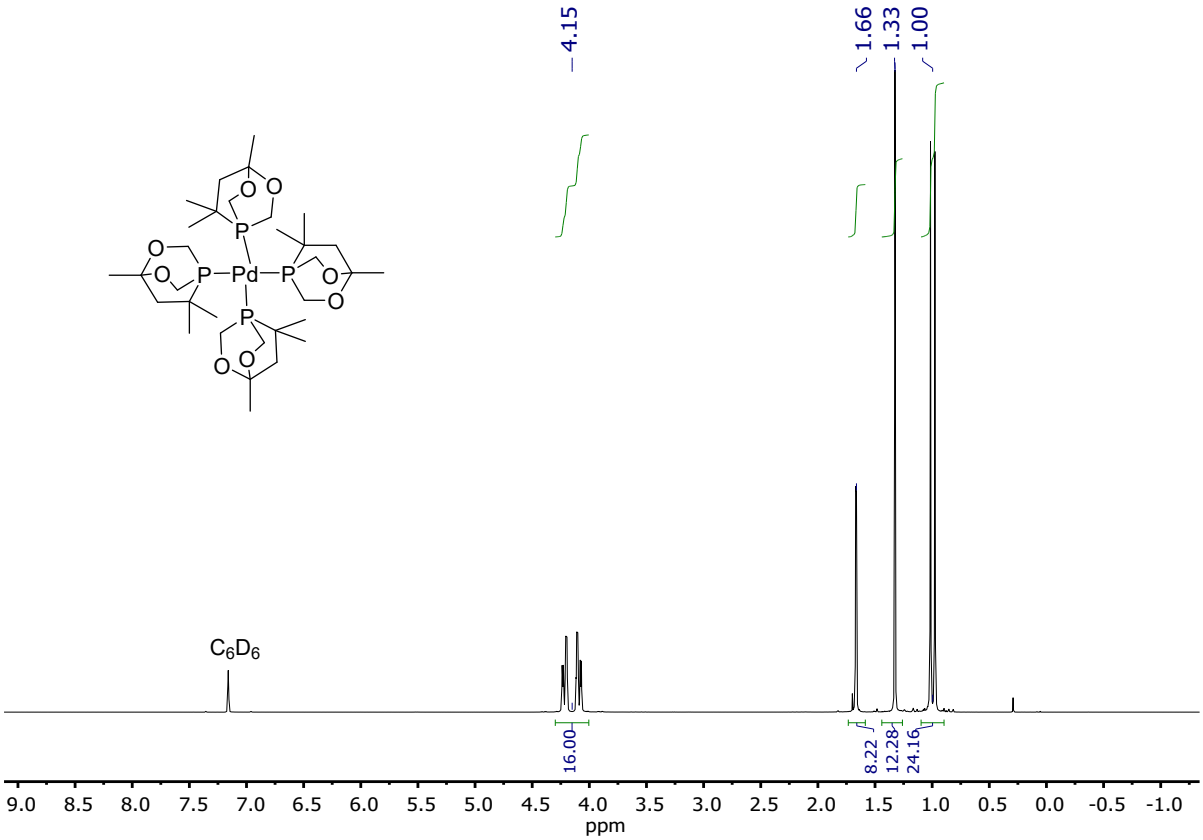

Figure S56. ^{1}H NMR (400 MHz, C_6D_6) spectrum of [Pd(**L1**)$_4$].

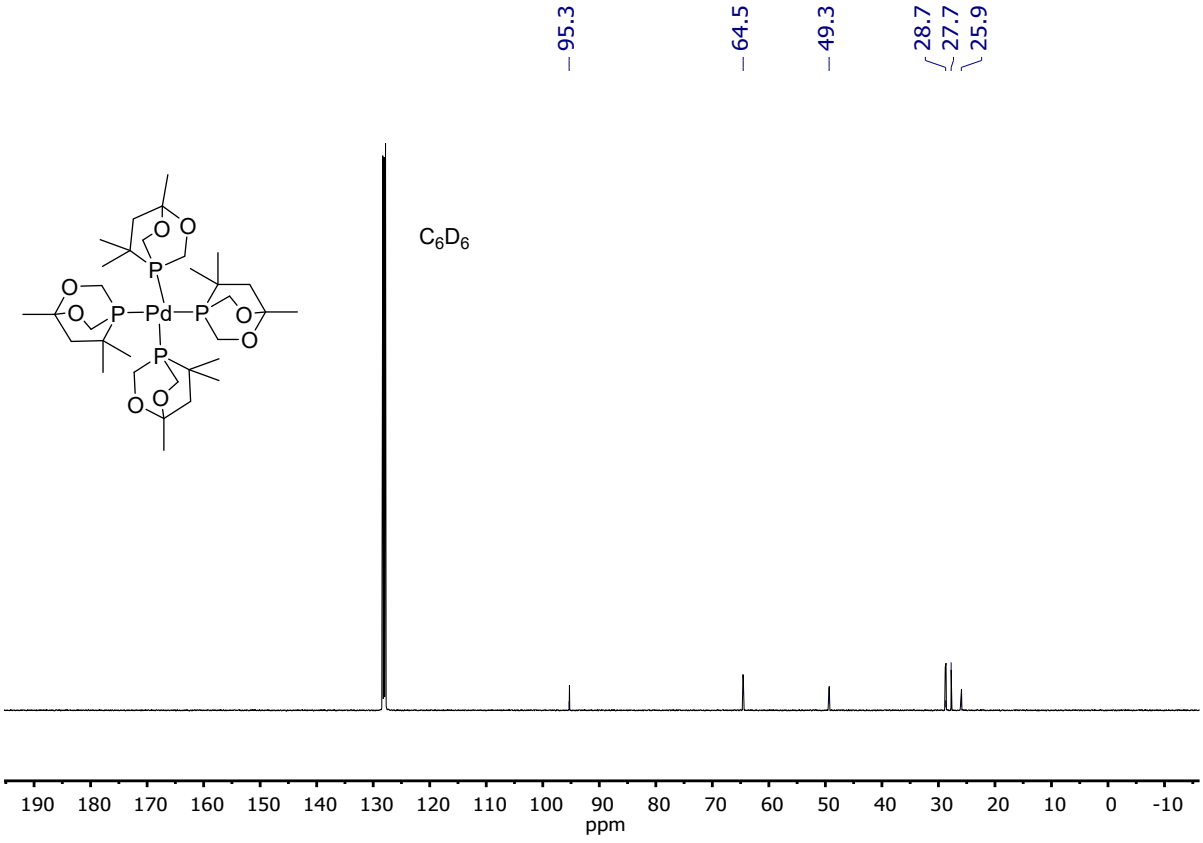

Figure S57. $^{13}C\{^{1}H\}$ NMR (101 MHz, C_6D_6) spectrum of [Pd(**L1**)$_4$].

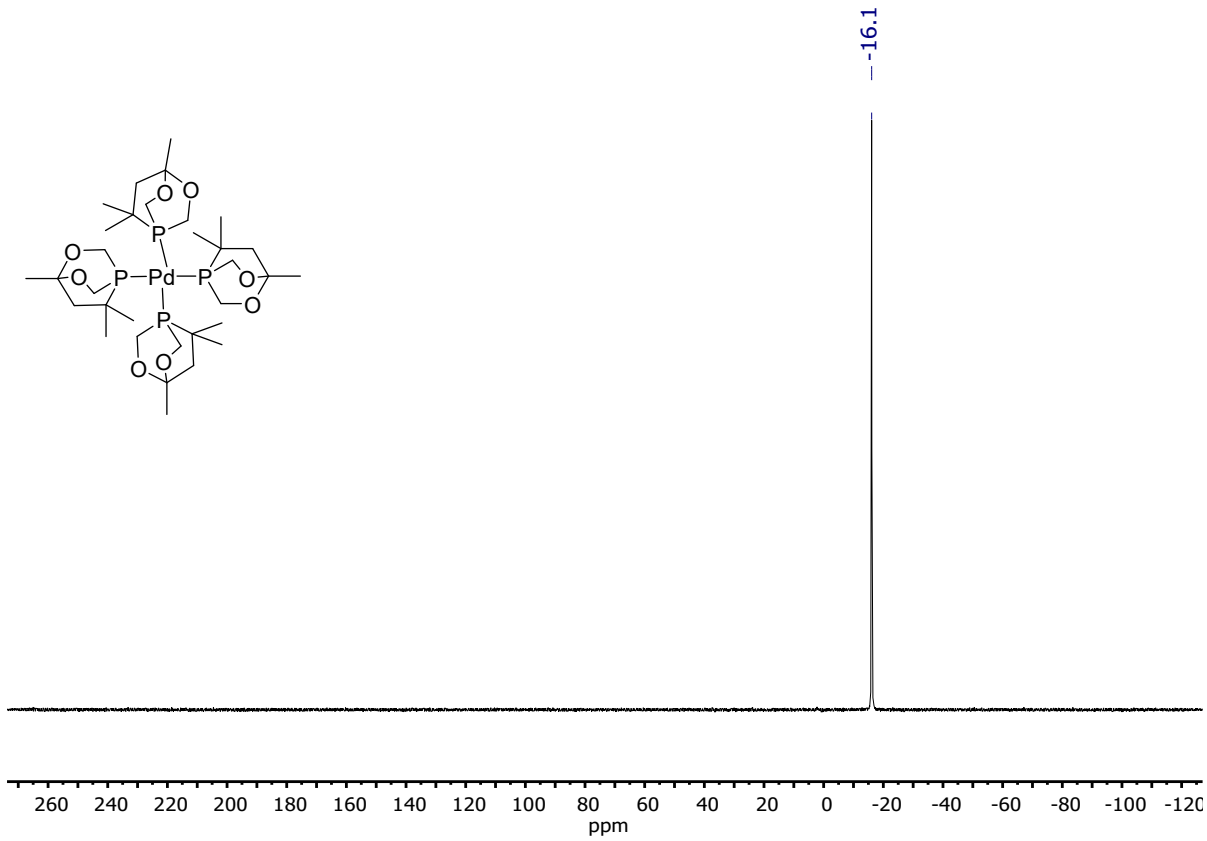

Figure S58. $^{31}P\{^{1}H\}$ NMR (162 MHz, C_6D_6) spectrum of [Pd(**L1**)$_4$].

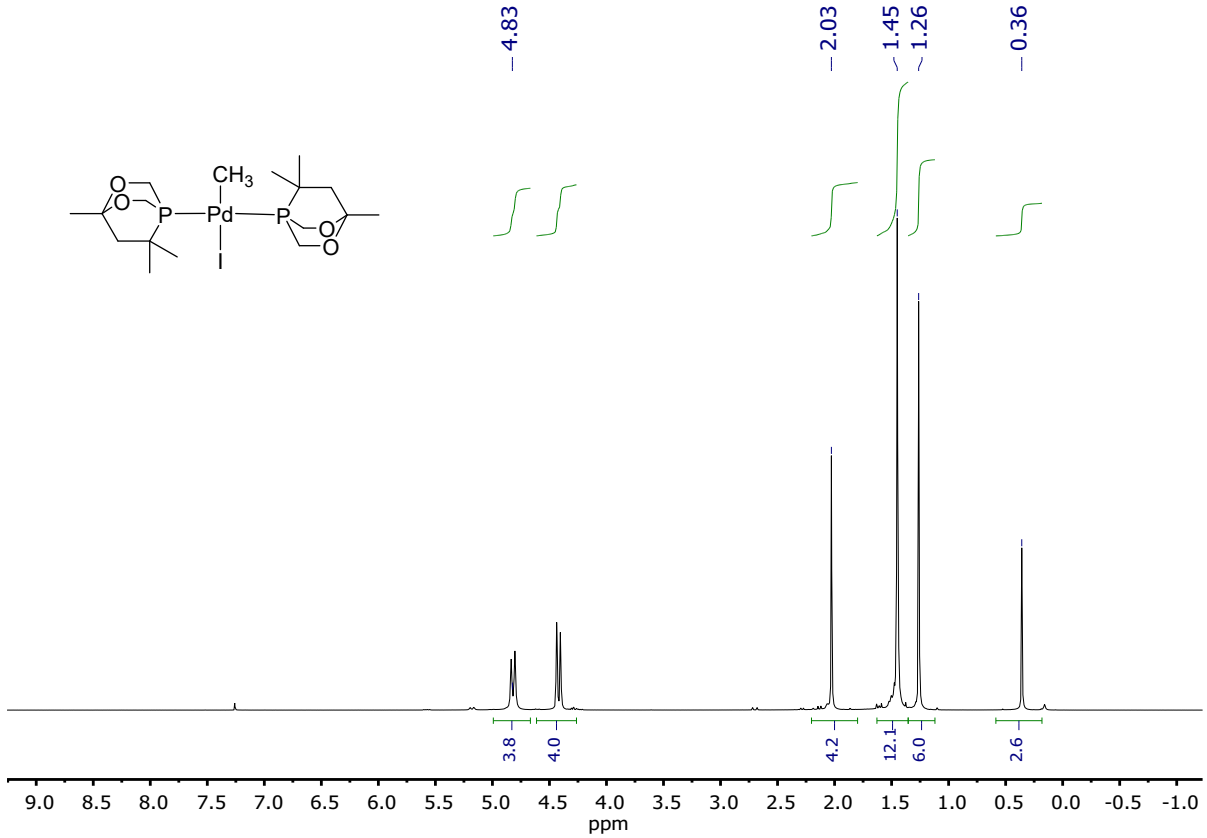

Figure S59. ^{1}H NMR (400 MHz, $CDCl_3$) spectrum of [Pd(**L1**)$_2$(CH_3)I].

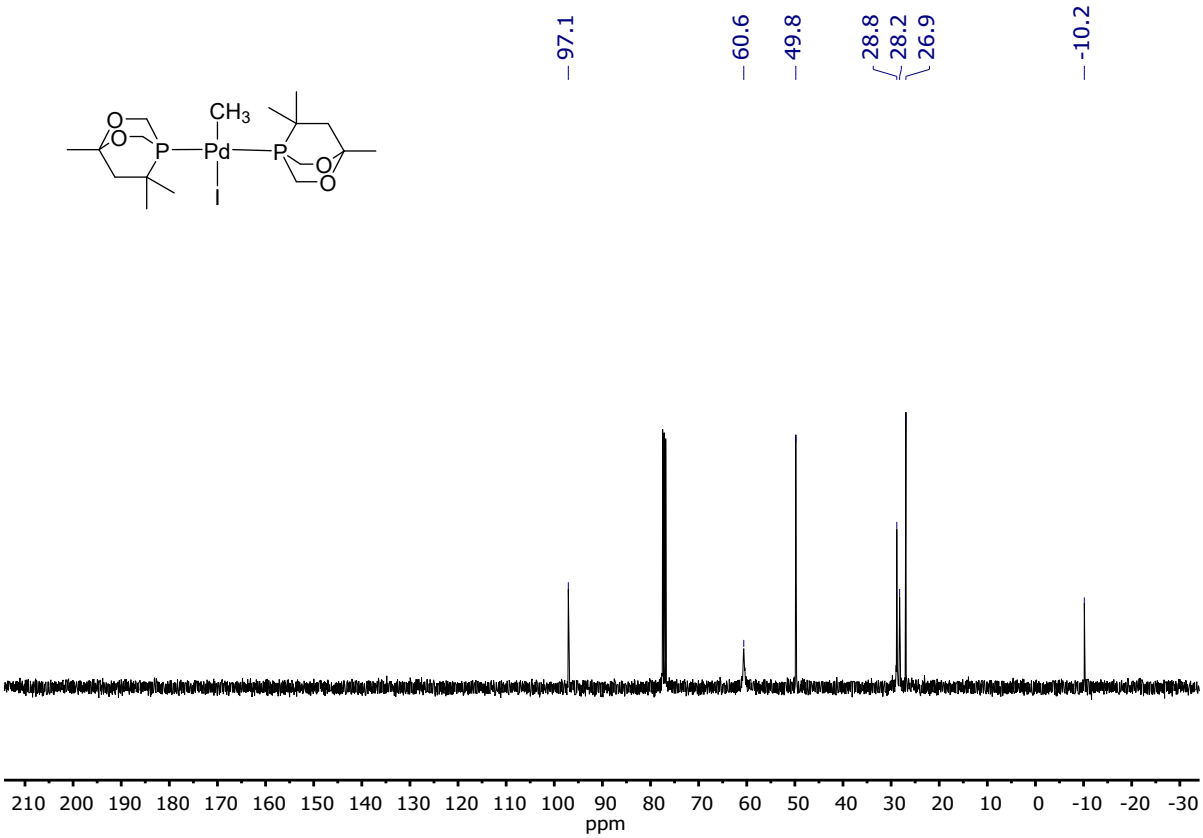

Figure S60. $^{13}C\{^{1}H\}$ NMR (101 MHz, $CDCl_3$) spectrum of [Pd(**L1**)$_2$(CH_3)I].

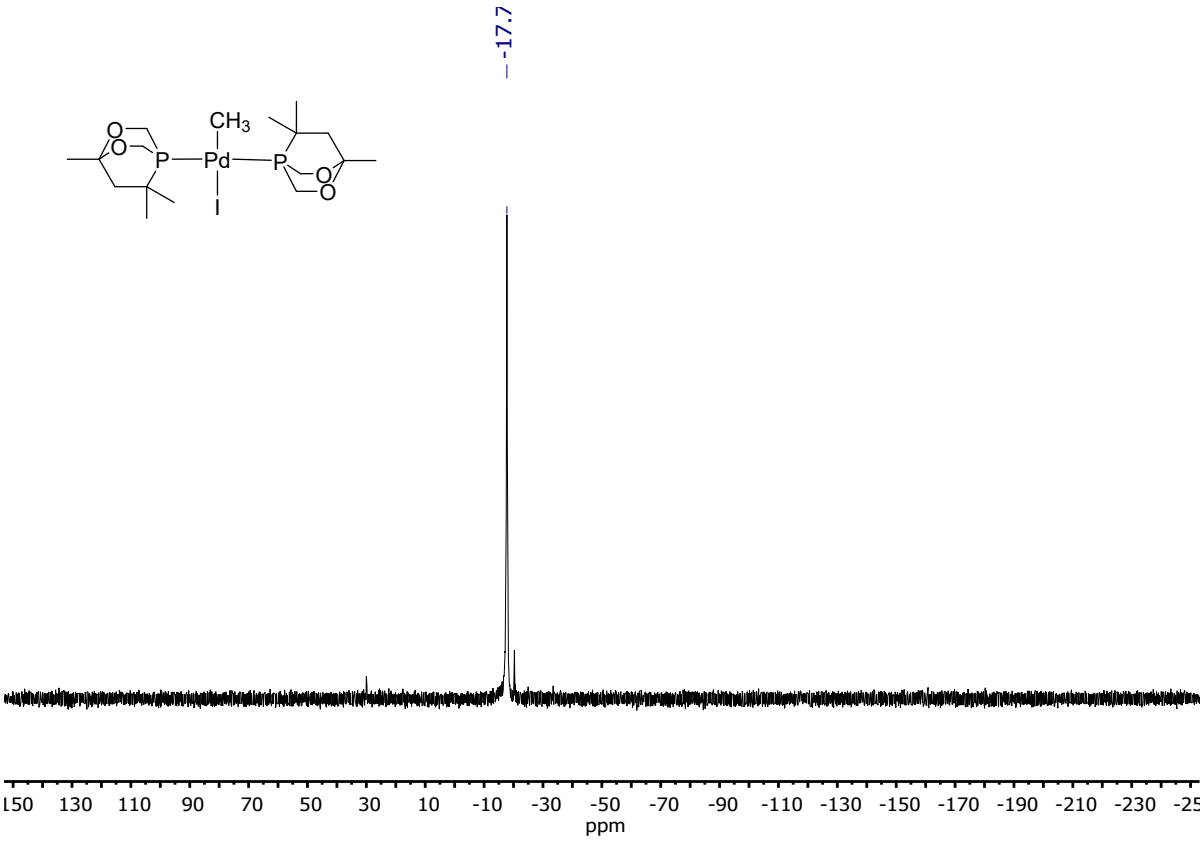

Figure S61. $^{31}P\{^{1}H\}$ NMR (162 MHz, $CDCl_3$) spectrum of [Pd(**L1**)$_2$(CH_3)I].

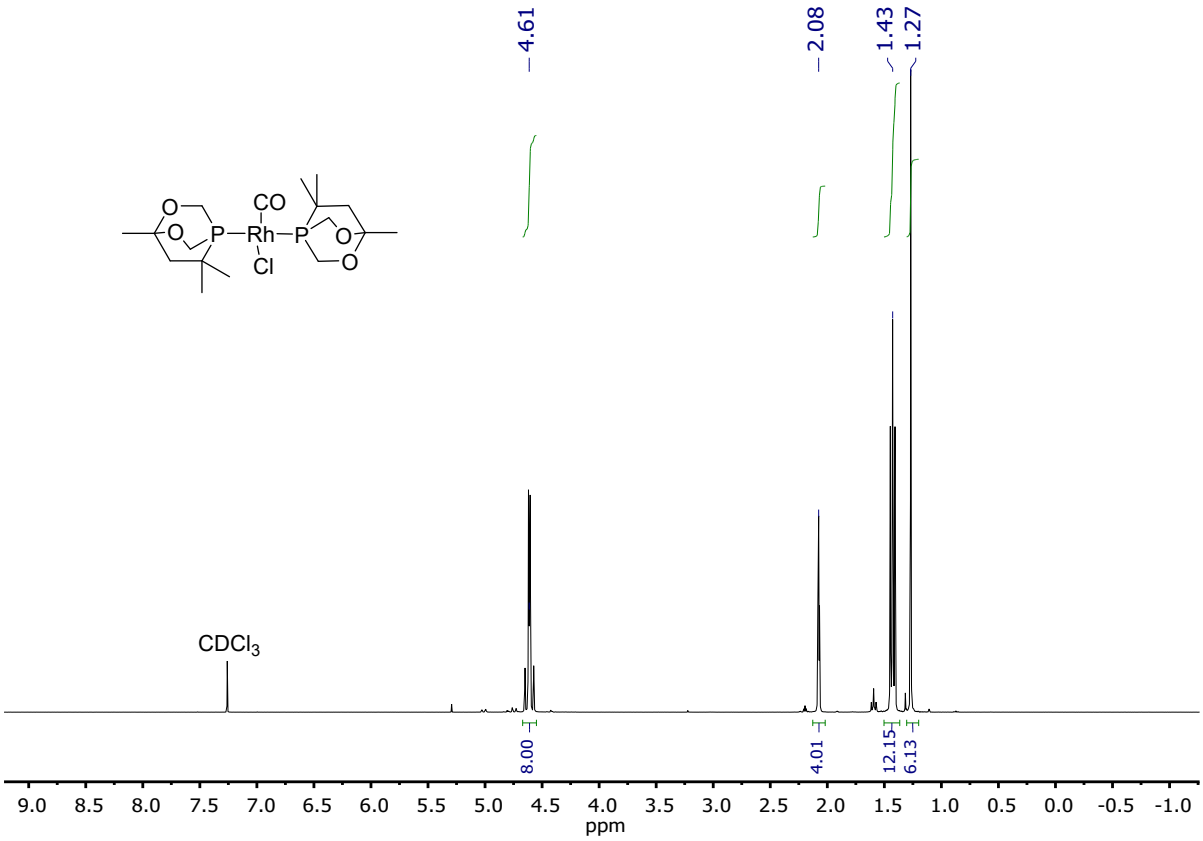

Figure S62. ^{1}H NMR (400 MHz, $CDCl_3$) spectrum of [Rh(CO)(**L1**)$_2$Cl].

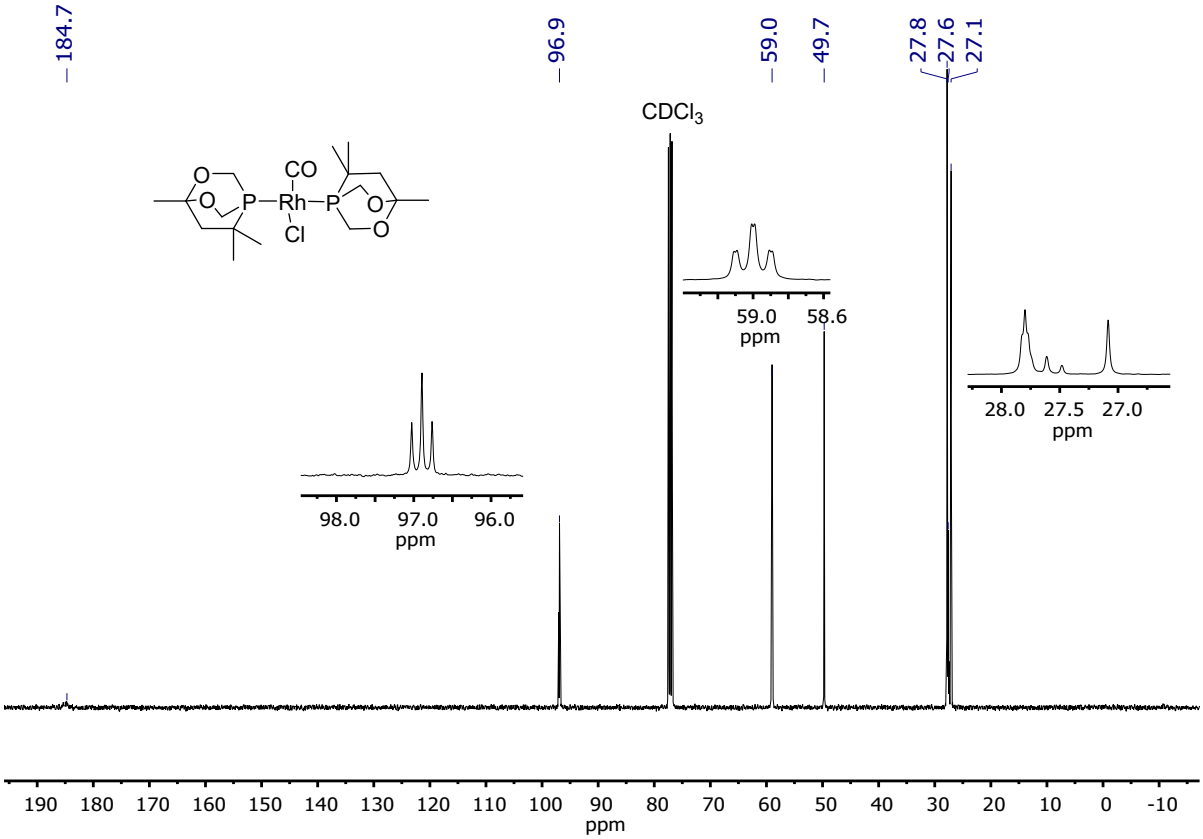

Figure S63. $^{13}C\{^{1}H\}$ NMR (101 MHz, $CDCl_3$) spectrum of [Rh(CO)(**L1**)$_2$Cl].

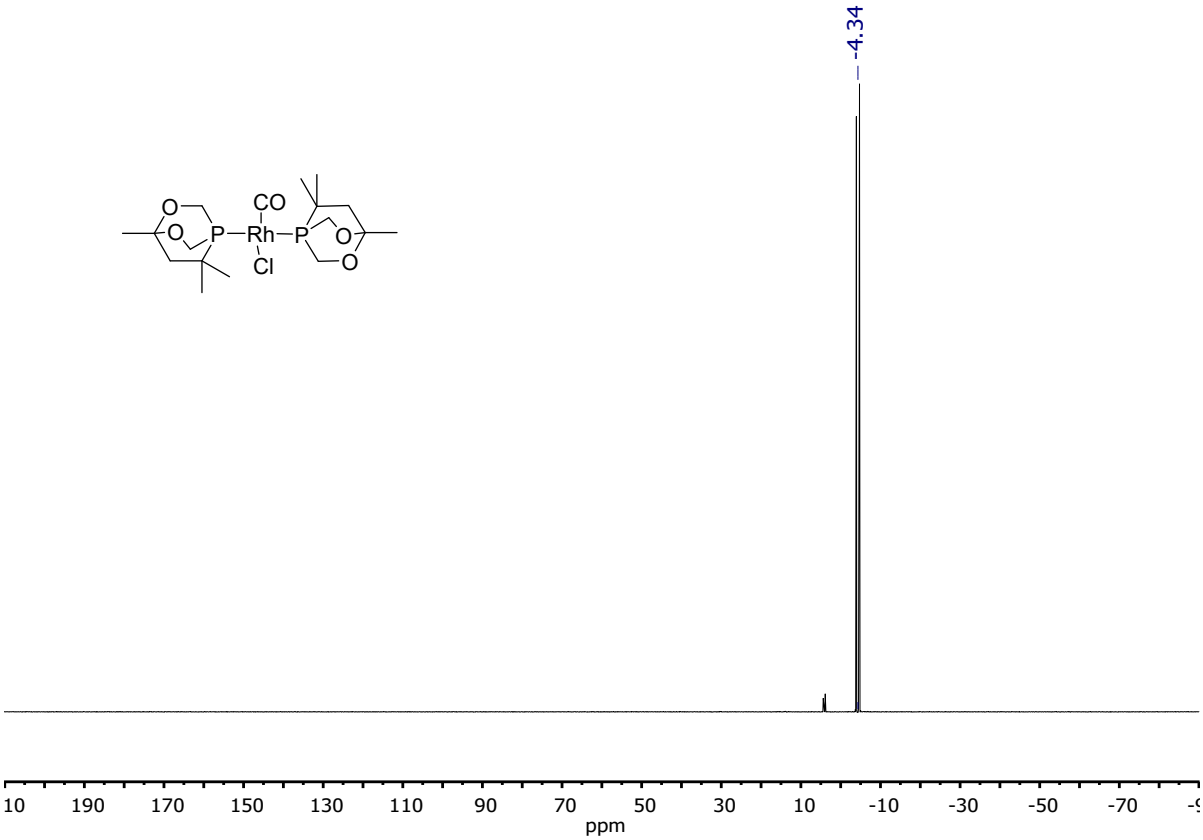

Figure S64. $^{31}P\{^{1}H\}$ NMR (162 MHz, $CDCl_3$) spectrum of [Rh(CO)(**L1**)$_2$Cl].

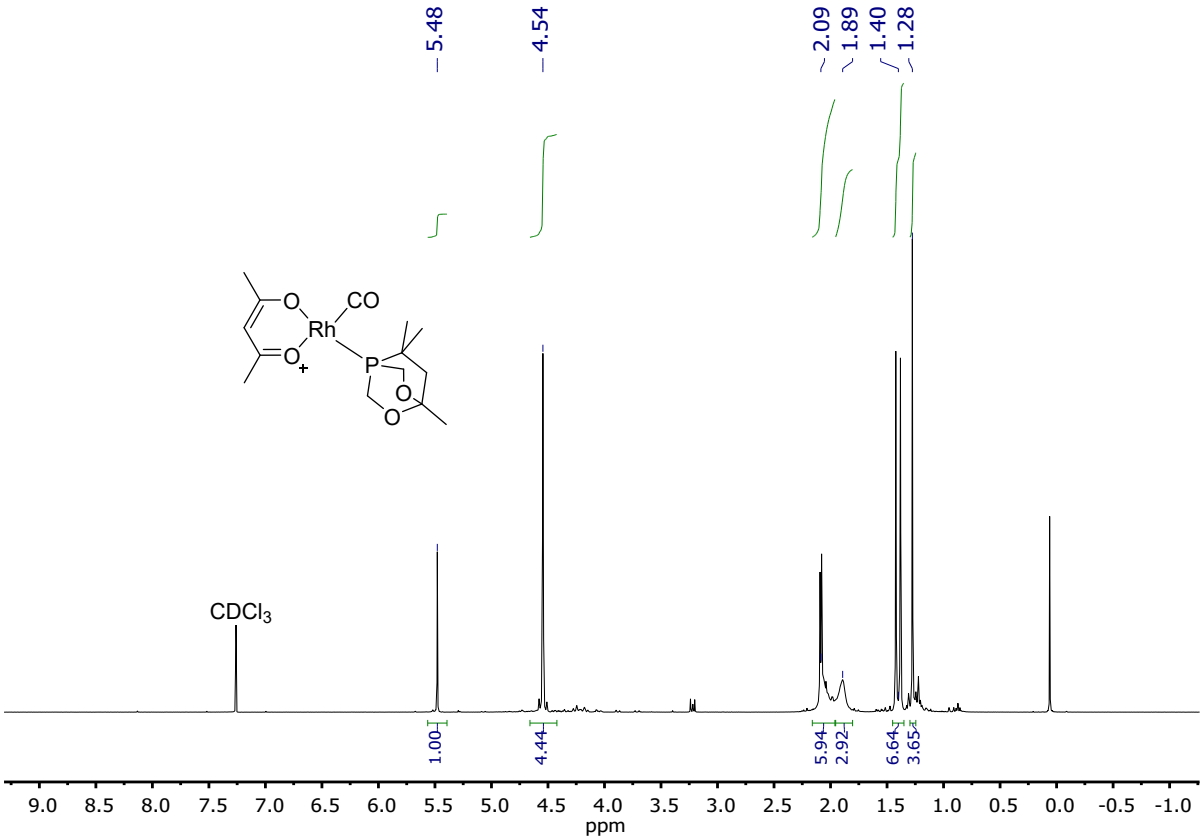

Figure S65. ^{1}H NMR (400 MHz, $CDCl_3$) spectrum of [Rh(acac)(CO)(**L1**)].

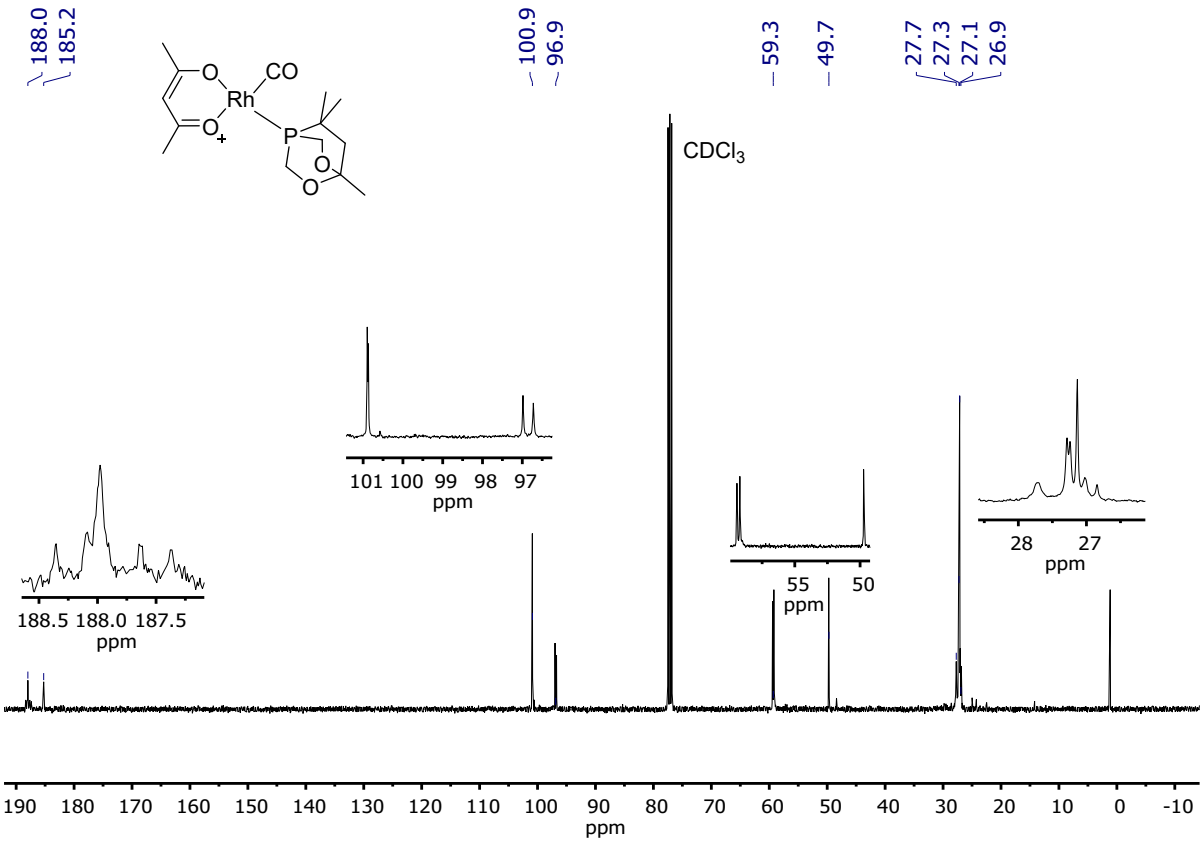

Figure S66. $^{13}C\{^{1}H\}$ NMR (101 MHz, $CDCl_3$) spectrum of [Rh(acac)(CO)(**L1**)].

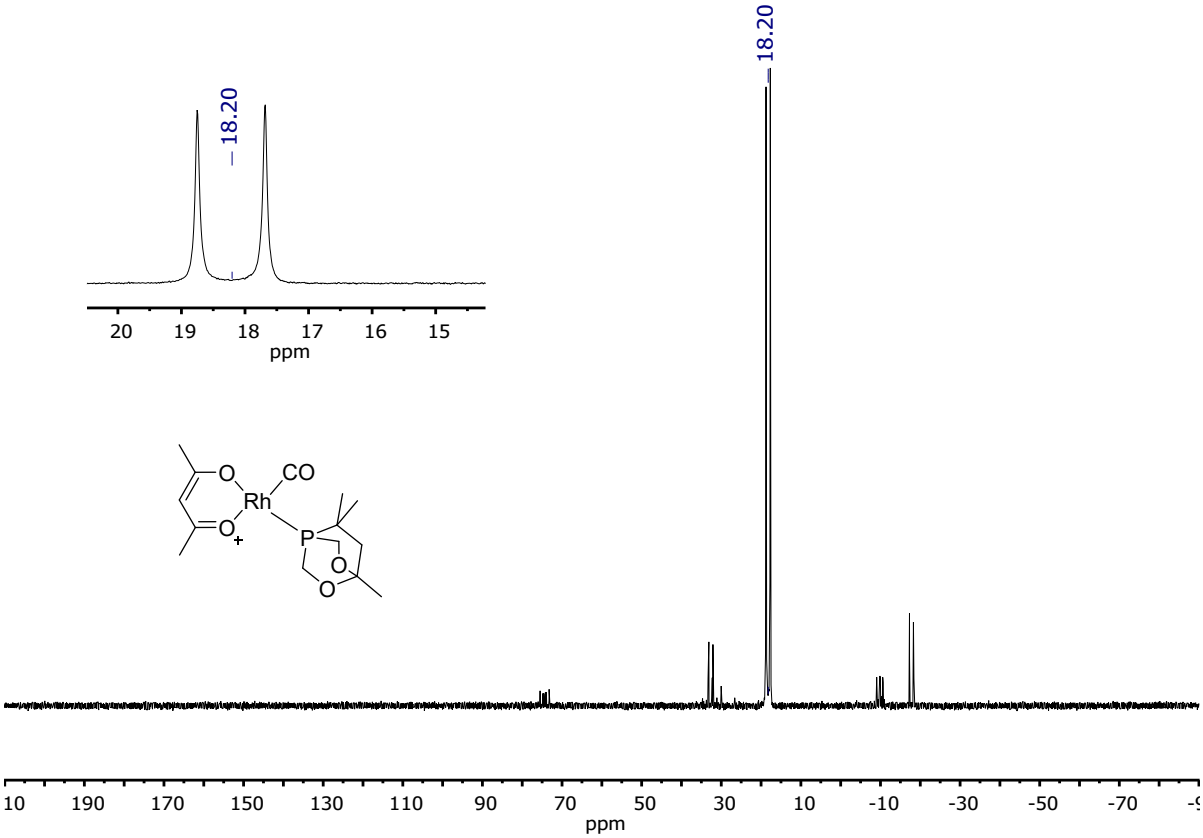

Figure S67. $^{31}P\{^{1}H\}$ NMR (162 MHz, $CDCl_3$) spectrum of [Rh(acac)(CO)(**L1**)].

3. Single Crystal X-ray Diffraction.

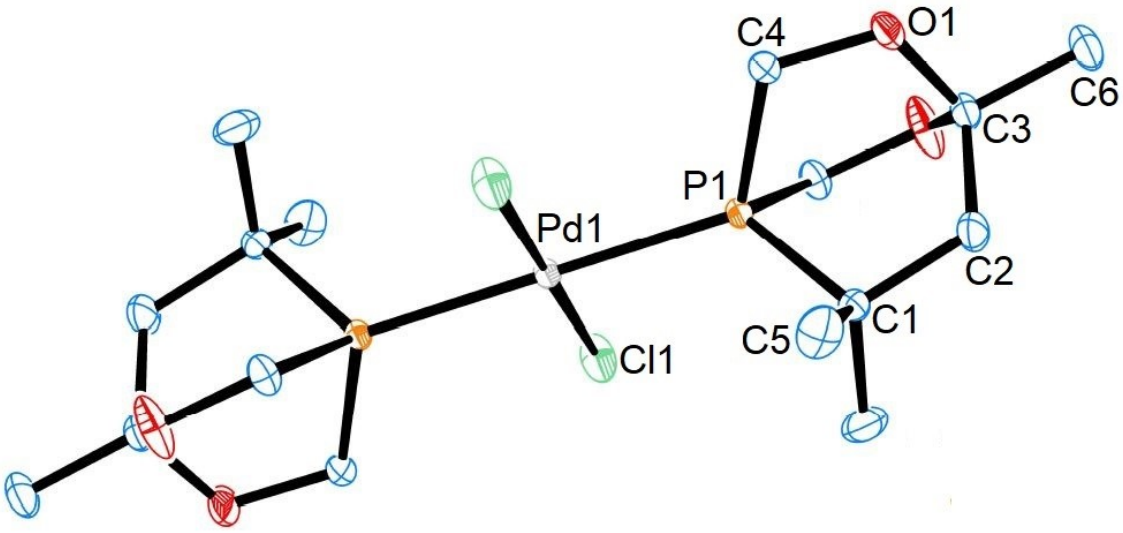

Figure S68. Molecular structure of [Pd(**L1**)$_2$Cl$_2$]. (thermal ellipsoids are drawn at 20% probability).

Table S1. Crystal data and structure refinement for [Pd(**L1**)$_2$Cl$_2$].

Identification code	CCDC 2301891
Empirical formula	$C_{16}H_{30}Cl_2O_4P_2Pd$
Formula weight	525.64
Temperature	300 K
Wavelength	0.71073 Å (MoKα)
Crystal system, space group	Monoclinic, C2/m
Unit cell dimensions	a = 11.7581(16) Å α = 90° b = 10.6856(15) Å β = 107.289(5)° c = 8.9245(11) Å γ = 90°
Volume	1070.6(2) Å^3
Z, Calculated density	2, 1.631 g/cm^3
Absorption coefficient	1.283 mm^{-1}
F(000)	536.0
Crystal size	0.28 × 0.21 × 0.1 mm

2θ range for data collection	4.78 to 52.726°
Limiting indices	−14<=h<=14, −13<=k<=13, −11<=l<=11
Reflections collected / unique	8777 / 1142 [R(int) = 0.0199]
Completeness to θ = 28.28	98.9 %
Absorption correction	Multi-scan
Refinement method	Full-matrix least-squares on F^2
Data / restraints / parameters	1142 / 0 / 69
Goodness-of-fit on F^2	1.079
Final R indices [I>2σ(I)]	R_1 = 0.0193, wR_2 = 0.0431
R indices (all data)	R1 = 0.0203, wR_2 = 0.0436
Largest diff. peak and hole	0.53 and −0.48 e.$Å^{-3}$

Table S2. Bond lengths [Å] and angles [°] for [Pd(**L1**)$_2$Cl$_2$]

Pd(1)-P(1)	2.2880(7)
Pd(1)-P(1)#1	2.2880(7)
Pd(1)-Cl(1)	2.2928(8)
Pd(1)-Cl(1)#1	2.2927(8)
P(1)-C(1)	1.832(3)
P(1)-C(4)	1.821(2)
P(1)-C(4)#1	1.821(2)
O(1)-C(4)	1.418(2)
O(1)-C(3)	1.409(2)
C(1)-C(2)	1.548(4)
C(1)-C(5)	1.522(3)
C(1)-C(5)#1	1.522(3)
C(3)-C(2)	1.506(4)
C(3)-C(6)	1.517(4)
P(1)-Pd(1)-Cl(1)	90.0
P(1)-Pd(1)-Cl(1)#1	90.0
P(1)#1-Pd(1)-Cl(1)	90.0
P(1)#1-Pd(1)-Cl(1)#1	90.0
Cl(1)#1-Pd(1)-Cl(1)	180.0
C(1)-P(1)-Pd(1)	121.43(9)
C(4)-P(1)-Pd(1)	116.78(6)
C(4)#2-P(1)-Pd(1)	116.78(6)
C(4)-P(1)-C(1)	100.16(9)
C(4)#2-P(1)-C(1)	100.17(9)
C(4)#2-P(1)-C(4)	97.41(14)
C(3)-O(1)-C(4)	117.55(17)

C(2)-C(1)-P(1)	104.91(19)
C(5)-C(1)-P(1)	109.97(14)
C(5)#2-C(1)-C(2)	111.26(17)
C(5)-C(1)-C(2)	111.26(17)
C(5)#2-C(1)-C(5)	109.4(3)
O(1)-C(4)-P(1)	111.19(14)
O(1)#2-C(3)-O(1)	109.9(3)
O(1)#2-C(3)-C(2)	110.76(17)
O(1)-C(3)-C(2)	110.76(17)
O(1)#2-C(3)-C(6)	106.10(16)
O(1)-C(3)-C(6)	106.10(16)
C(2)-C(3)-C(6)	113.0(3)

Symmetry transformations used to generate equivalent atoms: #1-x,1-y,-z ;#2+x,1-y,+z

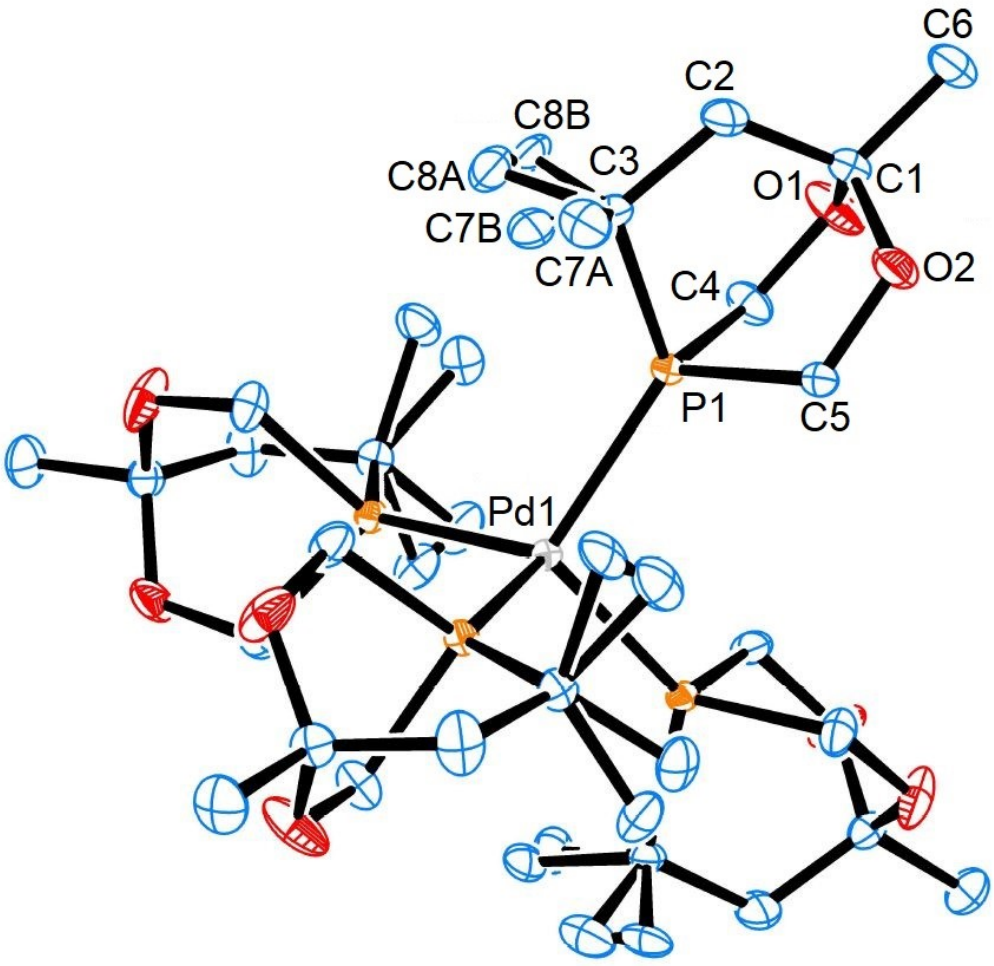

Figure S69. Molecular structure of [Pd(**L1**)$_4$]. (thermal ellipsoids are drawn at 20% probability).

Table S3. Crystal data and structure refinement for [Pd(**L1**)$_4$].

Identification code	CCDC 2081403
Empirical formula	$C_{32}H_{60}O_8P_4Pd$
Formula weight	803.08
Temperature	293(2) K
Wavelength	1.54184 Å (Cu-Kα)
Crystal system, space group	Tetragonal, I4(1)/a
Unit cell dimensions	a = 20.3803(2) Å α = 90° b = 20.3803(2) Å β = 90° c = 9.0334(2) Å γ = 90°
Volume	3752.08(11) Å^3
Z, Calculated density	4, 1.422 g/cm^3
Absorption coefficient	5.977 mm^{-1}
F(000)	1688
Crystal size	0.268 × 0.171 × 0.130 mm
2θ range for data collection	10.712 to 148.096°
Limiting indices	−10<=h<=24, −25<=k<=16, −6<=l<=10
Reflections collected / unique	2953 / 1830 [R(int) = 0.0238]
Completeness to θ = 28.28	96.0 %
Absorption correction	Gaussian
Refinement method	Full-matrix least-squares on F^2
Data / restraints / parameters	1830 / 0 / 126
Goodness-of-fit on F^2	1.094
Final R indices [I>2σ(I)]	R_1 = 0.0419, wR_2 = 0.1118
R indices (all data)	R_1 = 0.0439, wR_2 = 0.1140
Largest diff. peak and hole	0.72 and −0.62 e.Å^{-3}

Table S4. Bond lengths [Å] and angles [°] for [Pd(**L1**)$_4$]

P(1)-Pd(1)	2.3601(7)
Pd(1)-P(1)#1	2.3600(7)
Pd(1)-P(1)#2	2.3600(7)
Pd(1)-P(1)#3	2.3600(7)
P(1)-C(3)	1.870(3)
P(1)-C(5)	1.851(4)
P(1)-C(4)	1.849(4)
O(1)-C(4)	1.396(4)
O(1)-C(1)	1.401(4)
O(2)-C(5)	1.402(4)
O(2)-C(1)	1.403(4)
C(3)-C(8A)	1.506(15)
C(3)-C(8B)	1.560(18)
C(3)-C(2)	1.521(5)
C(3)-C(7A)	1.564(12)
C(3)-C(7B)	1.47(2)
C(1)-C(2)	1.493(5)
C(1)-C(6)	1.504(5)
P(1)#1-Pd(1)-P(1)#2	104.78(4)
P(1)#2-Pd(1)-P(1)	111.867(19)
P(1)#1-Pd(1)-P(1)#3	111.867(19)
P(1)-Pd(1)-P(1)#3	104.78(4)
P(1)#1-Pd(1)-P(1)	111.866(19)
P(1)#2-Pd(1)-P(1)#3	111.867(19)
C(3)-P(1)-Pd(1)	126.70(11)
C(5)-P(1)-Pd(1)	118.07(11)
C(5)-P(1)-C(3)	96.47(16)
C(4)-P(1)-Pd(1)	119.66(12)
C(4)-P(1)-C(3)	96.22(17)
C(4)-P(1)-C(5)	92.18(19)
C(4)-O(1)-C(1)	117.8(3)
C(5)-O(2)-C(1)	117.1(3)
C(8A)-C(3)-P(1)	112.4(6)
C(8A)-C(3)-C(2)	116.8(6)
C(8A)-C(3)-C(7A)	106.6(6)
C(8B)-C(3)-P(1)	105.5(7)
C(2)-C(3)-P(1)	109.0(2)
C(2)-C(3)-P(1)	109.0(2)
C(2)-C(3)-C(8B)	99.4(7)
C(2)-C(3)-C(7A)	102.2(5)
C(7A)-C(3)-P(1)	109.1(5)
C(7B)-C(3)-P(1)	110.8(7)
C(7B)-C(3)-C(8B)	108.5(8)
C(7B)-C(3)-C(2)	121.8(6)
O(2)-C(5)-P(1)	114.9(2)
O(1)-C(4)-P(1)	114.6(2)
O(1)-C(1)-O(2)	110.3(3)
O(1)-C(1)-C(2)	110.5(4)
O(1)-C(1)-C(6)	109.7(3)
O(2)-C(1)-C(2)	110.2(4)

O(2)-C(1)-C(6)	106.4(3)
C(2)-C(1)-C(6)	112.6(3)
C(1)-C(2)-C(3)	117.5(3)

Symmetry transformations used to generate equivalent atoms:
#1 5/4-y, 1/4+x, 1/4-z,
#2 1/4+y, 5/4-x, 1/4-z
#3 1-x, 3/2-y,+z

4. Calculation of Tolman Cone Angles

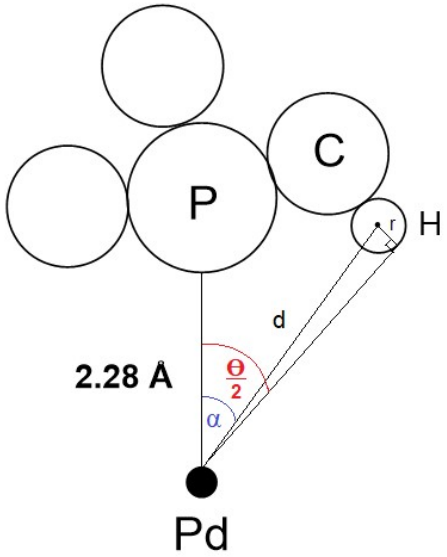

Figure S70. Definition of parameters for the calculation of Tolman Cone Angles (°).

Due to the asymmetric nature of ligand **L1**, substituent half-angles, $\frac{\theta_i}{2}$, were first measured for each substituent connected to the P donor atom. The average of the 3 measured half-angles was then doubled to get the overall Tolman Cone Angles (°), Θ. These calculations are represented in the following equations:

$$\theta = \frac{2}{3}\sum_i \frac{\theta_i}{2}$$

$$\frac{\theta_i}{2} = \alpha + \sin^{-1}\frac{r}{d} \times \frac{180}{\pi}$$

Where,

Θ = Tolman Cone Angle (°)

$\frac{\theta_i}{2}$ = Substituent half-angle (°)

α = Measured P-Pd-H angle (°)

r = Van der Waals radii of hydrogen (1.00 Å)[1]

d = Measured Pd-H distance (Å)

Pd-P distances of the XRD structures were first modified to 2.28 Å along the Pd-P axis with PerkinElmer Chem3D version 17.1.0.105. Alternatively, a dummy atom can be created 2.28 Å away from the P atom along the Pd-P axis to represent the Pd centre from which the Tolman Cone Angle measurements will be made. Mercury 2020.1 (Build 280197) was subsequently used to measure the above parameters for each substituent connected to the P donor atom.

As each substituent has multiple H atoms that could be considered as the cone outer limit, substituent half-angles for all possible H atom were calculated individually and the largest substituent half-angle of each substituent were taken to be plugged into the above equation to calculate the overall Tolman Cone Angle (°).

It should be noted that since Mercury measures distances and angles based on atom centres, an additional term has to be included to account for the Van der Waals radii of hydrogen atoms during Tolman Cone Angle calculations. For this, we followed the protocol of Müller and Mingos,[1] setting the Van der Waals radius of hydrogen to 1.00 Å and using trigonometry to derive the extra term to be added to the substituent half-angle.

Table S5. Measured distances and angles used to calculate Tolman Cone Angle for [Pd(**L1**)$_2$Cl$_2$].

XRD Structure	**C(3)**		**C(4)**		**C(7)/C(8)***		**Tolman Cone Angle**
	Pd-H	**P-Pd-H**	**Pd-H**	**P-Pd-H**	**Pd-H**	**P-Pd-H**	
[Pd(**L1**)$_2$Cl$_2$]	3.561 Å	39.96°	Symmetric with C(3)		3.472 Å	55.58°	123.24°

*The methyl groups C(7) and C(8) were symmetric with respect to Pd(1) resulting in identical Pd-H and P-Pd-H measurements.

Table S6. Measured distances and angles used to calculate Tolman Cone Angle for [Pd(**L1**)$_4$].

XRD Structure	C(7)		C(8)		C(1)/C(2)*		Tolman Cone Angle
	Pd-H	P-Pd-H	Pd-H	P-Pd-H	Pd-H	P-Pd-H	
[Pd(**L1**)$_4$]	3.624 Å	39.11°	3.614 Å	39.34°	3.685 Å 3.569 Å	54.27° 54.89°	120.75° (±0.38°)

*Due to disorder, 2 possible conformations were observed. Average Tolman Cone Angle between the 2 conformations is shown, with error of 1 standard deviation given in brackets.

Table S7. Measured distances and angles used to calculate Tolman Cone Angle for [Pd(**L4**)$_2$Cl$_2$].

DFT Structure	C(26)		C(29)		H(61)		Tolman Cone Angle
	Pd-H	P-Pd-H	Pd-H	P-Pd-H	Pd-H	P-Pd-H	
[Pd(**L4**)$_2$Cl$_2$]	3.718 Å	39.34°	3.646 Å	40.91°	5.064 Å	86.76°	139.95°

Density Functional Theory (DFT) calculations were performed with Gaussian 16 package[2] using the B3LYP[3] functional and the DEF2TZVPP[4] basis set on all atoms with Grimme dispersion correction[5] and Becke-Johnson damping.[6] All geometries were localised in the gas phase at the B3LYP level. Refined structure was confirmed to be at an energy minimum through frequency calculations.

Table S8. Cartesian coordinates for [Pd(**L4**)$_2$Cl$_2$].

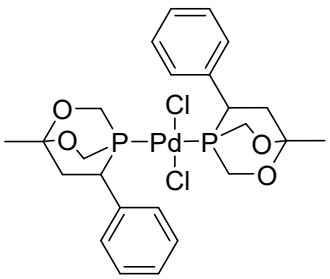

C(1)	6.158	-2.313	0.061
H(2)	6.146	-3.133	0.775
H(3)	6.873	-1.563	0.392
H(4)	6.459	-2.692	-0.914
C(5)	4.777	-1.704	-0.021
C(6)	3.141	-0.841	1.545
H(7)	3.091	0.102	2.085
H(8)	2.694	-1.615	2.172
C(9)	2.538	-2.420	-0.623
H(10)	1.874	-3.138	-0.145
H(11)	2.367	-2.456	-1.702
C(12)	4.684	-0.610	-1.096
H(13)	4.795	-1.088	-2.069
H(14)	5.530	0.062	-0.967
C(15)	3.364	0.204	-1.065
Cl(16)	0.024	-0.186	-2.323
O(17)	4.511	-1.141	1.266
O(18)	3.881	-2.779	-0.290
P(19)	2.178	-0.726	-0.010
Pd(20)	0.000	0.000	0.000
C(21)	-6.158	2.313	-0.061
H(22)	-6.147	3.133	-0.775
H(23)	-6.873	1.563	-0.392
H(24)	-6.459	2.692	0.914
C(25)	-4.777	1.704	0.021
C(26)	-3.142	0.841	-1.545
H(27)	-3.091	-0.102	-2.085
H(28)	-2.694	1.615	-2.172
C(29)	-2.538	2.420	0.623
H(30)	-1.874	3.138	0.145
H(31)	-2.367	2.456	1.702
C(32)	-4.684	0.610	1.096
H(33)	-4.795	1.088	2.069
H(34)	-5.530	-0.062	0.967
C(35)	-3.364	-0.204	1.065
Cl(36)	-0.024	0.187	2.323
O(37)	-4.511	1.141	-1.266
O(38)	-3.882	2.779	0.290
P(39)	-2.178	0.726	0.010
H(40)	-2.904	-0.196	2.051
H(41)	2.904	0.196	-2.051
C(42)	3.446	1.637	-0.595
C(43)	2.543	2.566	-1.116
C(44)	4.345	2.051	0.386
C(45)	2.546	3.881	-0.673

H(46)	1.831	2.247	-1.866
C(47)	4.348	3.369	0.829
H(48)	5.035	1.341	0.820
C(49)	3.450	4.288	0.302
H(50)	1.844	4.590	-1.091
H(51)	5.052	3.674	1.592
H(52)	3.454	5.313	0.648
C(53)	-3.446	-1.637	0.595
C(54)	-2.543	-2.566	1.116
C(55)	-4.345	-2.051	-0.386
C(56)	-2.546	-3.881	0.673
H(57)	-1.831	-2.247	1.866
C(58)	-4.348	-3.369	-0.829
H(59)	-5.035	-1.341	-0.820
C(60)	-3.450	-4.288	-0.302
H(61)	-1.844	-4.590	1.091
H(62)	-5.051	-3.674	-1.592
H(63)	-3.454	-5.313	-0.648
H(64)	0.815	-0.272	-0.004
H(65)	-0.815	0.272	0.004
H(66)	4.465	1.391	-0.970
H(67)	3.186	3.474	-1.072
H(68)	4.601	2.466	-0.614
H(69)	2.909	3.938	0.378
H(70)	4.178	3.893	-0.138
H(71)	3.531	5.382	0.490
H(72)	-4.465	-1.390	0.970
H(73)	-3.186	-3.474	1.072
H(74)	-4.594	-2.476	0.612
H(75)	-2.919	-3.935	-0.374
H(76)	-4.201	-3.894	0.141
H(77)	-3.518	-5.384	-0.485

5. Calculation of Ligand Buried Volume (%V_Bur)

Molecular structures obtained from X-ray crystallography: [Pd(**L1**)$_2$Cl$_2$] and [Pd(**L1**)$_4$], DFT calculations: [Pd(**L4**)$_2$Cl$_2$], or from the Cambridge Structural Database: [Pd(PPh$_3$)$_2$Cl$_2$] (CCDC reference: 1111617)[7] were subjected to ligand buried volume (%V_Bur) calculations using SambVca 2.[8] The transition metal atom (Pd) was set as the coordination centre and the Pd-P distance (metal-ligand distance) was set to 2.28 Å. Atoms not part of the ligand (e.g. Pd, Cl) were deleted and thus not considered in the buried volume calculation. Atomic radii were set

at Bondi radii and sphere radius set to 7 Å. Mesh spacing for numerical integration was set to 0.10 Å and hydrogen atoms were omitted from the calculation.

6. References

1. T. E. Müller; D. M. P. Mingos, *Transition Met. Chem.* 1995, **20** (6), 533-539.
2. M. J. Frisch, et al. *Gaussian 16 Rev. B.01*, Wallingford, CT, 2016.
3. A. D. Becke, *J. Chem. Phys.* 1993, **98** (7), 5648-5652.
4. F. Weigend, *Phys. Chem. Chem. Phys.* 2006, **8** (9), 1057-1065; F. Weigend; R. Ahlrichs, *Phys. Chem. Chem. Phys.* 2005, **7** (18), 3297-3305.
5. S. Grimme, *Wiley Interdiscip. Rev.: Comput. Mol. Sci.* 2011, **1** (2), 211-228.
6. E. R. Johnson; A. D. Becke, *J. Chem. Phys.* 2006, **124** (17), 174104; E. R. Johnson; A. D. Becke, *J. Chem. Phys.* 2005, **123** (2), 024101.
7. G. Ferguson; R. McCrindle; A. J. McAlees; M. Parvez, *Acta Crystallogr. B* 1982, **38** (10), 2679-2681.
8. L. Falivene, et al., *Organometallics* 2016, **35** (13), 2286-2293; L. Falivene, et al., *Nat. Chem.* 2019, **11** (10), 872-879.